TOWARD MODELING EROSION ON UNPAVED ROADS IN MOUNTAINOUS NORTHERN THAILAND

A DISSERTATION SUBMITTED TO THE GRADUATE DIVISION OF THE UNIVERSITY OF HAWAII IN PARTIAL FULFILLMENT OF THE REQUIREMENTS FOR THE DEGREE OF

DOCTOR OF PHILOSOPHY

IN

GEOGRAPHY

MAY 2000

by

Alan D. Ziegler

Dissertation Committee:

Thomas W. Giambelluca, Chair
Ross A. Sutherland
Everett A. Wingert
Deborah Woodcock
Guillermo H. Goldstein

We certify that we have read this dissertation; and that it is, in our opinion, satisfactory in scope and quality as a dissertation for the degree of Doctor of Philosophy in Geography.

_____

chair

_____

_____

_____

_____

Acknowledgments

I thank the following folks for their help in this research: Asuh, Atabuu, Atachichi, and Aluong (brawn); Kalaya (the General); Yun, Mae and Paa (kinsmanship); Paluk and Nadi Lamu (sharing their home), S. Yarnasarn, Geography, Chiang Mai University (support in Chiang Mai); J. Pintong, Agriculture Dept., Chiang Mai University (soil analyses); J. F. Maxwell (plant taxonomy and drinks); Mike Nullet and John Allison (engineering prowess); Chumnien and Amphai (support in Bangkok); T.T. Vana (field assistance in Thailand); Alexis Lee, J. Bussen, N. Thompson, J. Nagle, C.T. Lee, and M. Gilbeaux (lab/field assistance in Hawaii); Don Plondke (GIS); Sathaporn Jaiaree, and Sawasdee Boonchee, the Soil and Land Conservation Division of the Dept. of Land Development, Bangkok and Chiang Mai offices (expertise); Yinglek Pongpayack, the Soil Analysis Division of the Dept. of Land Development, Bangkok (soil analyses); Servillano Lamer, Department of Agronomy and Soil Science, University of Hawaii (support at UH test facility); C. Southern, and R. Gouda (construction and design of rainfall simulation apparatus); D. Ko, P. Malaspina, and E. Lind, Integrated Training Area Management Division, Schofield Barracks (use of ITAM facility at Schofield); Midwest Industrial Supply, Inc. (freely providing Soil Sement™).

I especially thank professors Thomas W. Giambelluca and Ross A. Sutherland for their advice, field assistance, and manuscript review during this project. This dissertation work was partially funded by the National Science Foundation Award (grant no. 9614259) and a seed money grant from the University of Hawaii. I was additionally supported by an Environmental Protection Agency Star Fellowship and a Horton Hydrology Research Award (Hydrological Section, American Geophysical Union); and I recieved travel money from the UH International Agreements Fund and the Arts and Sciences Advisory Council.

Abstract

Contributions of road networks and unstable agricultural activities to downstream sedimentation, water shortages, and flooding in mainland SE Asia are not easily determined because scientific understanding of runoff and erosion processes operating on roads is limited. This dissertation work, conducted within the Pang Khum Experimental Watershed (PKEW) in northern Thailand, supports that owing to low saturated hydraulic conductivity ($K_s \leq 16$ mm h^{-1}), Horton overland flow (HOF) generation occurs more frequently on unpaved PKEW roads than on other watershed surfaces having higher infiltrability (e.g., mean K_s for agricultural surfaces ranges from 130 to 320 mm h^{-1}). Because of frequent HOF generation, the road system contributes to stream sedimentation throughout the rainy season. The highly compacted (bulk density ≈ 1.45 Mg m^{-3}) PKEW road surface typically underlies a layer of loose material of finite depth. Instantaneous sediment transport (S_t) on roads varies because the supply of easily transported surface sediment is constantly altered by overland flow events, traffic, road maintenance, and mass wasting events, both during and between storms. As surface material is removed during an overland flow event, normalized S_t declines from an initial peak rate of ≈ 3 g J^{-1} to a steady rate of ≈ 0.5 g J^{-1}. The mechanical stress associated with vehicle passes during a storm increases the availability of loose material, producing 2-4 fold increases in S_t and sediment concentration (C_t) values. Herein, rainfall simulation data, surveys of traffic phenomena, and soil property measurements were used to parameterize the physics-based KINEROS2 model for simulating road runoff and erosion. During model validation, instantaneous discharge was simulated well (root mean squared error (RMSE) = 14%). However, because KINEROS2 equations do not “describe” road erosion processes accurately, S_t was simulated poorly (RMSE = 51.6%). To improve modeling, a methodology recognizing the dynamic erodibility (DE) of a road surface was introduced. By explicitly simulating removal of a layer of loose material, the DE modeling technique improved prediction of S_t (RMSE decreased to 35.4 %). Finally, a systematic approach is presented to implement DE modeling on any road surface where baseline erodibility and sediment availability can be quantified.

Table of Contents

Description **Page**

List of Tables

List of Figures

1. Introduction

1.1 IMPACTS OF UNSTABLE AGRICULTURAL PRACTICES AND ROAD SYSTEMS IN NORTHERN THAILAND

Current water shortage, flooding, and excessive sedimentation problems in lowland areas of Thailand are often blamed on agricultural practices of highland ethnic hilltribe groups, who have migrated to Thailand from China, Myanmar, and Lao over the last several decades. These groups, including the the Ahka, Hmong, Karen, and Lisu, traditionally practiced short-term swidden agriculture, involving the clearing of small (0.5-1.0 ha) plots on forested slopes for cultivation. Once crop production declined, the farmers moved to a new site, probably before their presence greatly impacted watershed hydrology and geomorphology. However, as mountain populations increased, available land decreased, thereby reducing the mobility of the swidden farmers. In response, traditional short-term, subsistence-based swidden practices were replaced by long-term, intensive cultivation of marketable crops (cf. Schmidt-Vogt, 1998, 1999). In some areas of northern Thailand, this intensified system has contributed to cumulative watershed effects both on-site locally and off-site downstream in major river systems, such as the Chao Praya. As a result, domestic and international conservation projects conducted in highland watersheds have focused primarily on the agricultural practices of ethnic minority groups. The international paradigm has traditionally been that swidden agriculture is synonymous with accelerated erosion.

This critical attention has helped foster a general perception that unwise agricultural practices of hilltribe minorities are the predominant cause of lowland water shortages, more frequent flooding, and excessive sedimentation. While improper cultivation techniques on steep slopes are certainly responsible for serious downstream effects in some areas, expansion of the rural road network may be equally or more important. The impacts of road systems, which have been rapidly expanding in the mountains of northern Thailand during the last three decades, have generally been overlooked by conservation projects. Road systems throughout the world are now generally recognized as important agents in disrupting watershed hydrological and geomorphological processes and contributing to adverse cumulative watershed effects (Reid, 1993; Montgomery,

1994). In some instances, road impacts may be greater than those of other recognized disruptive activities. Megahan and Ketcheson (1996) state the primary sediment source from logging activities in western USA is forest access roads, rather than other timber management activities (e.g., Megahan and Kidd, 1972). In a study near Melbourne Australia, Grayson et al. (1993) determined that timber harvesting activities did not greatly affect stream physical and chemical water quality, but improperly placed or poorly maintained roads contributed substantial sediment quantities to stream systems. In northern Thailand, unpaved mountain roads were found to disrupt hydrological and erosional processes disproportionately to their areal extent, compared with agriculture-related lands (Ziegler and Giambelluca, 1997a,b). This study lead to the hypothesis that in some watersheds in northern Thailand the impacts of roads are comparable to those of agricultural practices. However, to date, there is insufficient supportive research on hydrological and erosion processes operating on highly compacted road surfaces to fully assess their environmental significance, relative to agricultural lands. Furthermore, the methods and modeling tools available to assess road impacts are largely based on research on agricultural lands, and therefore, they may not be appropriate for studying road-related erosion.

1.2 THAILAND ROADS PROJECT

The Thailand Roads Project (TRP) was initiated in 1997 by Dr. Thomas W. Giambelluca, Dr. Ross A. Sutherland, and myself (all of the University of Hawaii, Geography Dept.) to study hydrological and geomorphological impacts of unpaved roads near Pang Khum village in northern Thailand (Figure 1.1). Objectives of TRP were to (1) construct a database of hydrologic, erosion, and soil-vegetation-atmosphere-transfer (SVAT) variables for several land-cover types; (2) determine the degree to which hydrologic processes in tropical watersheds are disrupted by roads; (3) establish the importance of roads in initiating hydrologic change and contributing to erosion processes—and in so doing, obtain a detailed understanding of erosion processes operating on and adjacent to road surfaces; and (4) quantify erosional and hydrological impacts associated with the expansion of road networks. In preparation for TRP, two pilot studies were conducted by the research team. The first, conducted in 1995, investigated runoff generation on mountainous roads at two sites in

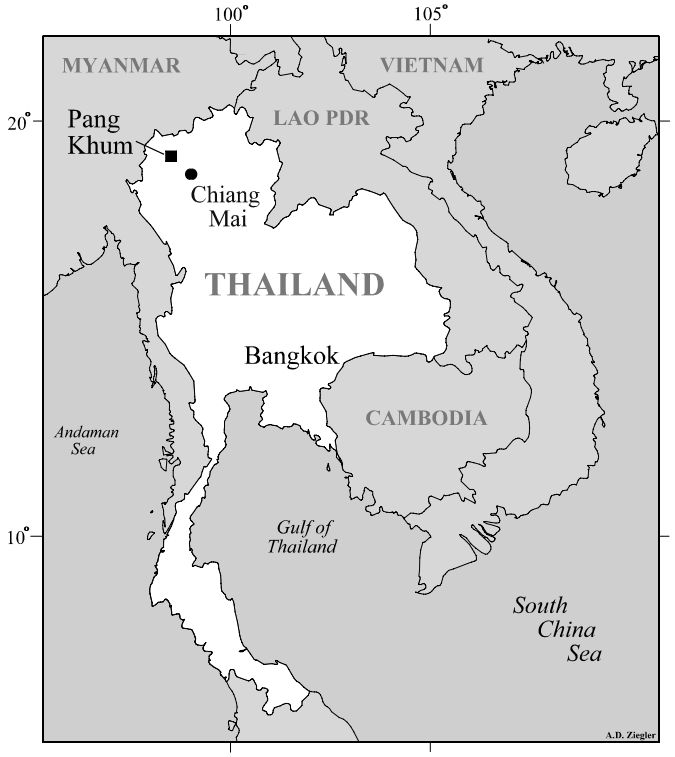

Figure 1.1. The study site is near Pang Khum Village in northern Thailand.

northern Thailand. The second, conducted in Hawaii in the fall of 1996, developed and tested the rainfall simulation methodology that would be the primary field research methodology in TRP. This dissertation results from my involvement in TRP from January 1997 to November 1999, and the two prior pilot studies. The dissertation work is a subset of that undertaken by TRP. It focuses primarily on the need for, and the development of, a realistic road erosion modeling methodology that will be used subsequently to achieve all the objectives of TRP.

1.3 OBJECTIVE OF THE DISSERTATION RESEARCH

The objective of this dissertation research is to employ field rainfall simulation experiments, soil property measurements, and surveys of road-related phenomena (e.g., traffic intensity, physical

dimensions) to develop a methodology that allows physically realistic modeling of runoff and erosion on unpaved roads in mountainous northern Thailand. Once developed, this methodology can then be used by others to quantify hydrological and erosional impacts resulting from road networks versus those from agricultural activities in steeply sloped areas of Montane Mainland Southeast Asia (MMSEA), which is the goal of the larger Thailand Roads Project. The modeling approach is designed to be applicable to all watersheds, tropical or temperate, lowland or highland. The work should allow managers and policy makers to better manage road networks in MMSEA.

1.4 LAYOUT OF THE DISSERTATION

This dissertation is composed of four experiments, Chapters 3-6, each working toward developing a modeling methodology for road erosion. Experiment I (Chapter 3) establishes the uniqueness of runoff generation and sediment transport of roads, compared with agricultural activities in the study area. Experiment II (Chapter 4) addresses the partitioning of total road erosion into splash and hydraulic erosion subprocesses, which is needed to parameterize the KINEROS2 physically-based model used in subsequent experiments. Experiment III (Chapter 5) shows the importance of vehicular traffic and maintenance practices in enhancing the erodibility of a road surface by detaching material that is subsequently removed during overland flow events. Experiment IV (Chapter 6), introduces the dynamic erodibility modeling methodology, which is based on the idea that road erodibility is a variable process, dependent on the amount of loose, easily entrained surface material present on the road. Additionally, the supply of this loose material varies in response to maintenance practices and traffic since the last overland flow event.

Chapter 2 provides the background needed to allow each experiment to be an independent work. All experiments are currently in press or have been accepted for publication (pending revision) in the following journals: *Earth Surface Processes Landforms* (Experiment I), *Water Resources Research* (Experiment II), *Earth Surface Processes Landforms* special issue on roads (invited, Experiment III), and *Hydrological Processes* (Experiment IV). A synthesis of this dissertation work will be published in *Agriculture, Ecosystems, and Environment* (invited).

2. Background

2.1 STUDY AREA: PANG KHUM EXPERIMENTAL WATERSHED

The study area for the dissertation research is near Pang Khum village (19°3'N, 98°39'E) in northern Thailand (Figure 1.1). Pang Khum is within the Samoeng District of Chiang Mai Province, approximately 60 km NNW of Chiang Mai, in the eastern range of the Thanon Thongchai Mountains. Field research was conducted in the 93.7-ha Pang Khum Experimental Watershed (PKEW; Figure 2.1). PKEW is part of the larger Khan River Basin, which drains into the Ping River, which in turn empties into the Chao Praya River. Bedrock is Triassic granite (field observation; Geological Map of Thailand, 1979). PKEW soils are Ultisols, Alfisols, and Inceptisols (Appendix A). Roads comprise < 1% of the PKEW area. Roads, access paths, and dwelling sites each comprise < 1% of the PKEW area. Approximately 12% of the basin area is agricultural land (cultivated, upland fields, and < 1.5 year-old abandoned); 13%, fallow lands (not used for 1.5-4 years); 31 and 12% are young (4-10 years) and advanced secondary vegetation, respectively; and 31% is disturbed, primary forest. The original pine-dominated forest has been altered by hundreds of years of swidden cultivation by Karen, Hmong, and, recently, Lisu ethnic groups. Most lower basin slopes are cultivated by Lisu villagers who migrated to Pang Khum from Mae Hong Son Province about 20 years ago. Population density in the area is now about 16 people km^{-1} (J. Fox, East-West Center, Honolulu, pers. comm.). Figure 2.2 shows the landcover in PKEW for 1995. The farming system now resembles a long-term cultivation system with short fallow periods, as opposed to the traditional Lisu long fallow system (cf. Schmidt-Vogt, 1998). Major crops include upland rice, corn, cabbage, onions, flowers, fruit, and some paddy rice. Opium was an important crop before government eradication began about 10 years ago.

Original forest was probably dominated by pine (J.F. Maxwell, Herbarium, Chiang Mai University, pers. comm., 1998). Some attempts have been made to regenerate deforested areas by planting *Pinus kisiya* Roy. ex Gord. Additionally, *Castanopsis diversifolia* King ex Hk. f., *Glochidion sphaerogynum* (M.-A.) Kurz, *Helicia nilagirica* Bedd., *Phyllanthus emblica* L., *Schima wallichii* (DC.) Korth, and *Styrax benzoides* Craib are commonly found in secondary forests. In the disturbed primary forests, *Castanopsis tribuloides* (Sm.) A. DC., *Lithocarpus elegans* (Bl.) Hatus. ex Soep., *Phoebe lanceolata* (Nees) Nees, *Rhus chinensis* Mill., *Saurauia roxburghii* Wall., and

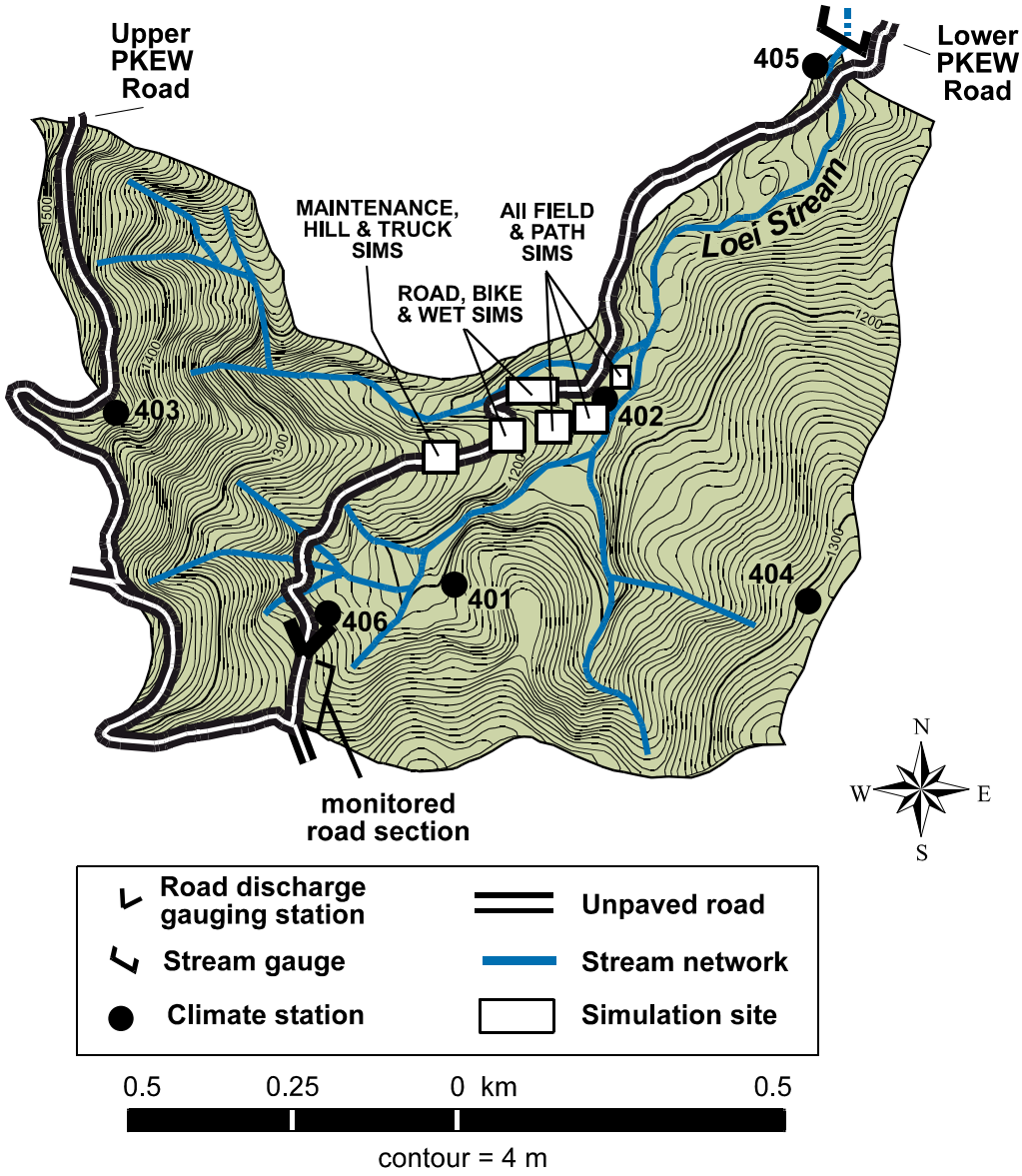

Figure 2.1. The 93.7-ha Pang Khum Experimental Watershed (PKEW).

Wendlandia tinctoria (Roxb.) CD. tinctoria are present. Understory vegetation in both primary and secondary forests commonly includes *Dioscorea glabra* Roxb. var. glabra, *Flemingia sootepensis* Craib., *Microstegium vagans* (Nees ex Steud.) A. Camus, *Panicum notatum* Retz., *Rubus blepharoneurus* Card., *Scleria lithosperma* (L.) Sw. var. lithosperma, *Setaria palmifolia* (Koen.) Stapf

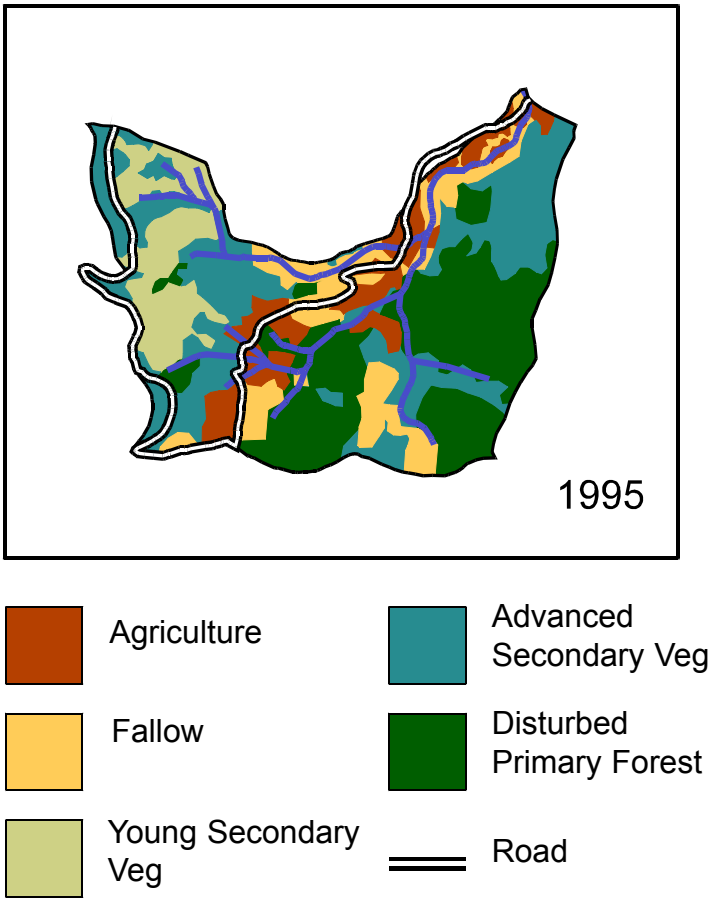

Figure 2.2. PKEW landcover in 1995; determined from airphoto interpretation (1:50,000).

var. palmifolia, *Thelypteris subelata* (Bak.) K. Iw., and *Thunbergia similis* Craib. Vegetation descriptions are based on surveys performed by J.F. Maxwell and me in the dry season of November and December, 1998. Some important wet-season species may therefore be absent from the description.

The Upper and Lower PKEW Roads are important source areas for sediment entering the stream channel network. At the beginning of the rainy season, loose road surface material that accumulates during the dry season is flushed by surface flow during the first few rainstorms. Thereafter, daily traffic detaches sediment and creates ruts for gully initiation. Filling of gullies with unconsolidated material, practiced by villagers as a means of temporary road repair, is an addi-

tional source of easily eroded material. Because HOF is frequently generated on roads (Ziegler and Giambelluca, 1997a), surface runoff consistently transports sediment and incises concentrated flow channels throughout the wet period.

2.2 ROAD EROSION MODELING

Although the geomorphological importance of unpaved roads has been recognized for almost a century (Gilbert, 1917), intensive road field research did not begin until after the mid-1970s (e.g., Anderson, 1975; Hafley, 1975; Megahan, 1975; Wald, 1975; Reid and Dunne, 1984). While recent studies in the Pacific NW have advanced understanding of road impacts (e.g., Jones and Grant, 1996, Megahan and Ketcheson, 1996; Bowling and Lettenmaier, 1997; Foltz and Elliot, 1997; La Marche and Lettenmaier, 1998; Thomas and Megahan, 1998; Wemple, 1998; Ketcheson et al., 1999; Luce and Black, 1999), the ability to assess the hydrological and erosional impacts of road versus nonroad activities is still developing. Physically based models can be important tools in understanding road disruption of basin functions, provided that (1) the model realistically describes underlying runoff generation and erosion processes, (2) necessary parameters and datasets can be obtained to force the model, and (3) validation can be performed to ensure model accuracy.

Early attempts at modeling road-related erosion include the RoSED model (Simons et al., 1977) and subsequent modifications (e.g., Simons et al., 1978; Ward, 1983). Few studies have attempted to derive road-related parameters used in the equations of physically based watershed runoff and erosion models (e.g., Simons et al., 1982; Ward and Seiger, 1983; Flerchinger and Watts, 1987; Luce and Cundy, 1994; Elliot et al., 1995, Ulman and Lopes, 1995). There are currently three dominant trends in road modeling: (1) building road features into the topology of versatile, physically based runoff/erosion models, such as KINEROS (e.g., Ziegler and Giambelluca, 1997b) or WEPP (Elliot et al., 1995); (2) incorporating road-related phenomena, e.g., interception of subsurface flow, into distributed soil-vegetation-atmosphere-transfer (SVAT) models (e.g., DHVSM, Wimosta et al., 1994; La Marche and Lettenmaier, 1998; Storck et al., 1998; Wigmosta and Perkins, unpublished); and (3) integrating road erosion data with spatial structures in geographical information system (GIS) models, such as ROADMOD (Anderson and MacDonald, 1998), and SEDMOD (Wold et al., 1998). Despite growing interest in modeling road erosion, no current modeling approach has been fully successful in simulating on-road erosion processes.

2.3. THE THREE-DIMENSIONAL ROAD PRISM

Understanding the principal hydrological and erosional processes on roads is essential to developing a modeling methodology. Results from the Thailand pilot study (Ziegler and Giambelluca, 1997 a,b) indicate the importance of focusing on the entire three-dimensional "road prism," as runoff generation, and subsequently sediment transport, are affected by both surface and subsurface hydrology. The conceptualized road prism in Figure 2.3, which is representative for most mountain roads in general, serves as the basis for the following definitions. One common source of road surface runoff (RO) is Horton overland flow (HOF). Because road surface infiltration rates are usually very low (owing to compaction), HOF is generated quickly on road surfaces (HOF_r) even during relatively low-magnitude rainfall events (Ziegler and Giambelluca, 1997a). In some instances, Horton flow generated on adjacent landuse surfaces (HOF_u) may flow onto the road surface, increasing runoff. Antecedent soil moisture content (Θ_n) also governs HOF generation: time to runoff (TTRO) is shorter on a wet road compared with the same road under dry conditions. Road surface Θ_n is affected by evaporation rate (EVAP) and by the depth to the underlying water table, which may also play an important role in overland flow generation. For example, saturation overland flow (SOF) occurs when the water table rises above the road surface, and the ground water exfiltrates onto the road. Based on preliminary work, SOF is currently believed to be rare in PKEW. Variability in the height of the rising water table is signified by the broken line and double arrow in Figure 2.3.

Once generated, surface runoff often remains on the road for tens to hundreds of meters until it typically exits at a stream crossing or onto the side of a hillslope (X_H). The high connectivity of the road system ensures that a large percentage of the surface flow is delivered to the stream network. In locations where runoff flows onto a hillside, water may either infiltrate (I) or cause channelization of the hillslope (e_C), developing flow paths that eventually terminate in the stream network. In PKEW, transport efficiency of on-road water to the stream network may exceed 75% (field-based estimate). Relatively small volumes of overland flow can entrain loose surface material resting on the road surface. As runoff flows down the road network, depth and velocity increase, thus shear stress increases. At some threshold, runoff erodes the compacted road surface (e_T); incision is often initiated in existing ruts or tire tracks.

Fundamentally, in the absence of gullying and mass wasting, erosion on the composite road surface is controlled by splash (e_s) and hydraulic erosion (e_h) sub-processes that operate on all sloping land surfaces. These processes are functions of (1) dynamic storm-related phenomena, including rainfall, infiltration, and local overland flow state (especially depth); and (2) soil surface erodibility properties, including shear strength. Owing to compaction, soil surface shear strength on roads is higher than on most other basin landuse types. Therefore, excluding extreme events, road surface materials are relatively resistant to detachment processes that could cause severe erosion on agricultural soils. Nevertheless, sediment transport on unpaved roads can be high when (1) large quantities of loose material have been deposited on the road surface before an overland flow event, (2) vehicular traffic during a storm detaches new material from the road surface; and/or (3) overland flow incises existing surface ruts/tracks. Loose surface sediment originates from mass wasting events, maintenance activities, and vehicular soil detachment, both during and between storms. These, and other phenomena/processes that enhance the erodibility of the road by supplying loose surface material, are referred to herein as "surface preparation" processes.

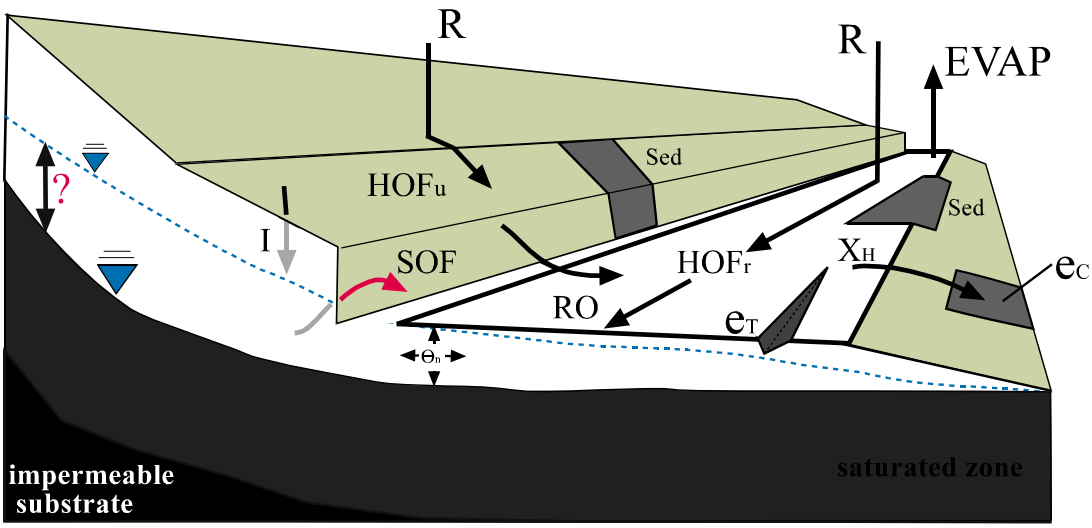

Figure 2.3. Fundamental hydrological and erosional processes of the 3-dimensional road prism: R is rainfall; EVAP is evaporation; I is infiltration; e_T is erosion of the road surface; e_C is hillslope channelization occurring below runoff exit points on the hillslope (X_H); orange shading shows sediment source areas (Sed); HOF is Horton overland flow occurring on the road (HOF_r) or upslope surfaces (HOF_u); SOF is saturation overland flow occurring when the water table (broken line) rises above the road surface.

3. EXPERIMENT I: Runoff generation and sediment production on unpaved roads, footpaths, and agricultural land surfaces in northern Thailand

3.1 ABSTRACT

Rainfall simulation was used to examine runoff generation and sediment transport on roads, paths, and three types of agricultural fields in PKEW. Because interception of subsurface flow by the road prism is rare in PKEW, work focused on Horton overland flow (HOF). Under dry antecedent soil moisture conditions, roads generated HOF in ≈1 min and have event runoff coefficients (ROCs) of 80% during 45-min, ≈105 mm h^{-1} simulations. Runoff generation on agricultural fields required greater rainfall depths to initiate HOF; these surfaces had total ROCs ranging from 0-20%. Footpaths are capable of generating erosion-producing overland flow within agricultural landscapes where HOF generation is otherwise rare. Paths had saturated hydraulic conductivity (K_s) values 80-120 mm h^{-1} lower than those of adjacent agricultural surfaces. Sediment production on roads exceeded that of footpaths and agricultural lands by more than eight times (1.23 versus < 0.15 g J^{-1}). Typically, high road runoff volumes (owing to low K_s, ≈15 mm h^{-1}) transported relatively high sediment loads. Initial road sediment concentrations exceeded 100 g L^{-1}, but decayed with time as loose surface material was removed. Compared with the loose surface layer, the compacted, underlying road surface was resistant to detachment forces. Sediment concentrations for road simulations were slightly higher than data obtained from a 165-m road section during a comparable natural event. Initial simulation concentrations were substantially higher, but were nearly equivalent to those of the natural event after 20-min simulation time. Higher sediment concentration in the simulations was related to differences in the availability of loose surface material, which was more abundant during the dry-season simulations than during the rainy season natural event. Sediment production on PKEW roads is sensitive to surface preparation processes affecting the supply of surface sediment, including vehicle detachment, maintenance activities, and mass wasting. The simulation data represent a foundation from which to begin parameterizing a physically based runoff/erosion model to study erosional impacts of roads in the study area.

3.2 OBJECTIVE

The objectives of this experiment are to (1) use rainfall simulation to quantify runoff generation and sediment transport on roads, footpaths, and agricultural lands and (2) compare data from small plot rainfall simulation experiments on roads with those from a natural rainfall event on a larger-scale road plot. The goal of this work is to examine whether processes operating on roads differ in type or magnitude from those on agricultural lands and to obtain parameters needed to simulate runoff and erosion using a physically based model (Experiment IV, Chapter 6).

3.3 METHODS AND MATERIALS

3.3.1 Study site

All work was performed within the 93.7-ha PKEW (Figure 2.2). Soil properties determined on the Lower PKEW Road and adjacent fallow fields are listed in Table 3.1. The Upper and Lower PKEW Roads are important source areas for material entering the stream channel network. At the beginning of the rainy season, loose road surface material accumulated during the dry season is flushed by surface flow during the first few rainstorms. Thereafter, light daily traffic (≈ 4 motorcycles and 2 trucks per day, Chapter 5) detaches more sediment and creates ruts for gully initiation. Filling of gullies with unconsolidated material is an additional source of easily eroded material. Because HOF is commonly generated on roads (Ziegler and Giambelluca, 1997a), surface runoff frequently transports sediment and incises concentrated flow channels throughout the wet period. During the largest rain event of 1998 (STORM, discussed below), HOF from the 1650 m Lower PKEW Road comprised 10% of the basin storm hydrograph for the first hour. Because road runoff exit points tend to be where the road intersects stream channels, conveyance efficiency to the stream network is ≈ 75% (based on field survey).

3.3.2 Simulation treatments

In February of 1998 and 1999 (dry seasons), 27 rainfall simulations were performed on a 50-m road section and five other surfaces within an upland rice field, including (1) hoed field, (2) upland field, (3) basin access path, (4) field maintenance path, and (5) fallow field. The rice field, consisting of 0.25 to 0.50 m rice stubble at the time of fieldwork (40-60% standing cover), was har-

Table 3.1. Soil Properties on and adjacent to the road surface at PKEW.

Descriptor/Property	Units	Road† Surface	Road Sediment	Upland Field
Sand fraction	%	54.4 ± 4.9	57.3 ± 8.2	57.1 ± 5.0
Silt fraction	%	24.0 ± 2.2	22.2 ± 3.8	21.2 ± 4.6
Clay fraction	%	21.7 ± 5.5	20.5 ± 5.5	22.0 ± 4.6
Dominant clay mineral	-	kaolinite††	-	kaolinite††
Particle density	Mg m^{-3}	2.55 ± 0.05	-	2.47 ± 0.06
$pH_{(1:5\ water)}$	-	4.9 ± 0.2	4.8 ± 0.3	5.6 ± 0.5
Organic carbon	%	2.5 ± 0.7	1.6 ± 0.6	3.5 ± 0.9
Total nitrogen	%	0.14 ± 0.03	0.13 ± 0.03	0.24 ± 0.03
Potassium	mg kg^{-1}	134 ± 68	319 ± 131	382 ± 118
Cation exch. capacity	$cmol_c\ kg^{-1}$	9.8 ± 2.6	-	14.7 ± 2.2
Calcium	$cmol_c\ kg^{-1}$	5.4 ± 3.1	-	16.3 ± 9.9
Magnesium	$cmol_c\ kg^{-1}$	0.58 ± 0.40	-	1.16 ± 0.52
Sodium	$cmol_c\ kg^{-1}$	0.14 ± 0.07	-	0.30 ± 0.09
Phosphorus	$cmol_c\ kg^{-1}$	0.34 ± 0.23	-	0.99 ± 0.32
% Exchangeable bases	%	63.1 ± 19.8	-	96.5 ± 8.9

† Road surface and upland field values were determined from eight and four 90 cm^3 surface cores, respectively; road sediment values were derived from sediment output of the 8 ROAD simulations; means are ± one standard deviation.

†† In addition to moderate amounts of kaolinite, the clay fraction also includes traces of illite, vermiculite, gibbsite, montmorillonite, and chlorite.

vested in November, 1997. Prior to simulation, the field was burned in a manner consistent with typical practice, except earlier in the season. A portion of the burned field was tilled with a traditional hand-held hoe. The upland field treatment was the unhoed burned field (≈ 90% bare ground). The 0.15-m-wide basin access path, used daily by 10 to 20 farmers, is the primary walking entry way into lower PKEW. The 0.14-m-wide field maintenance paths were created on the hoed surface by three Lisu farmers, wearing sandals, traversing up and then down a line 31 times. The fallow field consisted of < 0.5-m tall grasses and shrubs (≈ 80% standing cover). Hereafter, simulation surfaces are referred to as ROAD, HOED FIELD, UPLAND FIELD, PATH, FIELD PATH, and FALLOW FIELD (Table 3.2).

3.3.3 Measurement of physical properties

Prior to rainfall simulation, soil physical properties for each plot were measured either 1 m below or above the simulation plot. Surface bulk density (ρ_b) and antecedent soil moisture (Θ_n) were determined by sampling the upper 5 cm with a 90 cm^3 core ($n \geq 3$ for each plot), then oven drying for 24 h at 105° C. Subsurface bulk densities were determined similarly at 5 and 10 cm depths. Soil penetrability, a measure of the ease with which an object can be pushed into the soil (Bradford, 1986), was measured with a static Lang™ penetrometer (Gulf Shores, AL). The penetrometer provides an index of normal strength, termed penetration resistance (PR), for the upper soil surface, typically ≈ 0.5 cm in depth. Plot slope angles were determined with an Abney level. Saturated hydraulic conductivity was estimated from infiltration measurements taken *in situ* with Vadose Zone Equipment Corporation (Amarillo, TX) disk permeameters, linked to Campbell (Logan, Utah) 21X data loggers. Use of this instrument in PKEW is explained by Ziegler and Giambelluca (1997a).

3.3.4 Rainfall simulator and plot design

The rainfall simulator consisted of two vertical 4.3-m risers, each directing one 60° axial full cone nozzle (70 mm orifice diameter) toward the surface. Water from a refillable storage container (1850 L minimum) was fed to the simulator through 2.5 cm diameter PVC hose by a 750 W centrifugal pump and 2.5 kW gasoline-powered generator at 172 kPa (25 psi). This operating pressure produces rainfall energy flux densities (EFDs) of 1700-1900 J m^{-2} h^{-1}, which approximates energies sustained for 10-20 min during the largest annual PKEW storms (based on data from Ziegler and Giambelluca, 1997a). Tubular, sand-filled geotextile bags (3.0 m x 0.2 m x 0.1 m) were arranged to form rectangular plots. The bags were created from low permeability LINQ GTF 200 geotextile. Plot dimensions are shown in Table 3.2. Within PATH and FIELD PATH plots, the compacted path surface occupied only ≈18 and 16% of the respective areas; the remaining surfaces were similar to UPLAND FIELD and HOED FIELD, respectively. Nonpath surfaces were included within path treatments to investigate sediment transport from the entire path complex; i.e., erodible nonpath surfaces of relatively high infiltrability juxtaposed with compacted path surfaces that frequently generate HOF.

Table 3.2. Mean slope, antecedent soil mass wetness (w), rainfall intensity (r), and energy flux density (EFD) for rainfall simulation experiments.

Treatment	n†	plot dim (m)	slope (m m^{-1})	w (g g^{-1})	r (mm h^{-1})	EFD (J m^{-2} h^{-1})
ROAD	8	3.75 x 0.85	0.15 ± 0.02 a††	0.12 ± 0.03 b	105 ± 10 a	1774 ± 175 a
HOED FIELD	4	3.25 x 0.85	0.23 ± 0.02 b	0.06 ± 0.01 a	110 ± 13 a	1753 ± 218 a
UPLAND FIELD/PATH	7	3.25 x 0.85†††	0.20 ± 0.02 b	0.05 ± 0.01 a	107 ± 10 a	1818 ± 177 a
FIELD PATH	4	3.25 x 0.85	0.21 ±0.02 b	0.06 ± 0.01 a	105 ± 15 a	1807 ± 262 a
FALLOW	4	3.25 x 0.85	0.32 ± 0.02 c	0.04 ± 0.01 a	97 ± 7 a	1634 ± 125 a

† n is the number of "true" simulation replications; all replications were performed on previously untested plots.
†† Column values with same letter are NOT statistically different (ANOVA B-D, p = 0.05); values are ± one standard deviation.
††† PATH plot length was 3.75 m.

At the base of all plots, geotextile bags were aligned such that runoff was funneled into a shallow drainage trench. A V-shaped aluminum trough, inserted into the vertical trench wall, allowed event-based sampling. On nonroad plots, the trench face and triangular surface area immediately above the outlet were treated with a 5:1 mixture of water and Soil Sement™ (an acrylic vinyl acetate polymer from Midwest Industrial Supply, Inc., OH) to prevent sediment detachment on these nonplot areas. The ≈ 0.21-m^2 triangular area (in addition to plot areas above) contributed runoff, but not sediment. Rainfall was measured for 40 to 50 min with manual gauges placed on the plot borders. Energy flux density (J m^{-2} h^{-1}) of simulated rainfall was calculated as :

$$EFD = \frac{r}{V_{D_{50}}} \frac{mv^2}{2} \tag{3.1}$$

where r is event rainfall intensity (m h^{-1}) and V_{D50} is the volume (m^3) of the median-diameter (D_{50}) raindrop, determined by

$$V_{D_{50}} = \frac{4}{3}\pi \left(D_{50} \diagup 2 \right)^3 \tag{3.2}$$

In Eq. 3.1, m is the mass [kg] of the D_{50} drop, which is estimated as

$$m = (\rho_w - \rho_{air})\, V_{D_{50}} \tag{3.3}$$

where ρ_w and ρ_{air} are 1000 kg m^{-3} and 1.29 kg m^{-3}, respectively. Factor *v* in Eq. 3.1 is the fall velocity m s^{-1} of the D_{50} drop, determined by the equation from Best (1950):

$$v = V_{\max}\left(1 - e^{-\left(\frac{D_{50}}{b}\right)^{\beta}}\right) \tag{3.4}$$

with V_{max} = 9.5 (m s^{-1}), b = 1.77, and β = 1.147 (from Mualem and Assouline, 1986). Median drop size was estimated from nozzle manufacturer engineering data. Rainfall EFD is more informative than rainfall intensity because terminal velocity and drop size distributions from rainfall simulators differ from those of natural rainfall. Simulators with the same rainfall intensity, but different architectures, will have different EFDs.

3.3.5 Simulation data collection and calculations

Time to runoff (TTRO) was recorded during each event. Runoff samples were collected at TTRO, then again at 2.5, 5, or 10 min intervals. Most simulations were conducted for 60 min after TTRO; PATH simulations were conducted for only 45 min. Discharge was determined by measuring the time to fill of a 525 mL bottle. After settling, the supernatant was decanted and discharge samples were oven dried at 105°C for 24 h to determine mass of material transported. Sample discharge volumes were reduced to account for the presence of sediment. Values for instantaneous concentrations (C_t) were calculated as sediment mass per corrected discharge volume. Instantaneous discharge and sediment output values were adjusted to rates per unit area by dividing by filling time and plot area (plot areas for sediment and discharge calculations were different, see above). The rates were then divided by EFD values. Normalized instantaneous discharge (Q_t) and sediment output (S_t) therefore have units L J^{-1} and kg J^{-1}, respectively. Cumulative discharge (Q_{cum}) was calculated as total plot runoff volume prior to any time t, divided by EFD since TTRO. Calculated slightly differently, cumulative sediment (S_{cum}) output was total sediment mass at time t divided by EFD since the beginning of the simulation. Values were normalized differently because EFD prior to TTRO contributes differently to subprocesses controlling runoff generation and sediment transport: i.e. at the beginning of rainfall, sediment is detached by raindrop impact and material is transported downslope via rainsplash. In essence, energy prior to TTRO con-

tributes to the sediment supply that will be transported throughout the event after runoff commences. With discharge, rainfall is infiltrated, then ponded, before HOF generation. Only by contributing to surface sealing, which may speed up runoff generation, does energy prior to TTRO contribute to all-event discharge. Total normalized event discharge and sediment output are referred to as Q_{event} and S_{event}.

3.3.6 Measuring road discharge during natural events

To compare ROAD simulation data with discharge and sediment transport data from natural runoff events, a discharge collection station was constructed at the footslope of a 165-m road section near the watershed mouth (Figure 2.2). A trench was dug across the road to a depth and width of ≈ 0.5 x 0.75 m. Vertical trench walls were re-enforced with 4 mm steel. Depressions in the transitional area between the road surface and the reinforced walls were filled with concrete to prevent incision. The trench bottom was covered with corrugated aluminum roofing, which was shaped in a semi-circle and sloped (10%) to minimize sedimentation during events. The trench was covered by a perforated steel grate to accommodate traffic. A tipping bucket rain gauge (0.254-mm threshold) and datalogger were used to measure 1-min rainfall intensities at the site. A typical road cross-section was composed of ≈ 1.9 m of compacted track and 1.3 m of less compacted surface. This 3.2 m width represents the surface commonly traveled upon by vehicle (automobile and motorcycle), pedestrian, and animal traffic. Tracks were occasionally incised 5-15 cm. Nontrack surfaces often were often vegetated. Slopes for consecutive 20 m intervals starting at the trench were: 0.12, 0.23, 0.25, 0.18, 0.09, 0.07, 0.11, and 0.12 m m^{-1}. Discharge and sediment output values were measured similarly to those in the ROAD simulations. Values were divided by filling time, contributing area (3.2 m x 165 m), and event EFD, which was calculated using raindrop size data from Baruah (1973) and Eqs. 3.1-3.4.

3.3.7 Data analysis

Because simulation durations occasionally differed, most data were analyzed based on simulation times of 45 min. The lone HOED FIELD simulation producing runoff was conducted for only 25 min following TTRO. Because there was no replication, HOED was not included in statistical

analysis. Similarly, FALLOW FIELD was not included because none of the four replications produced runoff. All data were analyzed, after $\log_{10}$ transformation, using one-way analysis of variance (ANOVA), followed by post-hoc multiple comparison testing with the Bonferroni/Dunn test (B-D) when the F-values were significant at $p = 0.05$ (Gagnon et al., 1989). On compacted ROAD and PATH surfaces, ≈ 62% of the 250 PR values reached a maximum value of 6.7 MPa; rarely was the maximum reached on other surfaces. The distributions of road and path PR values were therefore truncated. Bounded data usually require special statistical treatment, but because ROAD and PATH data were substantially higher than those of the other surfaces, and the focus was not on differences between these two treatments, the use of ANOVA was justified. The nonparametric Spearman rank correlation coefficient (r_s) was used to evaluate the relationship between compaction indices (PR and ρ_b) and TTRO data.

3.4 RESULTS

3.4.1 Compaction indices

ROAD and PATH surfaces had statistically higher $\rho_{b(0\text{-}5\ cm)}$ and PR values, compared with the other surfaces ($p = 0.05$; Table 3.3). FIELD PATH, UPLAND FIELD, HOED FIELD, and FALLOW FIELD had surface ρ_b values statistically indistinguishable. ROAD and PATH surfaces had the highest PR values (means = 6.4 MPa); HOED FIELD and FALLOW FIELD were the least compacted surfaces by this measure (< 2.0 MPa). Compaction on roads and paths extended down to at least 15 cm, although subsurface values were not statistically different from those of the other surfaces (Table 3.3).

3.4.2 Instantaneous discharge and time to runoff

Figure 3.1 shows instantaneous discharge (Q_t) and other related runoff data for the simulation surfaces. Each data point is a mean of all simulations producing runoff. Each series begins at its mean time to runoff (TTRO). To indicate the proportion of rainfall transported from the plots as discharge, runoff coefficients (ROC = discharge volume/rainfall volume x 100%) based on mean rainfall data from all simulations are shown. Values below treatment identifiers represent rainfall depths falling on the plot before TTRO. Road surface runoff stands out, with mean TTRO occur-

Table 3.3 Mean values of compaction- and infiltration-related variables for six simulations.

Treatment	$\rho_{b(0 - 5\ cm)}$† (Mg m^{-3})	$\rho_{b(5 - 10\ cm)}$ (Mg m^{-3})	$\rho_{b(10 - 15\ cm)}$ (Mg m^{-3})	PR (MPa)	K_s (mm h^{-1})
ROAD	1.45 ± 0.13 (74) b	1.36 ± 0.11 (16) a	1.35 ± 0.10 (16) a	6.4 ± 0.4 (160) d	15 ± 9 (26) a
PATH	1.40 ± 0.11 (21) b	1.37 ± 0.09 (3) a	1.32 ± 0.14 (3) a	6.4 ± 0.7 (90) d	8 ± 5 (6) a
FIELD PATH	1.24 ± 0.11 (22) a	1.25 ± 0.16 (4) a	1.28 ± 0.12 (4) a	2.8 ± 1.1 (40) b	244 ± 88 (10) b
UPLAND FIELD	1.20 ± 0.09 (36) a	1.25 ± 0.15 (5) a	1.23 ± 0.13 (5) a	4.7 ± 1.4 (98) c	133 ± 77 (6) b
HOED FIELD	1.19 ± 0.06 (22) a	1.22 ± 0.03 (4) a	1.30 ± 0.07 (4) a	1.8 ± 1.2 (40) a	316 ± 129 (10)b
FALLOW FIELD	1.11 ± 0.05 (6) a	-	-	1.7 ± 0.9 (60) a	129 ± 38 (6) b

† ρ_b is bulk density at indicated depth; PR is penetration resistance, and K_s is saturated hydraulic conductivity; values are means ± one standard deviation; values in parentheses are sample sizes; values in each column with the same letter are NOT statistically different (ANOVA B-D, p = 0.05).

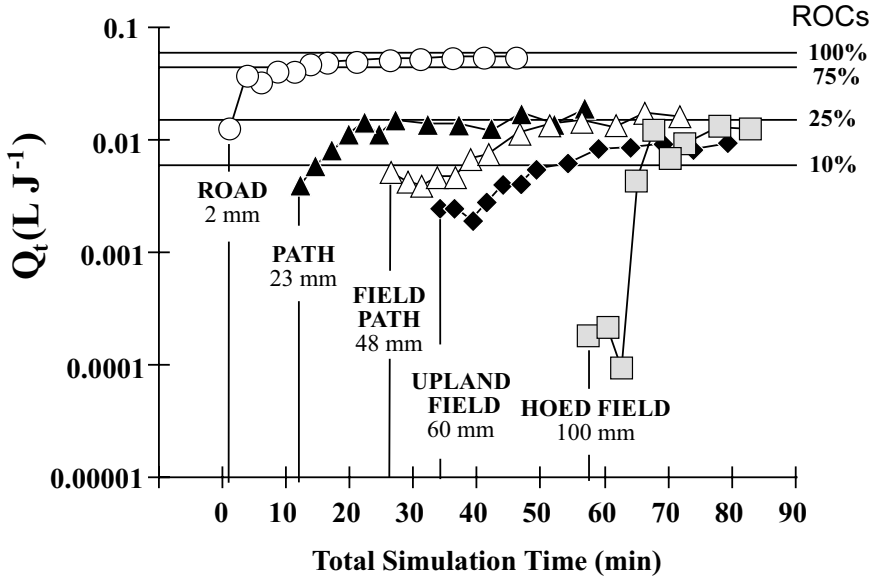

Figure 3.1. Normalized instantaneous discharge (Q_t) plotted since the beginning of rainfall simulation. Values are normalized by rainfall energy flux density (EFD) and plot area. Data series begin at mean time to runoff (TTRO). Values below surface identifiers refer to rainfall depths falling on the plot before TTRO. Runoff coefficients (ROCs) are based on rainfall intensity data for all simulations. HOED has no replication, as only one of four events produced runoff. FALLOW FIELD (not shown) did not produce runoff.

ring in ≈ 1 min. ROAD Q_t exceeded > 75% of rainfall after ≈ 15 min (total event ROC was > 80%). In marked contrast, FALLOW FIELD did not produce runoff after 60 min of simulated rainfall during four events; HOED FIELD produced runoff in only 1 of four events. TTRO for the lone HOED FIELD runoff event was ≈ 58 min, after ≈ 100 mm had fallen on the plot surface. TTRO was unique for all other surfaces, with runoff occurring first on PATH, then FIELD PATH, and finally UPLAND FIELD. Nonroad instantaneous ROC values were typically < 25%; FIELD PATH ROC was consistently < 15%.

3.4.3 Sediment output

Following preliminary analysis of sediment transport data, UPLAND FIELD (n = 4) and PATH (n = 3) treatments were combined into one group because their temporal responses were similar. Slope, antecedent soil moisture, rainfall intensity, and event EFD for the five remaining surface groups are summarized in Table 3.2. Table 3.4 lists mean values of TTRO, normalized total discharge, normalized total sediment output, and event sediment concentration for groups producing runoff. ROAD instantaneous sediment transport (S_t) values were often one order of magnitude higher than those of other surfaces (Figure 3.2). ROAD S_t was characterized by an output peak

Table 3.4. Mean runoff and sediment transport data for rainfall simulation experiments producing runoff.

Treatment	n	TTRO† (min)	Q_{TTRO} (mL J^{-1})	Event ROC (%)	S_{event} (g J^{-1})	C_{event} (kg m^{-3})
ROAD	8	1.1 ± 0.3a††	48 ± 1c	80 ± 6 c	1.23 ± 0.54 c	23 ± 10 b
HOED FIELD	1	57.8 -	7 -	5-	0.11 -	50 -
UPLAND FIELD/PATH	7	20.3 ± 8.5 b	13 ± 3 b	14 ± 5 b	0.05 ± 0.02 a	5 ± 2 a
FIELD PATH	4	34.1 ± 12.8 b	6 ± 2 a	6 ± 3 a	0.14 ± 0.09 b	35 ± 14 b

† TTRO is time to runoff; Q_{TTRO} is total discharge normalized by rainfall energy flux density (EFD) since runoff initiation; S_{event} is total sediment output normalized by EFD since beginning of simulated rainfall; C_{event} is total event concentration calculated from original data.

†† Values in a column with the same letter are NOT statistically different (ANOVA B-D, p = 0 .05); dash denotes treatment was not included in statistical analysis because n = 1; values are means ± one standard deviation.

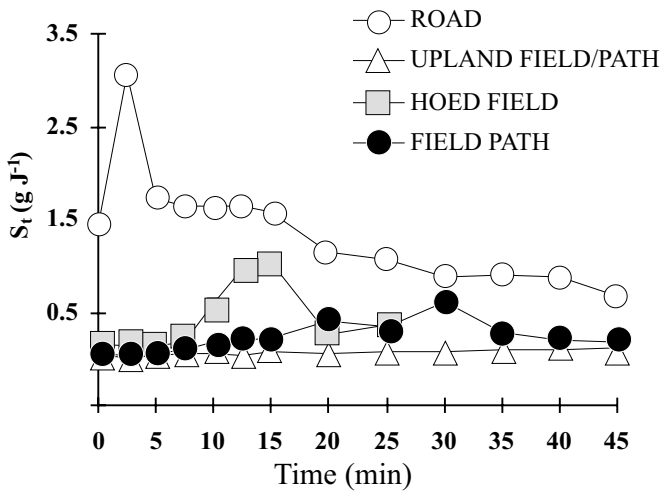

Figure 3.2. Instantaneous sediment output (S_t). FALLOW FIELD (not shown) produced no runoff.

within the first few min after TTRO, followed by a gradual decline throughout the remainder of the simulation. The response peak is related to flushing of easily transported, loose surface material. Normalized event sediment output was likewise an order of magnitude higher on the ROAD treatment (Table 3.4). Sediment transport for the other surfaces was initially very low following TTRO, with UPLAND FIELD/PATH values remaining relatively low for the entire simulation (Figure 3.2). HOED FIELD and FIELD PATH surfaces, however, experienced small output peaks, suggesting that detached material was available for transport on these recently worked surfaces once surface runoff reached sufficient depth and shear stress. Irregular discharge during the HOED FIELD experiment resulted from (1) windy conditions, which limited rainfall input to the plot surface and (2) a very rough surface, on which creation and destruction of flow-blocking microdams occurred. Low UPLAND FIELD/PATH S_t values are related to limited loose sediment on these surfaces and to high shear strength of the surface crust existing on the rice field.

3.4.4 Sediment concentration

In general, ROAD produced relatively high sediment output from relatively large runoff volumes (Figure 3.3a). ROAD instantaneous sediment concentrations (C_t) were initially ≈100 g L^{-1}, but

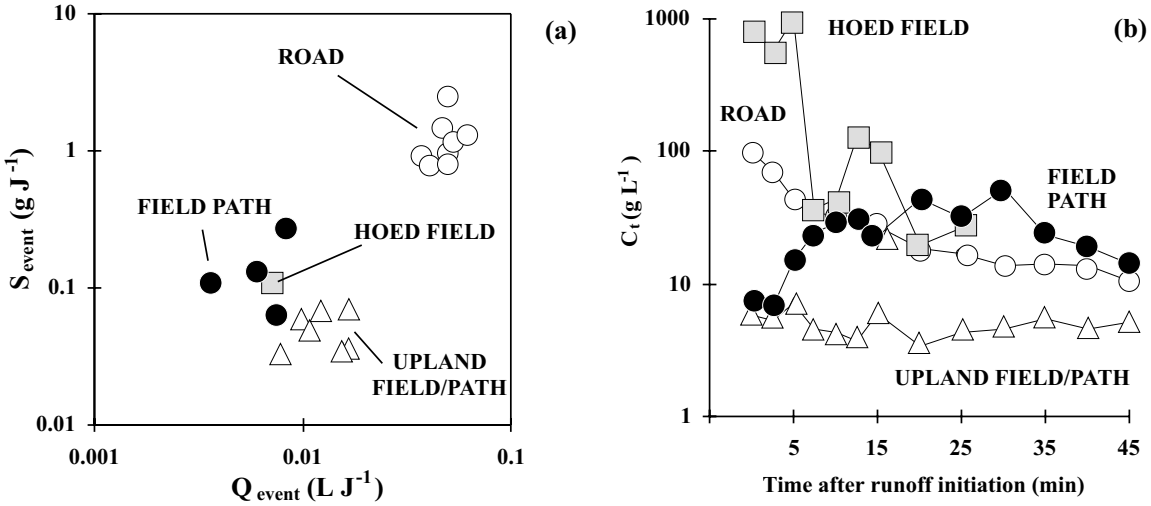

Figure 3.3. (a) Normalized event sediment output (S_{event}) versus normalized event discharge (Q_{event}). Sediment values were normalized by rainfall energy flux density (EFD) since the beginning of the simulation; discharge values were normalized by the energy since runoff initiation. (b) Instantaneous sediment concentration (C_t).

fell rapidly over time as loose material was flushed from the surface (Figure 3.3b). In comparison, the other surfaces produced less total sediment from smaller volumes of runoff (Figure 3.3a). Owing to very low discharge, HOED FIELD and FIELD PATH C_t values were at times the highest of all events; and total event concentrations for these surfaces were greater than those of ROAD (Table 3.4). However, total sediment output from these surfaces was minimal. Although more study is clearly needed to understand sediment transport on these surfaces, high C_t values are realistic, as hoeing detached a generous supply of loose material. Sediment concentration on the UPLAND FIELD/PATH treatments were the lowest of all treatments, again owing to surface resilience on the upland field.

3.5 DISCUSSION

3.5.1 Influence of compaction on K_s and runoff generation

Highly compacted surfaces, such as roads and paths, often have low infiltration rates because soil aggregates have been destroyed by compaction and the surface layer may be sealed by fine mate-

rial. Significant negative correlation existed between K_s and the two compaction indices, $\rho_{b(0\text{-}5cm)}$ and PR: r_s = -0.668 ($P < 0.0001$) and- 0.821 ($P < 0.0001$), respectively. Penetration resistance was sensitive to thin surface crusts not detectable with the 5-cm ρ_b core. With respect to runoff generation, TTRO showed strong negative correlation with ρ_b and PR: r_s = -0.766 ($P = 0.0008$) and r_s = -0.753 ($P = 0.001$), respectively. TTRO could be well predicted using step-wise regression from $\rho_{b(0\text{-}5cm)}$ and PR data: $R^2 = 0.822$ ($P < 0.0001$). Correlation between compaction indices and infiltration-related phenomena suggest easily obtained ρ_b and PR data can be used to extrapolate K_s and TTRO data sets, when sufficient experimentation is prohibited by time restraints or physically unfavorable conditions (e.g., steep slopes). The above correlations may change under wetter experimental conditions, because PR and TTRO are dependent on soil moisture.

Comparing HOED FIELD and FIELD PATH compaction and TTRO data is informative because the path treatment was created on the hoed surface. One research hypothesis was that compaction from walking would enhance HOF generation on the FIELD PATH surface. The small number of passes during dry antecedent moisture conditions increased $\rho_{b(0\text{-}5cm)}$ by < 5%, but significantly increased PR from 1.8 to 2.8 MPa (Table 3.3). Additionally, K_s was reduced by 23% as foot traffic destroyed most large aggregates and clods. Using the bulk density methodology, the shallow compaction on the hoed surface could not be detected, but the resulting thin mechanical crust was detectable using the penetrometer and disk permeameter. In terms of runoff generation, the foot traffic increased runoff generation: TTRO occurred after ≈ 34 min of rainfall during all four FIELD PATH events, compared with no runoff generation after 90+ min on three of the four HOED FIELD simulation experiments.

3.5.2 Erosion on path complexes

Juxtaposition of compacted footpaths with more-erodible planting surfaces could result in substantial surface erosion if sufficient HOF is generated on the path surfaces. TTRO data in Figure 3.1 support enhanced runoff generation on the path surfaces: i.e., PATH < UPLAND FIELD and FIELD PATH < HOED FIELD. Again, the compacted surface of PATH and FIELD PATH comprised < 20% of the simulation surface; the remaining surface was similar to UPLAND FIELD and HOED FIELD, respectively. The intention of including both path and nonpath surfaces in

simulation plots was to investigate the interaction of path-generated HOF with the erodible agricultural surface. For the two path treatments, runoff was initiated on the path portion of the simulation plot, and occurred on most of the PATH plot by the end of simulation. The nonpath portion of FIELD PATH did not contribute noticeably to runoff. Had path surfaces comprised the entire plot, TTRO would certainly have decreased and runoff would have increased for both treatments, as K_s on the compacted portion of the plots was lower than that of the field portion by 80-120 mm h^{-1} (Table 3.3).

Sediment transport was not substantial for either path treatment (Table 3.4, Figure 3.2), because (1) little HOF was generated on FIELD PATH (ROC < 15%), and (2) the nonpath surface of PATH had high strength (PR = 4.7 MPa), thereby resisting detachment/entrainment by rainsplash and path-generated HOF. Concentration data (Figure 3.3) support the potential for high sediment transport on complexes resembling FIELD PATH if sufficient HOF is generated. For example, FIELD PATH C_t values were the highest of all treatments ≈ 20 min after TTRO (Figure 3.3b), and relatively high S_{event} was generated from low discharge volumes (Figure 3.3a). Some sediment output was nonpath material entrained by on-path flow. Although walking impact enhanced runoff generation, it did not increase surface shear strength enough to resist hydraulic erosion. The path surface was susceptible to micro-rill incision and headward expansion as knick points migrated upslope (cf. flume studies of Bryan and Poesen, 1989; Merz and Bryan, 1993). Decreases in sediment output after ≈ 30 min runoff may be related to armoring. The hydrological behavior of the artificial NEW PATH surface may not represent compacted field paths that evolve over the course of a growing season. These older paths have ρ_b, PR, and K_s values more similar to those of the PATH, as opposed to NEW PATH. Thus, runoff generation may be better represented by the PATH treatment. If this is the case, and sediment output is similar to FIELD PATH, the potential for significant sediment transport exists.

3.5.3 Surface preparation and sediment transport

PKEW road surfaces have high sediment production rates in part because relatively high discharge volumes flush readily available, loose surface sediment. Discharge is high because road surfaces are highly compacted, thus infiltrability is low and a large percentage of rainfall becomes runoff

(Ziegler and Giambelluca, 1997a). Loose sediment is made available by surface preparation processes occurring between and during storms (Bryan, 1996). Surface preparation is any process that influences the availability, erodibility/detachability, or transport of surface material. For example, vehicle traffic is a principal mechanism responsible for detaching sediment during both dry and wet periods. Additionally, some sediment entrained during runoff events is redistributed on the road surface, and is available for transport during the next overland flow event. Although nonroad surfaces also undergo various surface preparation processes, surface runoff on these surfaces is more rare. Furthermore, vehicle detachment on roads is a daily phenomena; preparation processes on other lands occur less frequently. For example, weeding on agricultural lands, which breaks up crusted/compacted surfaces, may occur only a few times during the rainy period. Hoeing may occur only once annually.

Under dry antecedent soil moisture conditions, substantial sediment transport from PKEW agricultural surfaces will require significant rainfall depth (either as one large event, or as a series of showers that shorten TTRO by increasing soil moisture content) to generate significant HOF. Much less rainfall energy is required to generate runoff and remove loose surface materi-

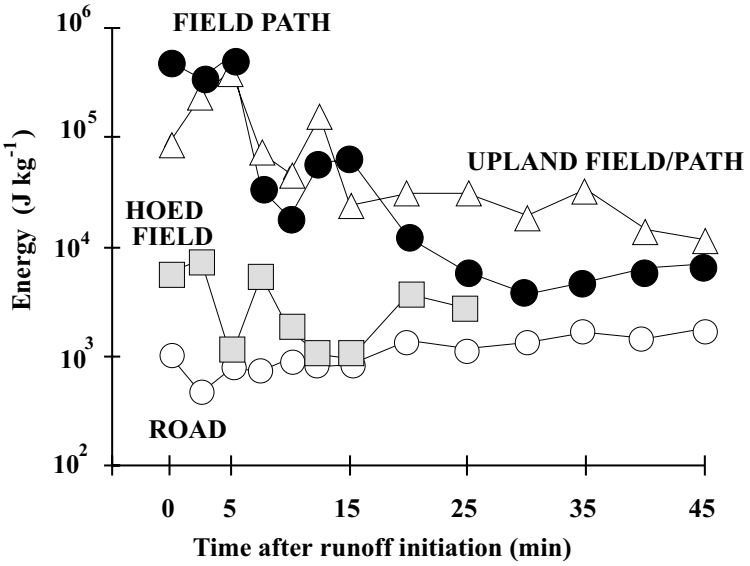

Figure 3.4. Energy required to remove 1 kg of sediment from the simulation plots.

al from roads. Figure 3.4 shows instantaneous rainfall energy needed to remove 1 kg of sediment from the small-scale simulation plots (Sutherland et al., 1996). ROAD has the lowest values, with agricultural surfaces typically having higher values. If rainfall prior to TTRO were included in this calculation, nonroad values would substantially increase, particularly those for the one HOED event that required ≈ 60 min of rainfall (EFD ≈ 1700 J m^{-2} h^{-1}) to produce runoff. At hillslope scales where roads channel runoff along the surface for substantial distances, sediment transport can be enhanced by high shear stresses that transport large aggregates and gravel not entrained by lower magnitude flows, such as those in the plot studies above. Furthermore, during high magnitude storm events, overland flow on long slopes can incise the compact road surface, especially in sections where ruts have already been formed.

3.5.4 Representativeness of the ROAD simulation data

One research goal was to use rainfall simulation data to assign parameters in KINEROS2 (Smith et al., 1995), a physically based model that will be used to describe road runoff and erosion processes (Chapter 6). Simulation data, obtained at a small scale, must therefore be representative of larger-scale natural phenomena, when normalized similarly. To assess the degree of similitude, ROAD Q_t and C_t were compared with data collected at the road discharge collection station during several natural rainstorms. This comparison is shown in Figure 3.5 for the rainstorm that most closely resembled the simulated events, both in intensity and duration (referred to hereafter as STORM). Rainfall intensities (Figure 3.5c) are plotted with respect to individual TTRO values (time 0). Simulated rainfall begins ≈1 min before TTRO. During the natural event, rainfall was first recorded 24 min before TTRO, with surface saturation, ponding, and interplot HOF also occurring well before runoff initiation. STORM rainfall intensity was highly variable compared with near-constant simulated rainfall intensity. During the high-energy portion of STORM (0-30 min), mean rainfall intensity (89 mm h^{-1}) was only slightly lower than the simulation rate of ≈ 105 mm h^{-1}. However, EFD was substantially higher for STORM (≈ 2640 vs. 1775 J m^{-2} h^{-1}), owing to median raindrop size being ≈ 50% larger than that of simulated rainfall.

Normalized ROAD and STORM Q_t were comparable during the first 30 min following TTRO when the natural rainfall rates were highest. Although falling limbs of the discharge hydro-

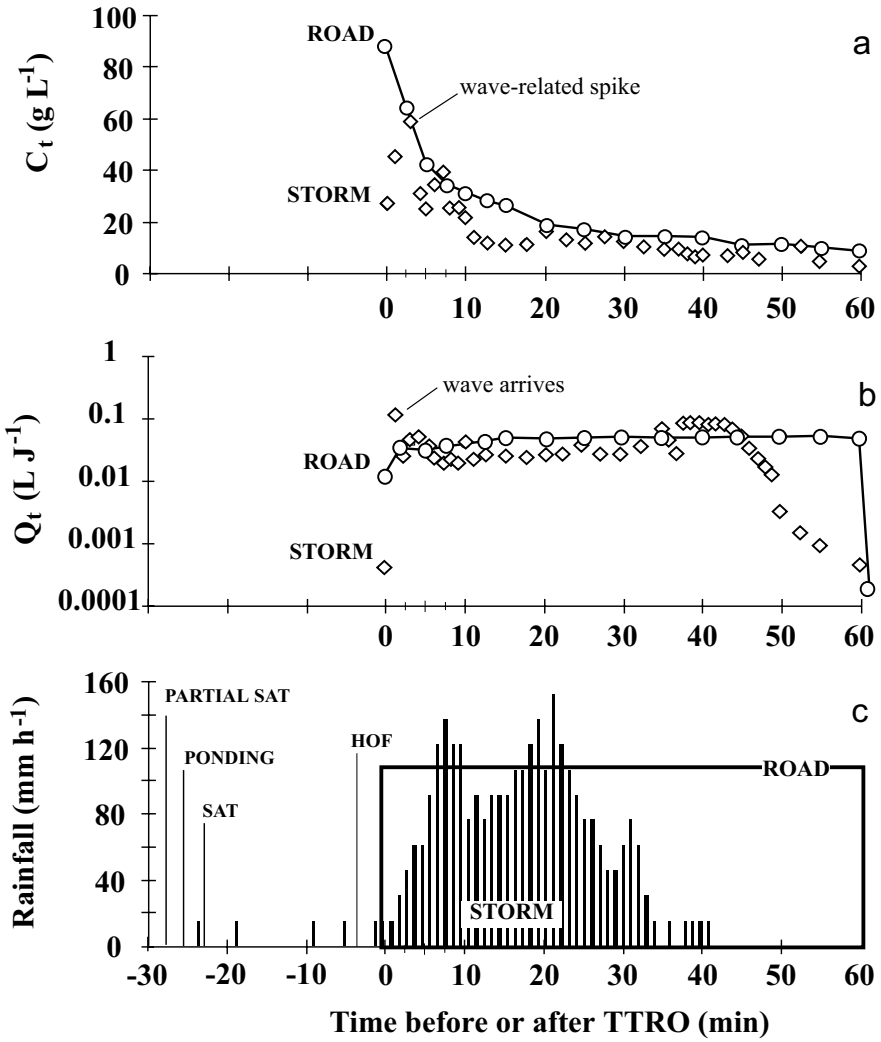

Figure 3.5. Comparison between simulated (ROAD) and natural event (STORM) (a) sediment concentration (C_t); (b) instantaneous discharge (Q_t); and (c) rainfall intensities. Discharge and sediment-related output data are plotted relative to their individual time to runoff (TTRO). Data from the simulation and natural event are normalized similarly. Partial saturation (PARTIAL SAT), ponding, saturation (SAT), and interplot Horton overland flow (HOF) correspond to the natural event.

graphs appear different, they are comparable when differences in plot lengths are considered. After rainfall was discontinued, ROAD plots typically drained in ≈ 0.75 min, time equivalent to ≈ 29 min when scaled to the 165-m monitored road section. The STORM falling limb ended after 24 min. One critical difference between the two data sets is that at the base of the road section, a 'wave' of runoff water arrived from upslope ≈ 1 min after TTRO (Figure 3.5b). This phenomena

was not detectable during small-scale ROAD simulations. The STORM C_t spike shortly thereafter (Figure 3.5c) was associated with the discharge wave, which brought both loose material from upslope and the energy needed to entrain sediment near the plot outlet. Prior to the concentration spike, ROAD C_t was much higher than STORM C_t. Afterwards, ROAD C_t was only slightly higher. Sediment transport decreased at both scales over time, as the supply of easily removed surface material became depleted. Post-event observations on the road section indicate a secondary mechanism contributing to the output decline may have been armoring, as sediment became oriented in crevices of road ruts.

ROAD C_t was higher than that of STORM despite raindrop impact energy and hydraulic energy being greater for the hillslope-scale natural event than for the simulation experiments. ROAD values were higher predominantly because simulations were performed in the dry season when ample loose material had collected on the road surface since the last HOF event several weeks prior. STORM was one of a series of wet-season rainshowers that continually depleted surface sediment created by traffic between events. Initial ROAD C_t values (≈ first 5 min) may be uncharacteristically high to represent wet season phenomena in general. However, they may be typical of concentrations achieved after long dry periods with frequent traffic or at the beginning of the rainy season before the dry season sediment accumulation is removed.

Comparing ROAD results with other field studies provides another opportunity to assess data integrity. The high initial C_t values are similar to those measured following truck passes in a 40-m^2 simulation plot in New Zealand (30 min, 32-38 mm h^{-1} events) (Coker et al., 1993). When compared with event concentration (C_{event}) and discharge (Q_{event}) data determined from culvert runoff during natural events for 10 road segments in Washington, USA (Reid and Dunne, 1984), ROAD data (unshaded circles in Figure 3.6) correspond most closely to roads undergoing heavy usage. Because PKEW roads are lightly used, these comparisons suggest that ROAD C_t values are high. However, ROAD values were similar to those of 30 min, 50 mm h^{-1} simulation experiments on ≈ 60 m^2 plots in two western states of the USA (Elliot et al., 1995); the ellipse in Figure 3.6 encompasses 24 data points that were generated from simulations at eight different sites, varying in soil type, during each of dry, wet, and very wet soil conditions. In addition, ROAD simulation values are only slightly higher than those recorded during seven storms on the monitored

PKEW road section in August 1998 (solid squares in Figure 3.6). General agreement between simulation and natural event data supports good similitude of the ROAD simulation data for natural phenomena in PKEW, but reveals limitations of comparing data at different scales. In addition, similar storm events on physically similar road sections could result in substantially different sediment output data if two sites differ in variables affecting erodibility (texture, clay mineralogy, shear strength, organic material, rock content) and/or availability of loose, entrainable material (as affected by age since construction, usage, maintenance activities, and mass wasting processes). High values from this study, compared with the Reid and Dunne findings on similar slopes, may relate to differences in soil erodibility, although one would surmise that soil originat-

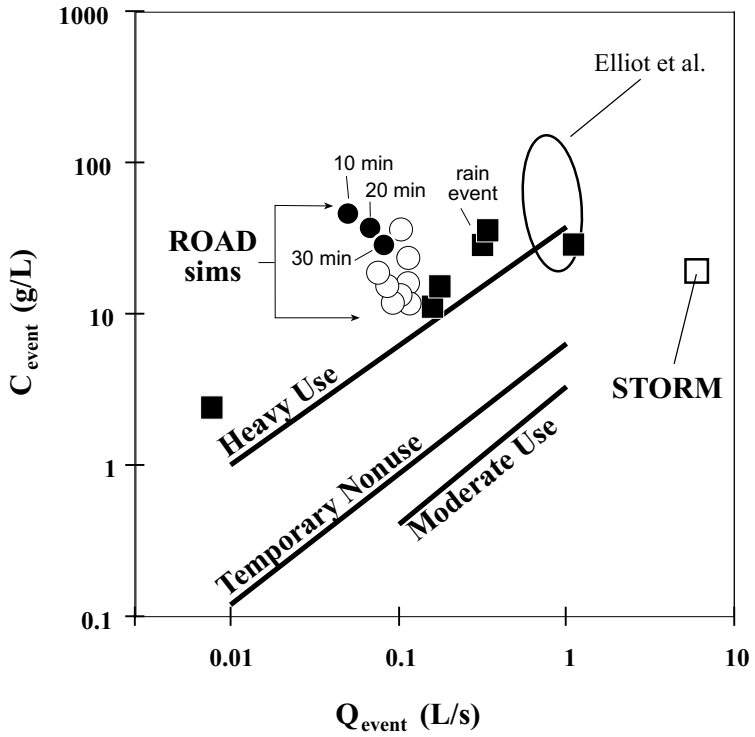

Figure 3.6. Total 'event' sediment concentration (C_{event}) plotted against total 'event' discharge (Q_{event}) for the ROAD simulations (unshaded circles) and the natural events (squares). Open square is STORM data from Figure 3.5. Mean values occurring at time = 10, 20, and 30 min during ROAD simulations are represented by filled circles. The labeled lines are fitted values determined on varying length roads during natural events in Washington state, for different levels of traffic (from Reid and Dunne, 1984). The ellipse surrounds 24 values determined in the simulation study of Elliot et al. (1995).

ing from the siltstone, sandstone, and graywackes bedrock material of the Washington study would be more erodible than the granitic-derived soil in PKEW.

Finally, the STORM value in Figure 3.6 does not continue the general trend of C_{event} increasing with Q_{event}, as suggested by the Reid and Dunne data and the lower-volume PKEW rainstorm events. PKEW road surfaces are composed of an erodible surface layer (loose material of limited supply) and a less-erodible underlying layer (compacted road surface). After some critical discharge volume has removed the loose material, sediment production diminishes because the underlying surface is resistant to detachment/entrainment.

3.6 CONCLUSION

Rainfall simulation was useful in ascertaining unique differences in runoff generation and sediment transport processes for roads, footpaths, and agricultural lands. Roads, having very low saturated hydraulic conductivities, generated runoff quickly (≈ 1 min) during high intensity events and produced event runoff coefficients > 80%. Agriculture-related land surfaces often required very large rainfall depths to produce overland flow when soils were initially dry. The dry season simulations may understate the importance of agricultural fields to a basin sediment budget, as erosion-producing HOF should occur more frequently under wetter soil conditions. Footpaths, like roads, increase the frequency of runoff, demonstrating their potential to enhance surface erosion by acting as source areas for surface runoff on agricultural lands where HOF is otherwise rare.

High road discharge volumes flushed loose sediment that had accumulated on the surface between or during rainfall events. Sediment transport on PKEW roads is initially high, then steadily declines over time as loose surface sediment becomes depleted. Sediment output is sensitive to processes altering the supply of loose surface material, and may be more affected by these processes than by the erodibility of the underlying compacted road surface. If large quantities of surface material are present, such as might occur before the first large wet-season storm, or following any extended dry period, sediment production can be substantial. When compared with discharge and sediment transport on a 165-m road section during natural events, simulation concentration data from this study were slightly higher. Some caution is therefore needed when using these results to validate a physically based erosion model (Experiment IV, Chapter 6).

4. EXPERIMENT II: Partitioning total erosion on unpaved roads into splash and hydraulic components: interstorm surface preparation and dynamic erodibility

4.1 ABSTRACT

Field rainfall simulation experiments at two sites are used to partition sediment transport on unpaved roads into splash and hydraulic erosion components. Rainsplash processes contributed 38 to 45% of total sediment output, with instantaneous contributions being variable throughout 60-min high-energy events. For low- and medium-magnitude rainstorms, splash erosion on roads is initially controlled by the removal of easily erodible material, followed by a dramatic reduction in sediment output associated with limited detachment from the resistant, highly compacted road surface. A conceptual model explaining temporal variations in splash and hydraulic erosion as functions of pre-storm surface preparation (via traffic, maintenance, mass wasting processes) is presented. For situations where loose sediment is readily available, rainsplash energy is less important to sediment detachment. If the loose layer is diminished (e.g., following an overland flow event) or protected by a surface crust, splash energy is needed to detach material from the road surface. Equations in most physically based erosion models do not predict temporal variations in road sediment transport that result from the removal of a loose surface layer of finite depth. A strategy that successfully treats this removal as changes in road erodibility is introduced.

4.2 OBJECTIVE

The objective of the study was to (1) provide a physical basis for parameterizing erosion equations for model sediment transport on unpaved roads; (2) identify temporal variations in erosion subprocesses and the underlying mechanisms causing variations; and (3) assess the ability of model equations to describe splash and hydraulic erosion processes on roads. This information is important for parameterizing the physically based model to be tested in Experiment IV, Chapter 6.

4.3 METHODS AND MATERIALS

4.3.1 Research Sites

Rainfall simulation was performed on two roads, one in Thailand, the other in Hawaii, USA. The Thailand site was in the Pang Khum Experimental Watershed (PKEW, Figure 2.2, described in

Chapter 2). The test road section is a relatively new detour bypassing a steep hillslope. Maximum slope was about 0.20 m m^{-1}. Ruts created from vehicle wheels incise the surface to depths of 0.10 to 0.15 m. Lowering from compaction and erosion processes is 0.1 m y^{-1}. Daily traffic includes approximately 4 motorcycle, 2 truck passes, and an occasional passing water buffalo. The Hawaiian study site is located at the base of the Waianae mountain range on Schofield Barracks (US Army) in central-west Oahu Island, Hawaii. Rainfall is seasonal, with about 75% of the annual 1000-1100 mm occurring from October to April. Unlike the Thailand site, there is typically no prolonged period without rainfall events large enough to generate surface runoff. Road surface material is a composite of Kolekole Oxisol, Helemano Inceptisol, weathered oxidic ash, and exposed regolith/bedrock (Soil Conservation Service, 1981). Slope on experiment road varies from about 0.05 to 0.35 m m^{-1}. The simulations were performed on an 80-m road section, for which the road surface lies 1-4 m below the adjacent roadside margin. Enhanced surface lowering results predominately from erosional and maintenance activities. Visible tracks and ruts are present on the road surface; however, traffic is now infrequent, as the section has been closed since slope failure below the experimental site in early 1997.

4.3.2 Rainfall Simulation Experiments

In August 1997, six rainfall simulation experiments were performed at the Hawaii site. Eight simulations were performed in PKEW in February, 1998. Each simulation run was a true replication, usually performed 6-10 m above the previous simulation plot. The simulator used at both sites consisted of two vertical, 4.3 m risers, each directing one 60° axial full cone nozzle (70 mm orifice diameter) toward the surface. The operating pressure of 172 kPa (25 psi) produced rainfall energy flux densities (EFD) of 1700-1900 J m^{-2} h^{-1} (100-115 mm h^{-1}), approximating energy sustained for 10-20 min during the largest annual PKEW storms (based on preliminary analysis of 2 years of rainfall data). Cylindrical, sand-filled, geotextile bags (3.0 x 0.2 x 0.1 m) were arranged to form two side-by-side rectangular subplots. For each simulation, one subplot was designated as a rainsplash treatment (referred to herein as SPLASH); the other was covered with 2-mm wire screen suspended 0.1 m above the road surface to retard raindrop energy (NO SPLASH). The design is similar to Hudson's (1957) mosquito gauze treatments of experiment no. 3 in Rhodesia. Sediment output from the NO SPLASH treatment is assumed to result entirely from hydraulic ero-

sion processes; and the difference between SPLASH (rainsplash + hydraulic erosion) and NO SPLASH (only hydraulic erosion) treatments represents the sediment contributed by rainsplash, i.e., detachment and rain-affected flow. Subplot dimensions for Schofield simulations were 3.50 (L) x 0.75 (W) m; the Thailand plots were slightly larger, 3.75 (L) x 0.85 (W) m. At the base of each sub-plot, geotextile bags were arranged to funnel runoff into a shallow drainage trench dug into the road surface. A V-shaped trough constructed from aluminum flashing was inserted into the vertical wall of the trench to allow event-based sampling. The face of the drainage trench and the triangular area below the main plot were treated with a 5:1 mixture of water and Soil Sement™ (an acrylic vinyl acetate polymer from Midwest Industrial Supply, Inc., OH) to prevent sediment detachment on these nonplot areas. The sealed triangular area (an additional plot length of 0.5 m) contributed only runoff to the plot output; and discharge values were corrected accordingly. Rainfall was measured during each event with 12 manual gauges placed on the plot borders. Table 4.1 shows physical properties associated with the road surfaces at the two sites. Mean values of plot slope, antecedent mass soil wetness, and simulation rainfall intensity are shown in Table 4.2.

Instantaneous discharge (Q_t), sediment output (S_t), and concentration (C_t) values were measured at time to runoff (TTRO) and then at 2.5 or 5 min intervals. Discharge volume was reduced to account for presence of sediment in the samples. Values of Q_t and S_t were adjusted to rates per unit area by dividing by filling time and plot area. The runoff coefficient (ROC) was cal-

Table 4.1. Physical properties of the unpaved road surface at the Thailand and Hawaii research sites

Descriptor/Property†	Units	Hawaii	Thailand	Tied P-value
$\rho_{b\ (0\ to\ 5\ cm)}$	Mg m^{-3}	1.32 ± 0.02††	1.42 ± 0.02	0.0008 (36, 48)
$\rho_{b\ (5\ to\ 10\ cm)}$	Mg m^{-3}	1.09 ± 0.06	1.36 ± 0.03	0.0004 (7, 16)
$\rho_{b\ (10\ to\ 15\ cm)}$	Mg m^{-3}	1.05 ± 0.05	1.36 ± 0.03	0.0004 (7, 16)
PR	MPa	5.8 ± 0.1	6. 4 ± 0.0	< 0.0001 (61, 160)
K_s	mm h^{-1}	28.4 ± 4.5	13.6 ± 2.1	0.0051 (12, 12)

†ρ_b is bulk density; PR is penetration resistance; K_s is saturated hydraulic conductivity. Tied P-values are the results of statistical testing with the nonparametric Mann-Whitney U test; values in parentheses indicate the sample number for Hawaii and Thailand, respectively; values < 0.05 reflect significant differences between Hawaii and Thailand sites

††Mean values ± one standard error.

Table 4.2. Median values for runoff-related and sediment transport-related data for the Hawaii and Thailand simulations.

	Slope (mm^{-1})	w† ($g\ g^{-1}$)	r ($mm\ h^{-1}$)	TTRO (min)	ROC (%)	f ($mm\ h^{-1}$)	S_{event} ($g\ m^{-2}$)	C_{event} ($kg\ m^{-3}$)
Thailand (n = 8)								
SPLASH	0.15 ab††	0.12 a	105 a	1.1 a	84 b	6.2 a	19.0 b	19.3 b
NO SPLASH	0.15 b	0.12 a	111 ab	1.5 ab	75 b	17.7 b	11.5 ab	13.3 ab
Hawaii (n = 6)								
SPLASH	0.13 ab	0.21 b	113 ab	1.5 ab	75 b	17.6 b	19.7 b	21.3 b
NO SPLASH	0.12 a	0.21b	129 a	2.4 b	62 a	36.6 c	8.4 a	10.3 a

† w is antecedent soil mass wetness, r is rainfall rate, TTRO is time to runoff, ROC is the total event runoff coefficient, f is steady-state infiltration rate, S_{event} is event sediment output, and C_{total} is total event concentration.

††Values in each column with the same letters are NOT statistically different at $\alpha = 0.05$, ANOVA followed by Bonferroni/Dunn post hoc testing on $\log_{10}$-transformed data.

culated at each sampling time as discharge rate / rainfall rate * 100%. Final event steady-state infiltration rate (f) was estimated as the difference in rainfall rate and discharge rate over the last 30 min of each simulation. This approximation assumes surface storage depressions are full; and thus the differences in rainfall and discharge rates are due to infiltration.

4.4. RESULTS

4.4.1 Runoff data

Table 4.2 contains mean runoff and sediment transport data for the Hawaii and Thailand simulations. At both sites, SPLASH treatments produce runoff sooner and have higher ROCs (i.e., greater discharge) than the NO SPLASH treatments. Final steady-state infiltration values are lower for SPLASH than for NO SPLASH treatments. These data collectively show that, even on highly compacted road surfaces, raindrop impact enhances runoff generation in a manner similar to that often occurring on cultivated soils (Flanagan et al., 1988; Römkens et al., 1990; Gimenez et al., 1992). In this respect, the main effect of rainsplash is to produce sealing of the surface by redistributing already-detached material, rather than causing aggregate breakdown.

4.4.2 Sediment output data

Total sediment transport (S_{event}) and sediment concentration (C_{event}) at both sites is higher for the SPLASH treatments than the NO SPLASH (Table 4.2). SPLASH sediment output is characterized by an initial flush of material, followed by a sharp decline, and then a stabilization in output toward the end of the 60-min simulations (Figure 4.1). NO SPLASH output is typically less than SPLASH; and in the Hawaii experiment output fluctuations are damped. In Figure 4.2 (c,d) total erosion (e_T) is partitioned into splash (e_s) and hydraulic erosion (e_h) components. Panels a and b show percent contributions of e_s and e_h to total erosion. At the Thailand site, e_h dominates e_T at the beginning of the simulation, but is only slightly greater than e_s after 60 min. In contrast, e_s at the Hawaii site is greater than hydraulic erosion for the first 20 min, after which e_h predominates. Total splash contribution to e_T at the Thailand and Hawaii sites is 37 and 48%, respectively. In comparison, Ulman and Lopes (1995) reported the e_s contribution to e_T to range from 44 to 60% for sites in Idaho and Colorado.

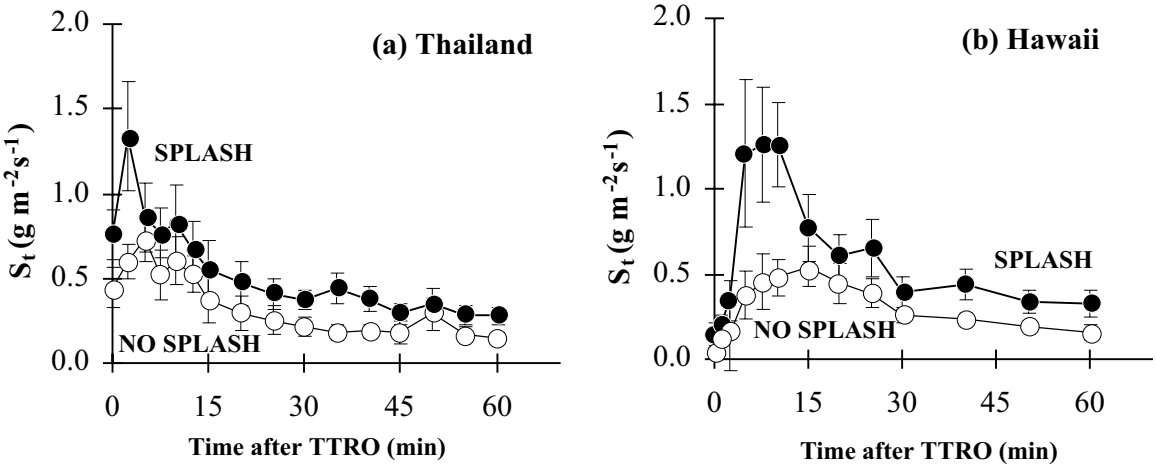

Figure 4.1. Temporal variation in mean sediment output for SPLASH and NO SPLASH treatments on (a) Thailand (n = 8) and (b) Hawaii (n = 6) unpaved road sites. Error bars represent ± one standard error; TTRO represents time to runoff. Under the assumptions of the investigation, NO SPLASH values result from hydraulic erosion processes and SPLASH values combine splash and hydraulic erosion processes.

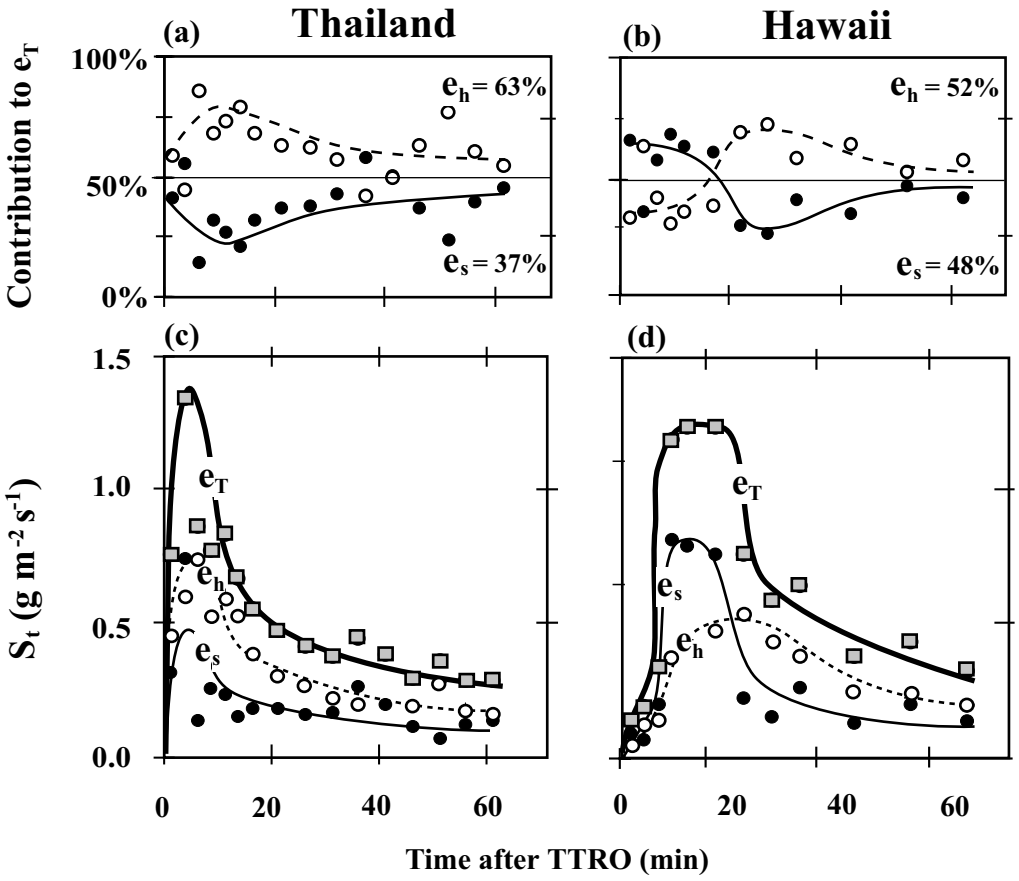

Figure 4.2. Time dependent sediment contributions (%) of splash (e_s) and hydraulic (e_h) erosion components to total sediment output (e_T) for (a) Thailand and (b) Hawaii experimental sites; and temporal variations of e_s, e_h, and e_T during 60 min of simulation for (c) Thailand and (d) Hawaii sites.

4.5 DISCUSSION

4.5.1 Role of surface preparation in road erosion

Surface preparation results from pre-storm events or processes that affect availability or transportability of sediment during storm events (cf., Bryan). Sediment detachment by vehicular traffic, maintenance activities, mass wasting events, and sediment deposition/removal during prior storms are important preparation processes affecting sediment availability. Temporal and spatial

variations in road sediment transport are related to pre-storm surface preparation, except, possibly, for high-magnitude events. For example, the early output peak during the Thailand dry-season simulations results from the flushing of loose, easily entrained material, which was generated on the road surface by vehicle detachment since the last overland flow event several weeks before (Figure 4.2c). The energy of flowing water was sufficient to entrain this material, as evidenced by the early importance of e_h to e_T. After the loose material was removed, however, splash energy was needed to entrain material from interrill areas adjacent to well-defined flowpaths into the rill system. By simulation's end, both hydraulic and splash subprocesses were greatly contributing to net erosion. Had less loose material been available at the beginning, e_T would likely have been more equally partitioned between e_s and e_h throughout the simulation. Time since the last overland flow event dictates the initial relationship between e_s and e_h. In general, holding traffic and maintenance constant, the longer the period between storms, the greater the opportunity for surface preparation to occur, and the greater the initial role of e_h in sediment transport.

Similarity in total sediment output (S_{event}, Table 4.2) at the Thailand and Hawaii sites suggest that the dissimilar e_s and e_h responses result largely from site-specific differences in surface preparation, as opposed to differences in soil erodibility. Because of differences in usage and rainfall seasonality, the abandoned Hawaii road had received less cumulative surface disruption than had the active Thailand road. Again, while the Thailand simulations were performed during a lengthy dry period, the Hawaii experiments were performed only two weeks after the last overland flow event. Prior to simulation, the Hawaii road surface contained a mechanical crust; and little loose surface material was present. During simulation, limited material could be entrained by surface flow alone. Rainsplash energy was important during the early simulation phase because it disrupted the crust and detached material. Had pre-storm traffic been greater, more loose material would have been present, and sediment transport would likely have resembled that on the Thailand road. At simulation's end, e_h was only slightly higher than e_s, as it was in the Thailand experiment. These data indicate that the fundamental differences in sediment transport response between the two sites resulted from availability of loose material, which was controlled by differences in cumulative surface preparation since the last overland flow event.

4.5.2 Dynamic erodibility and implications for modeling road erosion

Erosion model equations, which are based on experiments conducted on nonroad surfaces, do not predict an initial flush of loose material that was observed on the Thailand and Hawaii test roads. This is shown in Figure 4.3, where the observed e_s during the Hawaii simulations is compared with that predicted by the KINEROS2 splash erosion equation (Smith et al., 1995; Carl Unkrich, USDA-ARS, Tuscon, AZ, pers. comm.) and the WEPP interrill erosion equation (Flanagan and Nearing, 1995). Splash erosion in KINEROS2 is calculated by:

$$e_s = \begin{cases} c_f \; k(h)\, r^2 & q > 0 \\ 0 & q < 0 \end{cases} \tag{4.1}$$

where r is rainfall intensity (m s^{-1}), q is excess rainfall (m s^{-1}), k(h) is a function of surface water depth that reduces splash erosion as water depth increases, and c_f is a coefficient related to soil erodibility that partially controls the rate at which rainfall produces transportable material from the soil surface. Splash detachment in WEPP is embedded (along with the rain-affected flow phenomenon) within a general expression representing sediment delivery (D_i):

$$D_i = K_i \, I \, R \, S_f \, f(c) \tag{4.2}$$

where D_i has units of kg m^{-2} s^{-1}, K_i is the relative erodibility parameter (kg s m^{-4}), I is rainfall intensity (m s^{-1}), R is excess runoff (m s^{-1}), S_f is a slope factor (dimensionless), and f(c) is a function of canopy cover and/or surface residue (cf., Zhang et al., 1998). In Figure 4.3a, the WEPP response increases toward a limit that is approximately the maximum value. In contrast, e_s peaks near the beginning of the simulated event, then decreases (near monotonically) toward a limit that is a fraction of its maximum value. KINEROS2 splash output peaks early, falls, then stabilizes, largely in response to fluctuations in water depth. The observed e_s response is fundamentally different from the KINEROS2-predicted response in that it is controlled by the availability of entrainable material, not increasing water depth. Thus, equations that do not explicitly consider the removal of a finite layer of loose material will produce a poor prediction of temporal sediment transport for conditions similar to those examined on the Thailand and Hawaii roads.

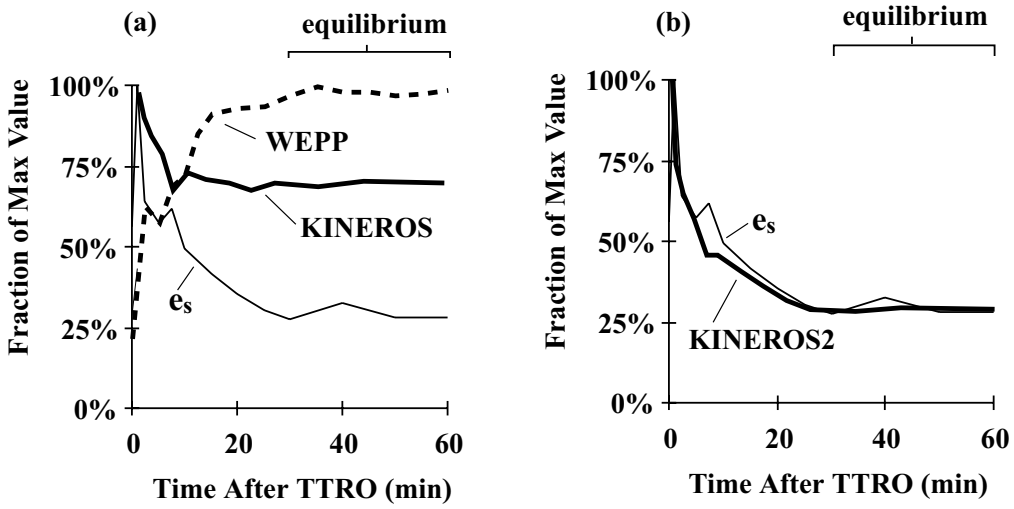

Figure 4.3. (a) Comparison of the measured splash component (e_s) with that predicted using KINEROS2 splash erosion equation (Eq. 4.1) and WEPP interrill erosion equation (Eq. 4.2). All values were derived from observed rainfall, runoff, water depth, and physical plot data from Hawaii road simulations. (b) Comparison of e_s with that predicted from the KINEROS2 equation using the dynamic erodibility concept (DE). For both panels a and b, data were normalized by dividing by the maximum value in each times series.

Removal of the loose surface layer can be simulated by allowing road erodibility to change throughout the event, e.g., c_f and K_i in Eq. 4.1 and Eq. 4.2, respectively. Normally, erosion is assumed to take place on uniform soil. Erodibility values are therefore held constant throughout simulated events. Our field simulation data, however, indicate the loose material that is initially removed is more erodible than the underlying compacted surface, which is eroded once the upper layer is removed. Road erodibility is therefore dynamic, changing in response to the availability of the loose surface material. Initial erodibility is determined by surface preparation; the erodibility after the loose material has been removed is that of the true road surface. Figure 4.3b shows the improvement of employing dynamic erodibility (DE) in simulating splash with KINEROS2.

4.6. SUMMARY AND CONCLUSIONS

Rainsplash enhances runoff generation and contributes greatly to sediment detachment/entrainment on unpaved roads. Even on these highly compacted surfaces raindrop impact reduces the infiltration rate in a manner similar to that occurring on aggregated agricultural and range land soils. Total event splash contribution to the total erosion process during 60-min rainfall simulations on two road surfaces ranged from 38 to 45%. On the Thailand test road, splash erosion was less than hydraulic erosionat all times during the simulation. On the Hawaii road however, spalsh erosion dominated hydraulic erosion for the first third of the event, then became less than hydraulic erosion for the last 40 min of the simulation. On compacted roads, variability in splash and hydraulic erosion subprocesses is initially controlled by the availability of surface sediment and finally by the shear strength of the underlying road surface. Pre-storm availability of loose material is a function of cumulative surface preparation since the previous overland flow event. Physically based erosion models that do not explicitly describe the removal of a loose material layer of finite depth will fail to predict road sediment transport response for roads where sediment preparation is important. If road erodibility is allowed to change during computer simulation (e.g., as in the DE methodology presented herein), removal of the loose surface layer can be simulated with conventional erosion models.

5. EXPERIMENT III: Interstorm surface preparation and sediment detachment by vehicle traffic on unpaved mountain roads

5.1 ABSTRACT

Road survey and field rainfall simulation experiments support that the erodibility of a road surface is dynamic. In the absence of extreme runoff events, dynamic erodibility results from the generation and removal of easily entrained surface material by human road surface maintenance activities, vehicular detachment, and overland flow events. Maintenance activities introduce, easily transportable material to the road surface where it can be entrained by overland flow. Traffic in dry conditions detaches material that is quickly removed during subsequent overland flow events. The pre-storm erodibility of a road is therefore largely a function of maintenance and vehicle activity since the last overland flow event. During rainstorms, vehicle passes increase sediment production by detaching/redistributing surface material and creating efficient overland flow pathways for sediment transport. However, if incision of tracks by overland flow does not occur, post-pass sediment transport quickly returns to pre-pass rates. Field rainfall simulation data suggest sediment transport resulting from during-storm vehicle passes is greatly influenced by the presence of existing loose material, which again is a function of prior road usage and maintenance activities. Incorporation of vehicular phenomena into physically based road erosion models may be possible by parameterizing both storm and inter-storm changes in the supply of loose surface material as changes in surface erodibility.

5.2 OBJECTIVE

The objective of this experiment was to use rainfall simulation to investigate sediment production associated with road maintenance practices in northern Thailand (i.e., manual filling of ruts), and to study sediment detachment by motorcycles and pickup trucks on unpaved roads. An additional objective was to establish links between road sediment production and various human activities by synthesizing physical property measurements, road usage information, and rainfall simulation results. This information is vital to the development of a general methodology for physically modeling road erosion (Experiment IV, Chapter 6).

5.3 METHODS AND MATERIALS

5.3.1 Survey of vehicle usage and surface physical characteristics

The following investigations were performed on the lower road running through the 93.7-ha PKEW (Figure 2.2, described in detail in Section 2.2): (a) a survey of vehicle usage; (b) measurements of cross-sectional physical characteristics; (c) an inventory of sediment sources; and (d) a survey of exit points for road runoff. The traffic survey was conducted for 225 h on 44 days between July, 1998 and February, 1999. During each survey session (usually 4 to 5 h beginning at an arbitrary time of day), each vehicle pass was recorded, noting the type of vehicle, road and weather conditions, and presence/absence of tire chains. Session values were converted to values of passes per 12-h work day using a simple weighting function. A total of 32 cross-sections were established 50 m apart, beginning 25 m inside the watershed boundary. One suite of cross-sectional measurements was conducted in the dry season, March, 1998; a second, 7 months later near the end of the wet season.

At each cross-section, numerous physical phenomena were recorded, including road width, surface condition (e.g., track vs. nontrack), two-dimensional slope, lowering estimates, rut/gully dimensions, and availability of loose surface material. Area-based volumetric and gravimetric estimates of surface material availability were determined by collecting surface sediment from a 0.10 m swath across the road surface at each cross-section. The loose material was collected with a brush and a trowel, taking care not to detach new material from the road surface. Also along the road, a detailed survey was made of sediment sources, preferential overland flow pathways, and runoff entry/exit points.

5.3.2 Rainfall simulation experiments

The rainfall simulator and plot design are described in Experiment I, Chapter 3. Three rainfall simulation experiments were conducted, including one investigating sediment transport on fill material used to repair the road surface (FILL). Two other experiments investigated sediment detachment during motorcycle (MOTORCYCLE) and truck passes (TRUCK). Data from the prior ROAD simulations (Chapter 3) were used as a road control. Experimental designs for each simulation are as follows:

(I) FILL simulations were performed in February 1999 on 1.3 m (W) x 3.75 m (L) plots on the steepest road section in PKEW (median slope = 0.18 m m^{-1}). For each of four FILL simulations on separate plots, a large surface rut (median dimensions = 0.45 m (W) x 0.13 m (D)) running length-wise down the slope was filled with soil taken directly from the roadside margin. The material was excavated and applied with a hand-held hoe by Lisu farmers in a manner consistent with typical road maintenance in PKEW. The fill material was compacted by stomping. Rainfall was applied for 45 min following time to runoff (TTRO).

(II) The MOTORCYCLE simulations were performed in February 1998 on the same plots as the ROAD simulations (Experiment I, Chapter 3), one day following the ROAD experiments. Thus, initial soil moisture was relatively high approximately 22 vs. a value of 12 g g^{-1} recorded during the ROAD experiments) and loose surface sediment was reduced from what normally would be expected during the dry season. Rain was applied to eight different pairs of 0.85 m (W) x 3.75 m (L) subplots for 10 min after TTRO. After rain cessation, a 100 cc Honda motorcycle (street tires = 5 cm wide, mass = 85 kg) was twice driven up and down through each plot. Thus, each wave of motorcycle activity consisted of four passes through the plot. After a 15-min delay to complete the passes, rainfall was applied for another 10 min period, followed by a second identical wave of motorcycle passes and a second 15-min delay. A final 30 min of simulated rainfall was then applied.

(III) TRUCK simulations were conducted on the four FILL simulation plots (described above) on the following morning, approximately 18 h after the FILL simulations ended. Rainfall was initially applied for 20 min. The research vehicle (1993 Isuzu Rodeo; street tires = 20 cm wide, mass = 1700 kg) was then driven once up and then back down through the test plot. Each plot was wide enough only to allow two of the four wheels to pass over the simulated surface; thus, during each pass phase the surface was exposed to detachment by a total of four tires. After a 10-min delay to complete the passes, rainfall was applied for 25 min. In all, four TRUCK simulations were conducted.

5.3.3 Rainfall simulator and plot design

The rainfall simulator consisted of two vertical, 4.3 m risers, each directing one 60° axial full cone nozzle (70 mm orifice diameter) toward the surface. The operating pressure of 172 kPa (25 psi)

produced rainfall energy flux densities (EFD) of about 1650-2040 J m^{-2} h^{-1} (100-120 mm h^{-1}), approximating energy sustained for 10-20 min during the largest annual PKEW storms (based on preliminary analysis of 2 years of rainfall data). Rainfall rate was measured during each event with several manual gauges placed on the plot borders. Cylindrical, sand-filled, low permeability geotextile bags (3.0 x 0.2 x 0.1 m) were arranged to form two side-by-side rectangular subplots. At the base of each sub-plot, geotextile bags were arranged to funnel runoff into a shallow drainage trench dug into the surface. A V-shaped trough constructed from aluminum flashing was inserted into the vertical wall of the trench to allow event-based sampling. Mean values of plot slope, pre-simulation soil wetness, rainfall intensity, and EFD for all simulation experiments are shown in Table 5.1.

5.3.4 Simulation data collection and calculations

During each experiment, instantaneous discharge and sediment output were recorded at time to runoff (TTRO), then again at 1.0, 2.5, or 5.0 min intervals until the end of simulation or until a scheduled break to conduct a vehicle passes. Discharge volume was reduced to account for presence of sediment in the samples. Instantaneous discharge and sediment output values were adjusted to rates per unit area by dividing by filling time and plot area. The rates were then divided by energy flux density (EFD) values of the simulated rainfall (described in Chapter 3). Normalized instantaneous discharge (Q_t) and sediment output (S_t) therefore have units m^3 J^{-1} and kg J^{-1}, respectively. Total normalized event discharge and sediment output, Q_{event} and S_{event}, were calculated as event total values divided by total event EFD. Runoff coefficients (ROCs) were calculated at each sampling time as the fraction of rainfall leaving the plot as discharge. Final event steady-state infiltration rates (f_{ss}) were estimated from the event rainfall intensity (r) and the final event runoff coefficient (ROCfinal, determined over the last 15 min of simulation time) as

$$f_{ss} = \left(100\% - ROC_{final}\right) r \tag{5.1}$$

This approximation assumes surface storage depressions are full; and thus the difference in rainfall and discharge rate is the f_{ss}.

Table 5.1. Mean slope, soil mass wetness, and rainfall variables for all simulation experiments

Treatment	n†	slope (m m^{-1})	w (g g^{-1})	r (mm h^{-1})	EFD (J $m^{-2}h^{-1}$)
FILL	4	0.20 ± 0.06††	0.10 ± 0.05	98 ± 11	1654 ± 188
ROAD††	8	0.15 ± 0.02	0.12 ± 0.03	110 ± 12	1836 ± 209
MOTORCYCLE					
Pre-pass	8	0.15 ± 0.02	0.22 ± 0.01	109 ± 12	1853 ± 198
Post-pass 1	8	0.15 ± 0.02	-	108 ± 16	1826 ± 269
Post-pass 2	8	0.15 ± 0.02	-	109 ± 16	1838 ± 262
TRUCK					
Pre-pass	4	0.20 ± 0.06	0.28 ± 0.01	104 ± 13	1665 ± 362
Post-pass	4	0.20 ± 0.06	-	120 ± 17	2037 ± 294

†w is pre-simulation mass wetness, r is rainfall rate, EFD is energy flux density; values are means ± one standard dev.
†† ROAD data are from Chapter 3.

5.3.5 Statistical Analysis

For comparing FILL with ROAD data, slope, antecedent soil wetness (w), r, event energy flux density (EFD), TTRO, Q_{event}, ROC, f_{ss}, S_{event}, and C_{event} data were analyzed using the nonparametric Mann-Whitney U-test (M-W U). For the MOTORCYCLE simulations, the data were $\log_{10}$-transformed then analyzed using one-way analysis of variance (ANOVA); multiple comparison testing was then conducted with the Fisher's protected least squares difference test (PLSD) when the F-values were significant at $p = 0.05$ (Gagnon et al., 1989). For comparison of MOTORCYCLE pre-pass S_t values with ROAD simulation data, repeated measures (RM) ANOVA was performed on $\log_{10}$-transformed data. The pre-pass and post-pass TRUCK simulation data were analyzed with M-W U.

5.4 RESULTS

5.4.1 Road survey

The traffic survey revealed the Lower PKEW Road receives 4.1 ± 0.5 (std. error) motorcycle and 1.8 ± 0.3 truck passes per 12-h work day. Daily motorcycle traffic is that from farmers going to

and from their fields. Truck traffic is generally from small pickups taking crops to the village or market; few villagers who utilize PKEW own a truck. Occasionally a caravan of 1 to 4 trekking jeeps will pass through. An army personnel transport truck (6 wheels, mass > 4400 kg) passes through once or twice a year carrying troops conducting opium eradication. Well-defined tire tracks/ruts exist throughout the entire 1.65 km length; in some areas a center motorcycle track parallels existing truck ruts. On steep sections, incised tracks provide a rough, exhilarating driving challenge during both wet and dry periods. Surface lowering, ≤ about 0.10 m y^{-1}, is detectable mainly on steep sections (≥ 0.15 m m^{-1}), which occupy < 30% of the total road length. This lowering value is based on one-year and five-year estimates made on the new detour section where the FILL simulations were conducted. In comparison, on one steep (> 0.20 m m^{-1}) section of the main artery leading to Pang Khum, lowering in excess of 0.75 m was observed during the 1996 rainy season.

Road cross-section measurements conducted in the 1998 dry season revealed 8.59 Mg (2.17 kg m^{-2}) of loose surface material on the Lower PKEW Road (1650 m (L) x 2.4 m (W) = 3960 m^2) Cross-sectional measurements taken during the rainy season verify significantly less (M-W U, tied-P value <0.0001) loose road material (3.13 Mg, 0.79 kg m^{-2}). Texture of this material, 58% sand, 19% silt, 23% clay, is indistinguishable from that of the compacted road surface and adjacent fields. Some locations with the greatest sediment depth were found on and immediately below the steepest roads sections, but no significant correlation existed between sediment depth and slope. Most surface material present during the survey is road material detached by vehicle traffic. Other nonroad sediment sources include (1) material removed from the roadside margin for repair; (2) infrequent bank failures (e.g., at entry points to upslope fields) and side slope slumping; (3) localized excavation sites for harvesting plants, insects, etc. Some of the wet-season material includes sediment deposited during prior overland flow events. The wet-season value, which is one-third that of the dry-season value, may be higher than what typically exists during the wettest part of the rainy season (June-August), for the survey was conducted during an extended dry period.

Conveyance efficiency (CE) of road runoff to the stream network varies spatially and temporally. For any given road section, erosion processes, maintenance, and mass wasting changes

the overland flow pathways and runoff exit points. During large storms, overland flow may bypass typical flow channels, thereby altering the conveyance efficiency. In PKEW, a total of 1263 m of the lower road terminates at the stream network. Assuming that runoff exiting elsewhere infiltrates on the hillside (supported by field observations) and that no evaporation or surface storage occurs, the maximum CE estimate for the Lower PKEW Road is 76%. During large storms, some overland flow leaves the road surface at ephemeral exits points, where it again infiltrates into the hillside. Factoring in these losses, the minimum CE estimate is 56%. For most storms, including STORM discussed below, estimated CE for the lower PKEW road is about 70% (field observation).

5.4.2 FILL simulations

Data in Table 5.2 show both hydrological and geomorphological differences between the FILL and ROAD simulations. For example, TTRO was much slower on the repaired/filled surface; additionally, total event discharge (Q_{event}) and event ROC were lower for FILL compared with the ROAD control. Bulk density of the fill surface was 1.05 Mg m^{-3} (taken *in situ* after the repair), significantly lower (M-W U, $\alpha = 0.05$, n=12) than the 1.42 Mg m^{-3} of the road surface. ROAD and FILL steady state infiltration rates were statistically indistinguishable, implying ending ROCs (thus final discharge) were similar. Total event sediment output for the FILL simulations was about 40% higher than for the ROAD simulations. Instantaneous sediment transport for the two simulation surfaces were very similar for the first 15 min, but then separated for the final 30 min, as FILL S_t remained relatively high, and ROAD S_t diminished (Figure 5.1a). Total sediment concentration was 2.5 times higher for the FILL versus the ROAD simulations (Table 5.2). Figure 5.1b shows FILL instantaneous sediment concentrations (C_t) to be consistently higher than those for ROAD. The maximum C_t during the FILL simulation was almost twice as high as that for ROAD (320 vs. 170 g L^{-1}).

5.4.3 MOTORCYCLE and TRUCK simulations

Runoff and sediment transport data from the MOTORCYCLE and TRUCK simulations are shown in Tables 5.2. For both types of simulations, post-pass phases had higher event discharge and

Table 5.2. Mean runoff and sediment transport data for all simulations

Treatment	TTRO† (min)	Q_{event} (L J^{-1})	ROC (%)	f_{ss} (mm h^{-1})	S_{event} (g J^{-1})	C_{event} (g L^{-1})
FILL	6.1 ± 3.4 a	0.043 ± 0.01 a	60 ± 14 a	12.0 ±11.3 a	1.7 ± 0.6 a	44 ± 9 b
ROAD††	1.1 ± 0.3 b	0.053 ± 0.01 a	82 ± 4 b	6.2 ± 4.1a	1.2 ± 0.6 a	21 ± 9 a
MOTORCYCLE†††						
Pre-pass	0.6 ± 0.3 b	0.013 ± 0.003 a	69 ± 10 a	16.4 ± 9.6 a	0.9 ± 0.4 a	17 ± 9 ab
Post-pass 1	0.4 ± 0.2 a	0.014 ± 0.003 a	75 ± 8 b	12.1 ± 8.4 a	1.3 ± 0.7 a	22 ± 10 b
Post-pass 2	0.3 ± 0.1 a	0.047 ± 0.008 b	86 ± 5 c	9.8 ± 5.1 a	2.8 ± 1.2 b	15 ± 6 a
TRUCK††††						
Pre-pass	0.8 ± 0.2 b	0.043 ± 0.007 a	73 ± 12 a	12.1 ± 11.8 a	1.2 ± 0.3 a	25 ± 7 a
Post-pass	0.5 ± 0.2 a	0.051 ± 0.007 a	86 ± 7 a	7.0 ± 6.6 a	3.8 ± 0.6 b	68 ± 8 b

†TTRO is time to runoff, Q_{event} is total normalized event discharge, ROC is the total event runoff coefficient (total runoff/total rainfall), f_{ss} is estimated steady-state infiltration rate (from Eq. 5.1), and S_{event} is normalized event sediment output, C_{event} is total event concentration; values are means ± one standard dev.

††ROAD and FILL data in each column with the same letter are NOT statistically different at p = 0.05, nonparametric Mann-Whitney U-test; ROAD data are from Chapter 3.

††† MOTORCYCLE simulation data in each column with the same letter are NOT statistically distinguishable at p = 0.05, ANOVA followed by Fisher's PLSD post hoc testing on $\log_{10}$-transformed data.

†††† TRUCK simulation data in each column with same letter are NOT statistically different at p = 0.05, M-W U.

ROCs. These increases may result from the creation of well-defined flow channels by the vehicle tires, but may also be artifacts of the post-pass phases having higher soil moisture values than the previous phases. The truck passes initiated significant increases in total event sediment output and concentration. The motorcycle passes increased sediment transport without causing the doubling in event sediment concentration that was present in the TRUCK simulations. Figures 5.2 and 5.3 show sharp increases in instantaneous sediment transport and concentration occurring immediately following truck and motorcycle passes. These spikes were soon followed by sharp declines to pre-pass values within 10-30 min.

5.5 DISCUSSION

5.5.1 Interstorm surface preparation

Although traffic in PKEW is light (based on definitions of Reid and Dunne, 1984), the roads are important sediment sources for material, particularly loose surface sediment, entering the stream

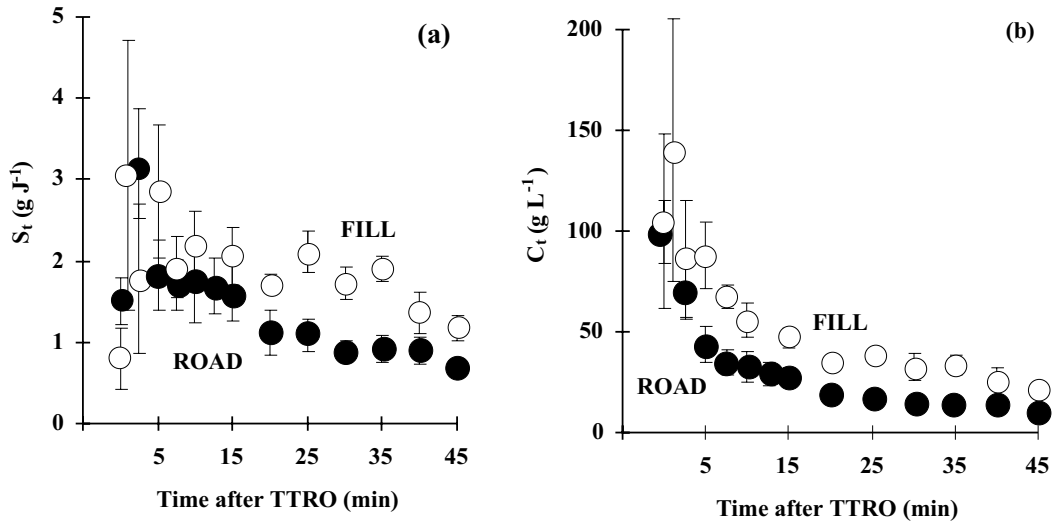

Figure 5.1. (a) Instantaneous sediment output (S_t) and (b) instantaneous sediment concentration (C_t) for the FILL and ROAD simulations. Data are means ± one standard error.

channel network. Abundance of loose road surface material at any given time is a function of vehicle traffic and other surface preparation processes occurring since the last overland flow event. Surface preparation refers to any phenomenon that contributes to the availability, erodibility/detachability, or transport of material (cf. Bryan, 1996) Interstorm preparation in PKEW is extensive during the 4-5 month dry season. During the wet season, the supply of loose material generated before each storm is diminished because the interstorm period is shortened. Importance in the length of the interstorm preparation period is illustrated in Figure 5.4a, where sediment transport on a road section during simulated rainfall after a long dry period (DRY) is compared with that on the same section one day following an approximately 80-mm rainfall event (WET, all data based on the ROAD and MOTORCYCLE simulations discussed below). Instantaneous sediment transport (S_t) for the DRY condition is significantly greater (RM ANOVA, $\alpha = 0.05$) than for WET at all time periods during the short, high-intensity (mean = 110 mm h^{-1}) event. Absent from the WET time series is the large initial flush of loose material that was present during the DRY time series. The material comprising this flush was generated by truck and motorcycle passes that occur for many weeks prior to the rainfall event. In the case of the WET

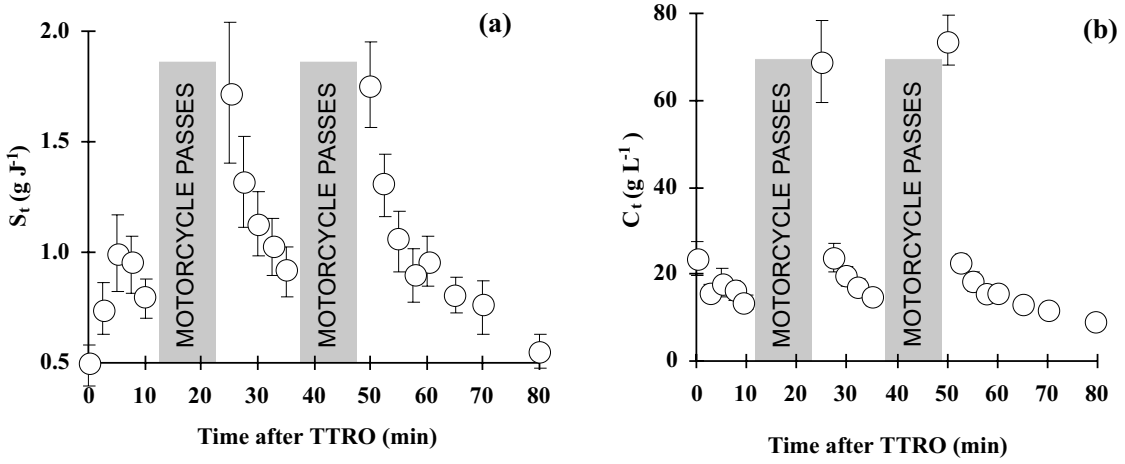

Figure 5.2 (a) Normalized instantaneous sediment output (S_t) and (b) instantaneous sediment concentration (C_t) for the pre-pass and two post-pass phases of the MOTORCYCLE simulations. Rainfall was stopped for 15 min to make the motorcycle passes. Each phase time series begins when runoff was generated. Values are means ± one standard error.

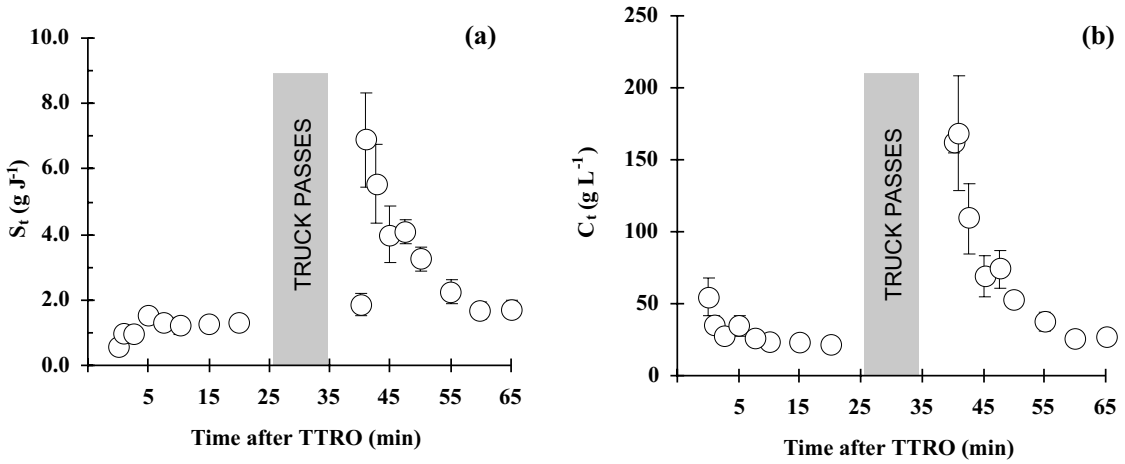

Figure 5.3. (a) Normalized instantaneous sediment output (S_t) and (b) instantaneous sediment concentration (C_t) for the pre-pass and post-pass phases of the TRUCK simulations. Rainfall was stopped for 10 min to make truck passes. Each phase time series begins when runoff was generated. Data are means ± one standard error.

simulation, the previous overland flow event on the previous day removed most loose surface material.

When interstorm sediment preparation is great, relatively small overland flow volumes can transport significant sediment loads. Figure 5.4b shows that one-third of the total sediment for the DRY road simulation is removed within the first 10 min of the 45 min event, when ROCs were far below event maximum values. Furthermore, nearly two-thirds of the material was removed before the midpoint of the storm (22.5 min). For shorter storm events, larger percentages of total event material will be removed early. For example, if the event lasts only 15 min, approximately 40% of the total sediment output will occur in the first 5 min. Figures 5.4a,b collectively indicate that if loose material is available, much will be transported soon after overland flow generation—even low-magnitude events are capable of entraining sediment on the road surface. Because of a high conveyance efficiency for the PKEW network, most of this material goes directly into the stream system

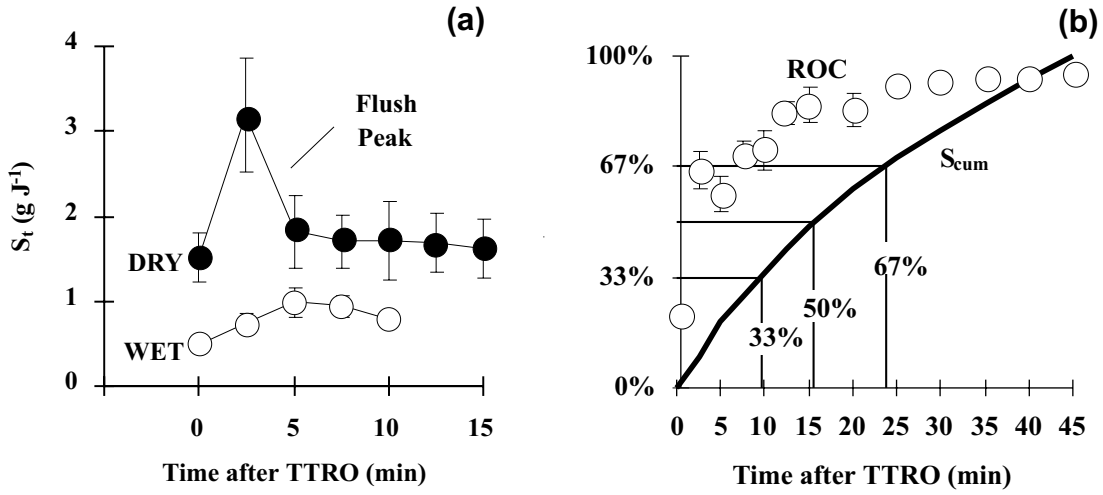

Figure 5.4.(a) Comparison of instantaneous sediment transport (S_t) on a road surface during DRY conditions with St one day after an 80 mm rainfall simulation event (WET). Values are means ± one standard error. (b) Cumulative sediment transport (S_{cum}) as a percentage of total output plotted with instantaneous runoff coefficients (ROC, dots) for the DRY road simulations shown in Figure 5.4a. Values are means ± one standard error.

5.5.2 Hydrological and geomorphological consequences of maintenance activities

Road maintenance is another interstorm preparation activity affecting sediment availability. In PKEW, less than 10% of the road requires some type of repair during or following the rainy season (field survey). Many attempts by villagers to make the road passable by filling gullies with cutslope material are quick-fix solutions, where much of the fill is quickly eroded during subsequent large storm events. The FILL simulations demonstrate the vulnerability of this type of repair. The fill material, being significantly less compacted than the road surface, infiltrated more rain water, delaying runoff generation by 5 min (Table 5.2). Throughout the simulation, the fill material temporarily stored rainwater that otherwise would have become HOF on the compacted road surface. During later stages of the simulation, subsurface stormflow exited the fill as return flow near the bottom of the plot. Post-event runoff from the ROAD simulation plots subsided within 1 min. In comparison, runoff continued on the FILL plots for several min after rainfall was discontinued. Although the fill had a higher infiltrability, water storage was limited; and the long-term infiltration rate was governed by that of the underlying, compact road surface. Thus, the repair represents a nonconsolidated layer resting atop a less-permeable surface that is subject to failure by two mechanisms: (1) sliding on the underlying compacted surface where infiltrated water flows laterally on steep road sections, and (2) surface erosion and incision by HOF.

With respect to surface erosion, both FILL and ROAD surfaces experienced an initial flush of easily removed surface material during rainfall simulation (Figure 5.1a). Again, much of the total event sediment for ROAD was removed in the first few minutes following runoff generation. In contrast, only a little more than half the total FILL output was transported after 25 min. Fluctuations in the FILL S_t data (e.g., 15 to 35 min) result from the creation and destruction of surface microdams (observed), processes that are common on bare, rough agricultural surfaces. FILL sediment response resembles a hybrid of that found on road and agricultural surfaces. To date, the FILL surface is the most erodible surface complex in PKEW—eclipsed perhaps only by field erosion resulting from HOF generated on agricultural maintenance paths. The term “complex” is used because it is the juxtaposition of an erodible material with a compact surface capable of generating sufficient HOF that produces high sediment output. Because the erodibility of this type of repaired surface is different from that of non-repaired road sections, it is important to discriminate between the two surface types when modeling.

5.5.3 Sediment detachment by vehicles

The MOTORCYCLE simulations demonstrate the role of vehicular traffic in enhancing sediment transport on unpaved roads during rain events (Figure 5.2, Table 5.2). Sediment transport during these experiments was relatively low because the simulation plots were used the preceding day for the ROAD simulations. The pre-pass simulation stage (0 to 10 min) demonstrates a supply-limited situation in which little loose surface material was present; most sediment output therefore, was material detached from the road surface by raindrop impact and rain-affected flow processes. By the end of this 10-min phase, S_t was probably approaching a baseline rate. Following the first wave of motorcycle passes, sediment output immediately doubled. Over the next 10 min S_t declined, but remained higher than the final pre-pass rate. Following the second set of motorcycle passes, S_t nearly doubled from the preceding value. Once again S_t declined during the remainder of the simulation. After about 15 min, S_t values were lower than those at the end of the pre-pass phase, indicating the motorcycle passes detached a limited supply of material that was removed in 10 to 15 min.

Although the passes created visible tire tracks, overland flow did not incise them—incision would have produced protracted, high S_t values. Nevertheless, the first motorcycle passes doubled total sediment production from what would have been expected without the disturbance (calculations based on S_t data from the 10-min post-pass phase). Similarly, the second motorcycle passes increased total sediment production by about 60% in the final simulation phase. Sediment concentrations increased significantly following each wave of the passes (Figure 5.2b). Concentration was significantly higher only at the initial post-pass sampling time when ROCs were still relatively low (about 40%). Just 2.5 min later when ROCs increased to about 80%, C_t values dropped to approximately their pre-pass values. This “elastic” response in C_t results from the detached material being stored temporarily within or near the well-defined tire tracks, where it could be removed quickly by channelized flow.

The S_t and C_t responses to truck passes were generally similar to those of the MOTORCYCLE simulations (Figure 5.3), with an exception being the magnitude of the sediment output spike following truck passes. TRUCK S_t increased to more than 5 times the pre-pass value, as compared with an approximate doubling of S_t following motorcycle passes. The greater TRUCK

response results from two conditions: (1) the TRUCK simulations were performed on a more erodible surface (the FILL simulation plots discussed above)—in fact, nearly all pre-pass TRUCK S_t values were ≥ the maximum MOTORCYCLE pre-pass S_t value; and (2) the heavier trucks (1700 vs. 85 kg) with wider tires (20 cm vs. 5 cm) detached more material than did the motorcycles. Following the truck passes, S_t peaked immediately, then declined over time. The final output value, however, remained higher than the final pre-pass value, indicating that the new material detached by the truck passes was not completely removed during the final 25 min of simulation. It may also indicate that incision of the newly formed truck tracks by overland flow was contributing substantially to sediment transport (incision on the fill was observed during some experiments). The truck passes generated 2.5 times more sediment output than would have been expected without the passes; this value is slightly higher than the doubling response witnessed during the first set of motorcycle passes. Initial post-pass sediment concentration (approximately 165 g L^{-1}) increased almost 8 times over the ending pre-pass values. Somewhat different from the MOTORCYCLE concentration response, post-pass TRUCK C_t remained high for several minutes. Unfortunately, because the TRUCK and MOTORCYCLE simulation methodologies were different, it is not possible to estimate reliably how much more sediment was detached by the truck versus the motorcycle passes.

5.5.4 Vehicle detachment in a prior study: a comparison

Similar to this study, Coker et al. (1993) found elevated sediment concentrations following truck passes (2 passes of a 3000 kg, 6-wheel dump truck) on a wet road during simulated rainfall (400 m^2 plot, 30 min, 38 mm h^{-1}) in the Marlborough Sounds of New Zealand. In all, 5 groups of two passes were made approximately 5 min apart. Immediately following dump truck passes, sediment concentrations at one site initially rose by an order of magnitude to > 120 g L^{-1}. Within 2.5 min, C_t fell to roughly the pre-pass value. For each successive pair of truck passes, large post-pass C_t peaks were generated; however, successive peak values constantly decreased, with the final peak value only reaching about 60 g L^{-1}. In comparison, the diminishing concentration peak phenomena did not occur during the MOTORCYCLE simulations, and the post-pass TRUCK C_t values didn't return to the range of pre-pass values until after about 10 to 15 min.

Aside from being related to differences in soil erodibility, differences between the simulation results and those in the Marlborough experiment are likely related to surface preparation. The Marlborough plots were raked prior to simulation to insure the presence of a loose layer of uniformly distributed material. Most loose material on the Thailand plots was removed by prior rainfall simulation events. Therefore, most of the post-pass sediment transport during the MOTORCYCLE and TRUCK simulations was that of newly detached material. Post-pass sediment output at Marlborough was probably a combination of material detached by the truck passes and loose pre-simulation material that the dump truck passes redistributed into efficient overland flow pathways (i.e., newly formed tracks). Concentration peaks declined over time not because the passing trucks were necessarily detaching less material, but probably because the supply of loose surface material became depleted over the course of the simulation. Some differences between the two studies could be related to scale, as sediment output on the small-scale Thailand plots is sensitive to sediment detachment at the bottom of the plots. Nevertheless, these two field-based studies emphasize that vehicle-induced sediment output is substantially influenced by availability of loose surface material, which is influenced by pre-event surface preparation, e.g., traffic (cf., Reid and Dunne, 1984).

5.5.5 Toward modeling vehicular traffic

The rainfall simulations have provided knowledge about two specific mechanisms by which vehicular traffic influences sediment transport on unpaved roads: (1) interstorm surface preparation; and (2) detachment of new material and/or redistribution of existing material during rain storms. Both mechanisms generate new material to be flushed from the road surface either during the next overland flow event (in the case of interstorm preparation) or within the next few minutes (in the case of detachment during an overland flow-producing storm). A third mechanism, incision of tire ruts/tracks, was not investigated.

An on-going goal in erosion research is to use physically based models to simulate sediment production on unpaved roads (Simons et al., 1977; 1978; Ward, 1985; Elliot et al., 1995). This endeavor is difficult because model sediment transport equations, which are often based on agricultural or range land experiments, typically do not describe the observed sediment

transport response on unpaved roads poorly (e.g., that of ROAD in Figure 5.1a). The next chapter introduces the dynamic erodibility (DE) methodology to simulate the initial flush of loose material and the ensuing decay in sediment transport by explicitly modeling the removal of a finite layer of loose material. The DE methodology recognizes erodibility changes both as material is detached during the interstorm period and during a storm as surface sediment is removed by overland flow. Initial erodibility for any given storm is a function of sediment availability; once all loose material is removed, erodibility is that of the compacted road surface.

Surfaces represented by FILL above, can be modeled with DE by assigning repaired road sections initial erodibility parameters that are higher than those of the surrounding compacted road surface. Eventually erodibility will decrease as the easily transported material is removed. Again, extreme events where gullying and mass wasting occur are not considered. Other researchers have reported decreases in road erosion rates over time following grading on gravel roads (Luce and Black, 1999) and road construction (e.g., Megahan, 1974, Riley, 1988, and Beschta, 1978). In most cases, the decline results, in part, from preferential depletion of fine, highly erodible fractions (others have referred to this process as armoring, e.g., Megahan, 1974; Black and Luce, 1999). With DE, one would treat preferential depletion as a shift to a less erodible material (i.e., the course and/or consolidated material left behind).

Modeling vehicle detachment during storms is difficult because users must simulate the process by manipulating model splash and hydraulic erosion parameters. A plausible approach using DE is to treat vehicle-induced increases in the supply of surface material as temporary increases in road erodibility. In the case of interstorm surface preparation, erodibility is a function of sediment availability, which is related to total traffic since the last overland flow event. Modeling vehicle passes during a storm requires employing DE at a shorter time scale. Sediment transport following a vehicle pass increases because a new limited supply of material becomes available on the road surface where it can be entrained immediately by overland flow. For modeling, each pass marks the transition to a higher state of erodibility. After the new material is removed, sediment transport rate—hence erodibility—returns to that of the pre-pass state.

Figure 5.5 conceptualizes modeling vehicular detachment during a storm employing DE. Sediment production on the road surface (S_{Road}, from ROAD data) decreases over time as easily entrained surface material is removed. Thus, for a lengthy storm without during-event traffic a road surface passes through several states of decreasing erodibility. Initial road erodibility (E_n) is determined by sediment availability. Times T_1 and T_2 mark transitions to states of lower erodibility (i.e., $E_n > E_{n-1} > E_{n-2}$). The thin line represents the sediment output generated following a vehicle pass (based on post-pass TRUCK S_t rates minus the pre-pass equilibrium rate). The thick line is the combined sediment production from the road and that generated by the truck pass: $S_{Road+Truck} = S_{Road} + S_{Truck}$. The passing of the truck immediately produces a transition to a higher erodibility state (i.e., $E_{n+1} > E_n$). After several minutes of high sediment production, $S_{Road+Truck}$ declines; and at time T_3, the surface erodibility switches to the preceding value, E_n. As time progresses, erodibility values reduce to E_{n-1} at T_4; then E_{n-2} at T_5.

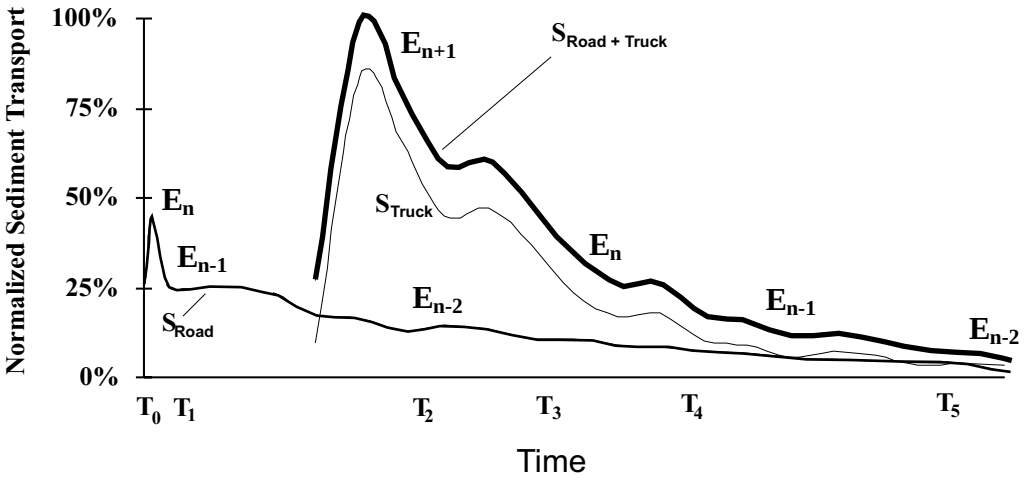

Figure 5.5. Conceptual methodology for modeling vehicular detachment during a storm. S_{Road} is sediment transport on the road surface. S_{Truck} is the sediment transport resulting from truck passes. $S_{Road+Truck}$ is the total sediment transport following the truck passes. All values are normalized by dividing by the maximum $S_{Road+Truck}$ value. Values of E (where $E_n > E_{n-1}$) represent the road surface erodibility, which decreases as loose material is removed and increases as vehicle passes detach new material from the compacted road. T_n values mark transitions to lower erodibility states (described in the text). The time scale is on the order of 2-3 h.

A model from a prior study (Megahan, 1974) provides a basis for assigning post-pass erosion rates:

$$\varepsilon_t = \varepsilon_n + k\, S_o\, e^{-kt} \qquad (5.2)$$

where ε_t represents the erosion rate at a disturbed site; ε_n is the erosion rate of the site prior to disturbance; S_o is the amount of material made available by the disturbance; k is the recovery potential for the disturbed site; and t is time. Incorporating the Megahan model into the conceptual model shown in Figure 5.5 is accomplished simply by substituting E_{n+1} and E_n for ε_t and ε_n, respectively in Eq. 5.2.

At present, there are few experimental data for prescribing various S_0, k, and erodibility values. The MOTORCYCLE and TRUCK simulations generally indicate that erodibility doubles following a set of passes for about 15 to 30 min (assuming relatively high, stable rainfall and overland flow). In another "truck" study conducted in Hawaii (unpublished data) post-pass S_t values returned to approximately the pre-pass maximum values after about 20 min following two passes of a pickup truck having similar mass as the Isuzu used in Thailand (Figure 5.6). Total sediment

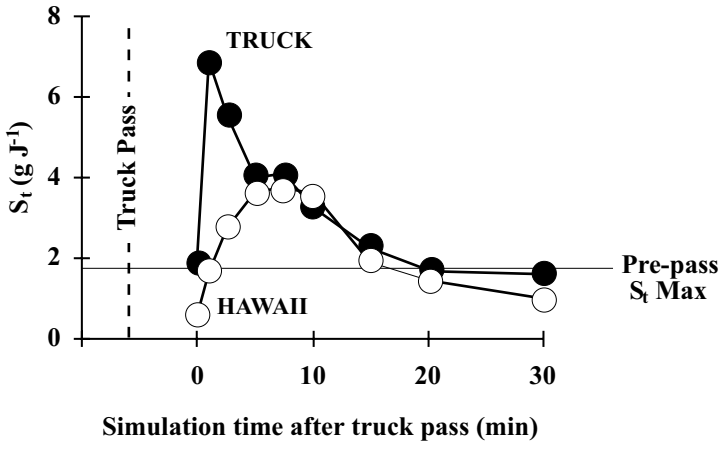

Figure 5.6. Comparison of post-pass instantaneous sediment transport (S_t) for the TRUCK simulations in Thailand and a prior study in Hawaii. In both experiments, post-pass values decrease to approximately the pre-pass maximum value after about 20 min (33 and 40 mm of rainfall for the HAWAII and THAILAND simulation, respectively).

output attributed to the HAWAII truck passes was less than that determined in the TRUCK simulations, emphasizing that various states of erodibility are inherently determined by the physical properties of the road soil surface. Erodibilities will probably have to be determined experimentally for different locations. Although the knowledge base to make such prescriptions is nascent, Figure 5.5 represents a framework from which to direct future research.

5.6 CONCLUSION

Knowledge of pre-storm surface preparation phenomena, especially vehicular and maintenance activities, is crucial to understanding sediment transport on unpaved roads. During typical rainfall events where overland flow does not greatly incise the surface, much of the sediment transported on PKEW roads is loose, easily entrained material that was present prior to the event. This loose material is predominantly generated by vehicular detachment and maintenance activities during the interstorm period. In general, for any given usage level, the longer the interstorm period, the greater the supply of loose material; thus, the greater the event sediment transport. Vehicular traffic during rainstorms initiates high sediment transport rates by detaching new material from the road surface and creating efficient overland flow paths. Additionally, a vehicle pass redistributes existing loose material into flow paths where it can be entrained. Sediment transport response to a vehicle pass is therefore related to interstorm surface preparation, as well as to the more obvious variables associated with the passing vehicle, *in situ* soil, and rain event. Because the supply of loose material is in constant flux, the road behaves like a surface with changing erodibility. Through adopting this concept of dynamic erodibility, one can parameterize maintenance and vehicular activities during physically based modeling of road-related erosion.

6. EXPERIMENT IV: Erosion prediction on unpaved mountain roads in northern Thailand: validation of dynamic erodibility modeling using KINEROS2

6.1 ABSTRACT

Work investigated the application of the event- and physics-based KINEROS2 runoff/erosion model for predicting overland flow generation and sediment production on unpaved mountain roads. Field rainfall simulations provided independent data for model calibration and validation. Validation showed KINEROS2 could simulate total discharge, sediment transport, and sediment concentration on small-scale road plots, for a range of slopes, during simulated rainfall events. Predicted hydrographs for aggregated validation experiments had root mean square errors (RMSEs) ≤ 25% using the calibration parameter set. KINEROS2, however, did not accurately predict time-dependent changes in sediment output and concentration (RMSE > 50 and 100%, respectively). In particular, early flush peaks and the temporal decay in sediment output were not predicted, owing to the inability of KINEROS2 to model removal of a surface sediment layer of finite depth. For typical events in the study area, material from the upper layer is predominantly detached and entrained by surface overland flow. During long events, sediment transport declines as supply of loose superficial material becomes depleted. Modeled erosion response was improved by allowing road erodibility to vary during an event. Assigning unique model erosion detachment parameters to periods defined by road surface sediment availability improved RMSE of predicted sediment transport by 30-40% for the validation events. A predictive relationship was shown to exist between road erodibility states and road surface sediment depth. This relationship allows implementation of the dynamic erodibility (DE) method for events where pre-storm sediment depth is estimated from road usage since the last overland flow event.

6.2 OBJECTIVE

The objective of this experiment is develop a methodology for using the KINEROS2 model for predicting road runoff and erosion on unpaved roads in northern Thailand. KINEROS2 will be validated using discharge and sediment transport data from several small-scale field rainfall simulation experiments on unpaved roads in PKEW. Refinements, based on the change in erodibility of a road surface, will then be introduced to improve model prediction.

6.3 METHODS AND MATERIALS

6.3.1 Soil physical property measurements

All work for this experiment was performed on the lower road in PKEW (Figure 2.2; described in detail in Section 2.1). Soil properties determined on this road are listed in Table 6.1. Moisture retention data (soil moisture characteristic) were determined from 45 cm^3 cores collected from the road surface using standard procedures described in Klute (1986). Five matric potentials (ψ) were selected with a range from -5 kPa to -1500 kPa. Preferential porosity was computed as the difference in water content between ψ = 0 kPa (saturation) and that at -10 kPa (Mbagwu, 1997). Mesoporosity was computed as the difference in water content between ψ at -100 kPa and -10 kPa; microporosity, between ψ at -1500 kPa and -100 kPa (Mbagwu, 1997). Methods for determining other soil properties are described in Chapter 3. Description of measuring cross-sectional physical characteristics are described in Chapter 5.

6.3.2 Rainfall simulation

In February 1998 and 1999, rainfall simulation experiments were conducted on the Lower PKEW Road (locations shown in Figure 2.2). Eight simulations (ROAD) were conducted on a road section with slope ranging from 0.13 to 0.18 (m m^{-1}). Four simulations were performed on the steepest road section in PKEW (HILL, slope = 0.29 m m^{-1}). One day following the ROAD simulations, an additional simulation was performed on each ROAD plot to investigate sediment transport during successive storms (WET). The rainfall simulator, plot design, and calculations of instantaneous concentrations (C_t), discharge (Q_t), and sediment output (S_t) are described in previous chapters.

6.3.3 KINEROS2

KINEROS2 (Smith et al., 1995), the second-generation version of KINEROS (Woolhiser et al., 1990), is an event- and physics-based runoff and erosion model. Application and testing of KINEROS is documented elsewhere (Smith, 1976; Zevenbergen and Peterson, 1988; Smith et al., 1995). Dynamic, distributed flow modeling in KINEROS2 is well-suited to describe road runoff and erosion processes in PKEW, where (1) runoff generation is dominated by HOF, with minimal

Table 6.1. Soil Properties of the road surface soil at PKEW

Descriptor/Property	Units	n	mean ± SD
Sand fraction	%	8	54.4 ± 4.9
Silt fraction	%	8	24.0 ± 2.2
Clay fraction	%	8	21.7 ± 5.5
Dominant clay mineral	-	4	kaolinite†
Saturated hydraulic conductivity	mm h^{-1}	26	15.0 ± 8.6
Wetness at saturation (also saturated porosity)	m^3 m^{-3}	26	0.44 ± 0.05
Water retained at -330 kPa	m^3 m^{-3}	5	0.30 ± 0.01
Water retained at -1500 kPa	m^3 m^{-3}	5	0.13 ± 0.01
Preferential porosity	m^3 m^{-3}	5	0.10 ± 0.03
Meso-porosity	m^3 m^{-3}	5	0.07 ± 0.01
Micro-porosity	m^3 m^{-3}	5	0.15 ± 0.01
Bulk density (0-5 cm)	Mg m^{-3}	74	1.45 ± 0.13
Bulk density (5-10 cm)	Mg m^{-3}	16	1.36 ± 0.11
Bulk density (10-15 cm)	Mg m^{-3}	16	1.35 ± 0.10
Penetration resistance	MPa	160	6.4 ± 0.4
Particle density	Mg m^{-3}	8	2.55 ± 0.05
pH(1:5 water)	-	16	4.8 ± 0.3
Organic carbon	%	16	1.6 ± 0.6
Total nitrogen	%	16	0.13 ± 0.03
Cation exchange capacity	$cmol_c$ kg^{-1}	16	9.8 ± 2.6
Exchangeable Bases	%	16	63.1 ± 19.8

† In addition to moderate amounts of kaolinite, PKEW soil also contains traces of illite, vermiculite, gibbsite, montmorillonite, and chlorite.

contributions from interception of subsurface flow by the road prism and (2) sediment transport on the road surface varies throughout the course of a storm. The following description of KINEROS2 is based on Smith et al. (1995) and C. Unkrich (unpublished manuscript, Southwest Watershed Research Center, USDA-ARS, Tuscon, AZ):

Horton overland flow simulation in KINEROS2 utilizes the kinematic wave method to solve the dynamic water balance equation:

$$\frac{\partial h}{\partial t} + \frac{\partial Q}{\partial x} = q(x,t) \tag{6.1}$$

where *h* is water storage per unit area, *Q*(x,t) is water discharge, x is distance downslope, t is time, and q(x,t) is net lateral inflow rate. Solution of Eq. 6.1 requires estimates of time- and space-dependent rainfall r(x,t) and infiltration f(x,t) rates:

$$q(x,t) = r(x,t) - f(x,t) \tag{6.2}$$

The infiltration model in KINEROS2 utilizes several parameters describing a one- or two-layer soil profile: saturated hydraulic conductivity (K_s), integral capillary drive or matric potential (G), porosity (ϕ), and pore size distribution index (λ). The coefficient of variation for K_s can be specified to account for spatial variation in infiltration. Inclusion of two soil layers allows modeling a restrictive surface or subsurface layer. The general one-layer infiltrability (f_c) model is a function of cumulative infiltration (I):

$$f_c = K_s\left[1 + \frac{\alpha}{e^{(\alpha I/B)} - 1}\right] \tag{6.3}$$

where α is a parameter related to soil type (fixed at 0.85 in KINEROS2) and $B = (G + h_w)(\Theta_s - \Theta_i)$, where h_w is surface water depth and the second term, unit storage capacity, is the difference of effective saturation (Θ_s) and soil moisture (Θ_i).

Simulating erosion involves solving the dynamic sediment mass balance equation:

$$\frac{\partial (AC_s)}{\partial t} + \frac{\partial (QC_s)}{\partial x} - e(x,t) = q(x,t)\, c(x,t) \tag{6.4}$$

where A is cross-sectional area, C_s is local sediment concentration, e is net erosion/deposition rate, q(x,t) is water inflow rate and c(x,t) is the corresponding concentration of the inflowing water. KINEROS2 does not explicitly separate rill and interrill erosion processes (often there are no rills); rather it divides e_T into two additive components: rainsplash (e_s) + net hydraulic erosion (e_h). Splash erosion is calculated from Eq. 4.1. Flow-induced net hydraulic erosion is the difference between particle detachment (dependent on slope, flow depth, flow velocity, particle size) and deposition. In KINEROS2, e_h is calculated as a function of current local sediment concentration C_s(x,t) and transport capacity (C_{mx}):

$$e_h = c_g(C_{mx} - C_s)A \tag{6.5}$$

where A is cross-sectional area of the flowing water; and c_g is a transfer rate coefficient, which is equal to soil particle settling velocity (v_s) / hydraulic depth (h) during deposition; and c_g is less than v_s/h during erosion on cohesive soils.

Drainage basins in KINEROS2 are treated as a cascading network of surface, channel, and pond elements. Channels receive flow from adjacent surfaces or upslope channels. Rectangular surfaces may be cascaded or arranged in parallel to represent complex topography or erosion features. A road section could be represented as one element or subdivided into parallel flow planes representing distinct features, such as ruts, gullies, or tracks. Each element is characterized by assigning parameter values that control runoff generation and erosion processes. Dynamic, distributed flow modeling in KINEROS2 requires a temporal record of rainfall rate at one or more spatial locations.

6.3.4 Model calibration and model error assessment

Five of the eight ROAD simulation events were randomly chosen to produce a model calibration dataset (events 1,2,4,5, and 7). Nonrectangular simulation plots were modeled in KINEROS2 as a singular rectangular element, having length and area equal to those in the field simulations; element widths were reduced to give equal areas. Median measured instantaneous and total discharge Q ($m^3\ s^{-1}$), sediment transport S (kg s^{-1}), and sediment concentration C (kg m^{-3}) values for observed event (ROAD12457) were compared to the time series predicted by KINEROS2. Element parameters controlling runoff generation (e.g., capillary drive and K_s) and erosion processes (e.g., splash erosion and soil cohesion coefficients), which were initially assigned based on physical property data, were adjusted during calibration to reduce the error in predicted Q and S. Five measures of model error or performance were used:

Percent error in total estimate:

$$E_{total} = \frac{(P_{total} - O_{total})}{O_{total}} 100 \qquad (6.6)$$

Percent error in peak value estimate:

$$E_{peak} = \frac{(P_{peak} - O_{peak})}{O_{peak}} 100 \qquad (6.7)$$

Root mean square error (%):

$$RMSE = \sqrt{\frac{1}{n}\sum_{i=1}^{n}\left(P_i - O_i\right)^2}\ \frac{100}{\overline{O}} \tag{6.8}$$

Coefficient of determination:

$$CD = \frac{\sum_{i=1}^{n}(O_i - \overline{O})^2}{\sum_{i=1}^{n}(P_i - \overline{O})^2} \tag{6.9}$$

Model efficiency (ME, Nash and Sutcliffe, 1970):

$$R^2 = 1 - \left(\frac{\sum_{i=1}^{n}(O_i - P_i)^2}{\sum_{i=1}^{n}(O_i - \overline{O})^2} \right) \tag{6.10}$$

where P_{total} and O_{total} are event total predicted and observed values; P_{peak} and O_{peak} are peak event predicted and observed values; P_i and O_i are predicted and observed instantaneous values; and $\overline{O}$ is the mean of the observed data. If predicted and observed values are equal, E_{total}, E_{peak}, RMSE, CD, and R^2 produce optimal values of 0, 0, 0, 1, and 1. Lower limits for E_{total}, E_{peak}, RMSE, and CD are zero; model efficiency R^2 can be negative. CD indicates the proportion of total variance of observed data that is explained by the predicted data. A negative R^2 value indicates model values are worse estimates than the observed mean (Loague and Green, 1991). Appropriateness of these error indices are described elsewhere (Green and Stevenson, 1986; Loague and Green, 1991). Calibration first focused on reducing E_{total} to ± 0.5% for runoff; further refinements were then made to produce a better fit of the predicted runoff hydrograph, as indicated by the other performance indices (i.e., RMSE, CD, and ME). The subsequent adjustments maintained an E_{total} of ± 0.5%. Following runoff calibration, adjustments were made to splash and hydraulic detachment parameters to first reduce S total error ± 0.5%, and then produce the best fit of modeled versus observed values, as defined by RMSE, CD, and ME. Changing sediment detachment parameters do not produce detectable differences in predicted runoff in KINEROS2.

6.3.5 Model validation

Validation of the ROAD12457 parameter set (Table 6.2) was performed on three datasets: (1) the three ROAD simulations not used for calibration (events 3,6, and 8); (2) the HILL simulations;

Table 6.2. The ROAD12457 parameter set following calibration.

Parameter†	Description	Value	Units	Calculated/estimation method
TH	Thickness of soil layer 1	0.15	m	Field examination of soil profile
$K_{s,1}$, $K_{s,2}$	Saturated hydraulic conductivity	4.05	mm h^{-1}	Reduced from Table 6.1 value during calibration
C_vK_s	Coefficient of variation for K_s	0.61	-	Table 6.1
G_1	Layer 1 capillary drive	15	mm	Reduced during calibration from value in Rawls et al. (1982) for sandy clay loam.
G_2	Layer 2 capillary drive	36	mm	Same as for G_1
λ	Pore size distribution index	0.25	-	Rawls et al. (1982) for sandy clay loam
SAT	Initial relative saturation	0.47	-	Calculated as pre-storm soil wet ness divided by wetness at saturation
f_1, f_2	Layer 1 and 2 porosity	0.43	m^3 m^{-3}	Estimated at soil wetness at saturation
c_f	Rain splash coefficient	261.6††	s m^{-1}	Determined during calibration from estimated value (Figure 6.2)
c_g	Soil cohesion coefficient	0.0196††	-	Same as for c_f
RELIEF	Average microtopo-graphic relief	100	mm	Field measurements
SPACING	Average microtopo-graphic spacing	0.40	m	Field measurements
ρ_s	Particle density	2.55	Mg m^{-3}	Table 6.1
MAN	Manning's n roughness coefficient	0.015	$ft^{1/6}$	Comparison of field conditions with values in Morgan (1995)
INT	Interception depth	0	mm	Field measurements
ROCK	Volumetric rock fraction of the soil column	1	%	Field measurements

† Subscripts refer to an upper (1) or lower (2) soil layer utilized by the infiltration subcomponent.

†† For dynamic erosion (DE) modeling, c_f = 139.95 and c_g = 0.0105.

and (3) the WET simulations. The first dataset allowed validation under initial conditions similar to those of ROAD12457. The HILL dataset allowed validation on a steeper road section, with drier antecedent moisture conditions and different surface preparation than ROAD12457. Surface preparation refers to events/phenomenon contributing to availability, detachment, or entrainment of surface material (e.g., vehicular traffic, maintenance, mass wasting, Chapter 5). The WET dataset allowed validation during typical wet season conditions, i.e., when high initial soil moisture content produces rapid runoff generation and prior HOF events have reduced loose surface sediment availability. One validation goal was to identify parameters sensitive to physical differences related to topography, soil moisture, and surface preparation.

6.4 RESULTS

6.4.1 Model calibration

Table 6.3 lists rainfall intensity, storm duration, plot slope, an index of initial soil moisture (SAT in Table 6.2), runoff (RO), total sediment output (S), and total sediment concentration (C) for rainfall simulation events modeled during KINEROS2 calibration and validation experiments. Events are referred to by simulation type (i.e., ROAD, HILL, or WET) and one or a string of digits indicating a specific simulation number, or referring to the median values of several sites (e.g., ROAD368, refers to the median of ROAD simulations 3, 6, and 8).

Median instantaneous discharge (Q_t), sediment transport (S_t), and concentration (C_t) values for calibration event ROAD12457 are shown with KINEROS2-predicted values in Figure 6.1. Following parameter optimization, errors in predicted total RO and S were ≤ 0.5 % (Tables 6.4-6.5). The Q_t time series is well-modeled by KINEROS2 (RMSE = 14%; CD ≈ 0.80; R2 = 0.84); modeled peak discharge is underestimated by only ≈ 3% (Figure 6.1a). Substantially higher prediction error exists for instantaneous and peak S_t and C_t (Tables 6.5-6.6). The sediment peak in the first 20 min of the event, and the corresponding high C_t values, are not predicted by KINEROS2 (Figure 6.1 b,c). RMSE for predicted S and C are > 50 and 100%, respectively; and S_t and C_t peaks are underestimated by > 41 and 78%, respectively. Only during the middle third of ROAD12457 is S_t well-described by KINEROS2. Low E_{total} for KINEROS2-predicted S results from a balance of under-prediction of S_t at the beginning of the event, and over-prediction toward the end.

Table 6.3. Summary of event characteristics and output for rainfall simulation experiments used for validation of KINEROS2.

	Event/plot variables†				Total outputs		
Sim id	r ($mm\ h^{-1}$)	Duration (min)	Slope ($m\ m^{-1}$)	SAT	RO (mm)	S (kg)	C ($kg\ m^{-3}$)
ROAD1	91	61.2	0.14	0.54	75.7	5.0	16.7
ROAD2	110	60.8	0.14	0.53	98.4	6.2	16.0
ROAD3	94	61.5	0.13	0.40	72.2	5.6	19.7
ROAD4	107	61.4	0.13	0.26	95.2	9.4	24.9
ROAD5	100	61.2	0.14	0.47	84.1	4.4	13.2
ROAD6	116	60.6	0.18	0.43	95.0	5.4	14.3
ROAD7	108	61.2	0.18	0.41	91.5	13.5	37.3
ROAD8	112	60.9	0.17	0.38	96.1	4.6	12.1
ROAD12457	107	61.2	0.14	0.47	91.5	6.2	16.7
ROAD368	112	60.9	0.17	0.40	95.0	5.4	14.3
HILL1	108	46.6	0.24	0.25	61.2	13.3	57.5
HILL2	131	47.0	0.24	0.25	86.4	15.7	48.3
HILL3	92	46.4	0.29	0.27	56.7	17.0	79.6
HILL4	123	46.2	0.29	0.12	76.7	15.7	54.3
HILL	115	46.5	0.26	0.25	69.0	15.7	55.9
WET1	90	10.9	0.14	0.74	12.6	0.78	15.6
WET2	100	11.3	0.14	0.78	12.3	0.79	16.2
WET3	93	10.8	0.13	0.74	9.8	0.54	14.1
WET4	102	10.5	0.13	0.74	14.8	2.04	34.8
WET5	113	10.5	0.14	0.84	16.3	0.57	8.8
WET6	127	10.3	0.17	0.82	18.3	0.66	9.1
WET7	118	10.7	0.18	0.84	14.4	0.96	16.8
WET8	120	10.5	0.17	0.85	13.3	0.33	6.2
WET	108	10.6	0.14	0.80	13.9	0.72	14.8

†r is rainfall intensity; Duration is total simulation time; SAT is initial relative saturation; RO, S, and C are total runoff, sediment output, and concentration.

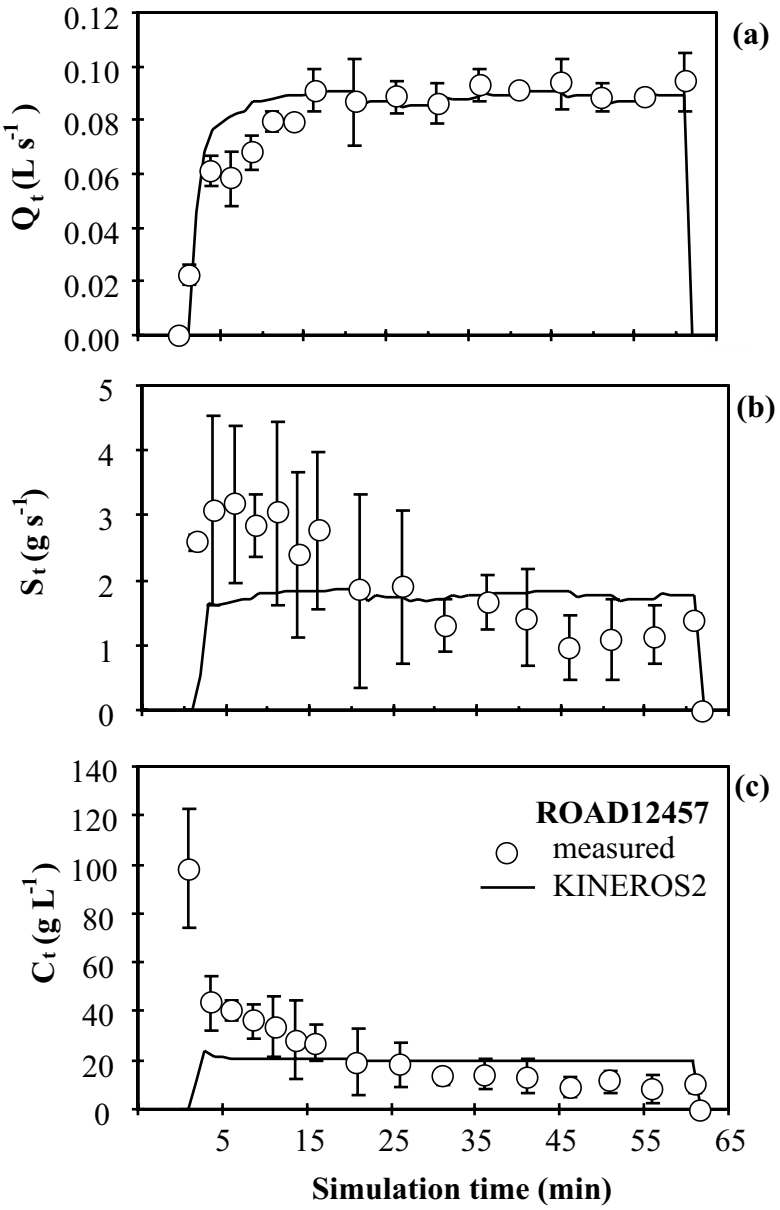

Figure 6.1. Comparison of (a) discharge (Q_t), (b) sediment transport rate (S_t), and (c) concentration (C_t) between measured rainfall simulation data (circles) used in model calibration and KINEROS2-predicted values. Measured values are medians from ROAD events 1,2,4,5, and 7; error bars are ± one median absolute deviation about the median. KINEROS2 was run using the calibration parameter set (Table 6.2).

Table 6.4. Errors between observed and KINEROS2-predicted runoff.

	Observed (mm)	Predicted (mm)	E_{total}† (%)	E_{peak} (%)	RMSE (%)	CD (r^2)	ME (R^2)
ROAD12457††	91.5	91.1	-0.47	-3.44	14.0	0.82	0.84
ROAD368	95.0	91.2	3.84	-2.22	23.4	0.80	0.65
ROAD3	72.2	80.9	12.03	-1.96	29.6	0.87	0.52
ROAD6	95.00	103.1	8.47	34.21	62.5	0.37	-1.15
ROAD8	96.2	100.0	4.02	-9.46	22.6	0.92	0.68
HILL	69.0	74.2	7.52	-1.11	17.6	0.79	0.81
WET	13.9	16.5	18.98	0.43	21.5	0.67	0.85

† E_{total} is error in total output estimate (Eq. 6.6); E_{peak} is error in peak estimate (Eq. 6.7); RMSE is root mean squared error (Eq. 6.8); CD is coefficient of determination (Eq. 6.9); ME is model efficiency (Eq. 6.10).

†† Events modeled using dynamic erodibility methodology have same discharge values as event reported here.

Table 6.5. Errors between observed and KINEROS2-predicted sediment output.

	Observed (mm)	Predicted (mm)	E_{total}† (%)	E_{peak} (%)	RMSE (%)	CD (r^2)	ME (R^2)
ROAD12457††	6.22	6.23	0.22	-41.2	51.6	1.64	0.77
ROAD368	5.39	7.92	46.8	-41.9	87.1	0.72	0.44
ROAD3	5.63	4.96	-11.9	-68.5	75.9	2.14	0.61
ROAD6	5.39	9.83	82.3	-26.3	117.9	0.76	0.09
ROAD8	4.63	8.88	92.1	-36.0	96.8	0.51	0.32
HILL	15.69	10.66	-32.1	-67.0	70.1	3.22	0.62
WET	0.72	1.25	73.4	56.2	84.0	0.34	0.38
ROAD12457 DE††	6.22	6.47	4.04	-3.93	35.4	1.11	0.89
HILL DE	15.69	14.64	-6.69	-21.9	44.6	0.97	0.85
ROAD3 DE	5.63	5.23	-7.07	-61.3	71.4	1.55	0.66
ROAD6 DE	5.39	8.07	49.6	-39.9	92.3	0.91	0.44
ROAD8 DE	4.63	6.84	48.0	-26.9	64.5	0.63	0.70

† E_{total} is error in total output estimate (Eq. 6.6); E_{peak} is error in peak estimate (Eq. 6.7); RMSE is root mean squared error (Eq. 6.8); CD is coefficient of determination (Eq. 6.9); ME is model efficiency (Eq. 6.10).

†† Events modeled using dynamic erodibility methodology have same discharge values as event reported here.

††**Table 6.6. Errors between observed and KINEROS2-predicted sediment concentration.**

Sim id	Observed ($kg\ m^{-3}$)	Predicted ($kg\ m^{-3}$)	E_{total}† (%)	E_{peak} (%)	RMSE (%)	CD (r^2)	ME (R^2)
ROAD12457††	16.7	20.1	20.6	-78.4	104.8	3.05	0.38
ROAD368	14.3	25.5	78.3	-69.1	102.1	1.44	0.49
ROAD3	19.7	18.0	-8.36	-77.6	118.6	3.03	0.32
ROAD6	14.3	28.1	95.9	-82.7	154.9	3.68	0.23
ROAD8	12.1	26.1	115.2	-72.5	84.2	1.72	0.60
HILL	56.0	44.9	-19.7	-84.5	116.5	7.94	0.29
WET	14.8	22.3	50.4	51.6	88.4	0.45	0.35
ROAD12457 DE††	16.7	20.9	25.1	-64.7	97.0	2.04	0.47
HILL DE	56.0	61.7	10.3	-61.9	103.4	2.23	0.44
ROAD3 DE	19.7	19.0	-3.33	-67.2	113.3	2.09	0.38
ROAD6 DE	14.3	23.0	60.8	-76.9	141.5	3.24	0.36
ROAD8 DE	12.1	20.1	65.8	-63.0	62.8	1.88	0.78

† E_{total} is error in total output estimate (Eq. 6.6); E_{peak} is error in peak estimate (Eq. 6.7); RMSE is root mean squared error (Eq. 6.8); CD is coefficient of determination (Eq. 6.9); ME is model efficiency (Eq. 6.10).

†† Events modeled using dynamic erodibility methodology have same discharge values as event reported here.

6.4.2 The ROAD12457 parameter set

The calibration stage produced a parameter set (ROAD12457) for use during model validation. In the ROAD12457 parameter set (Table 6.2), the soil is modeled as a two-layer column, with the upper layer having thickness (TH) 0.15 m. Layer one depth was determined from field profile observations and bulk density measurements (Table 6.1). Numeric subscripts in Table 6.2 refer to upper (1) or lower (2) soil layers (depth is not specified). The parameter specification approach initially used field-measured values; changes having physical basis were then allowed during calibration. For example, field-measured K_s (15.0 mm h^{-1}) was replaced by 4.1 mm h^{-1}, a value slightly less than the rainfall simulation-derived estimate of steady state infiltration (5.4 mm h^{-1}, Table 4.2). The original coefficient of variation for the K_s data was retained for C_vK_s. Capillary drive values G_1 and G_2 for the highly disturbed road surface were reduced by an order of magnitude during calibration from recommended values for sandy clay loam soils (Rawls et al., 1982). Pore size distribution index (λ) corresponds to that of sandy clay loam soil in Rawls et al. (1982). Initial soil saturation (SAT) was calculated as initial soil moisture divided by soil moisture at saturation (Table 6.1). RELIEF refers to vertical changes in microtopography over the prescribed SPACING interval. Porosity (ϕ) and particle density (ρ_s) were determined *in situ* (Table 6.1).

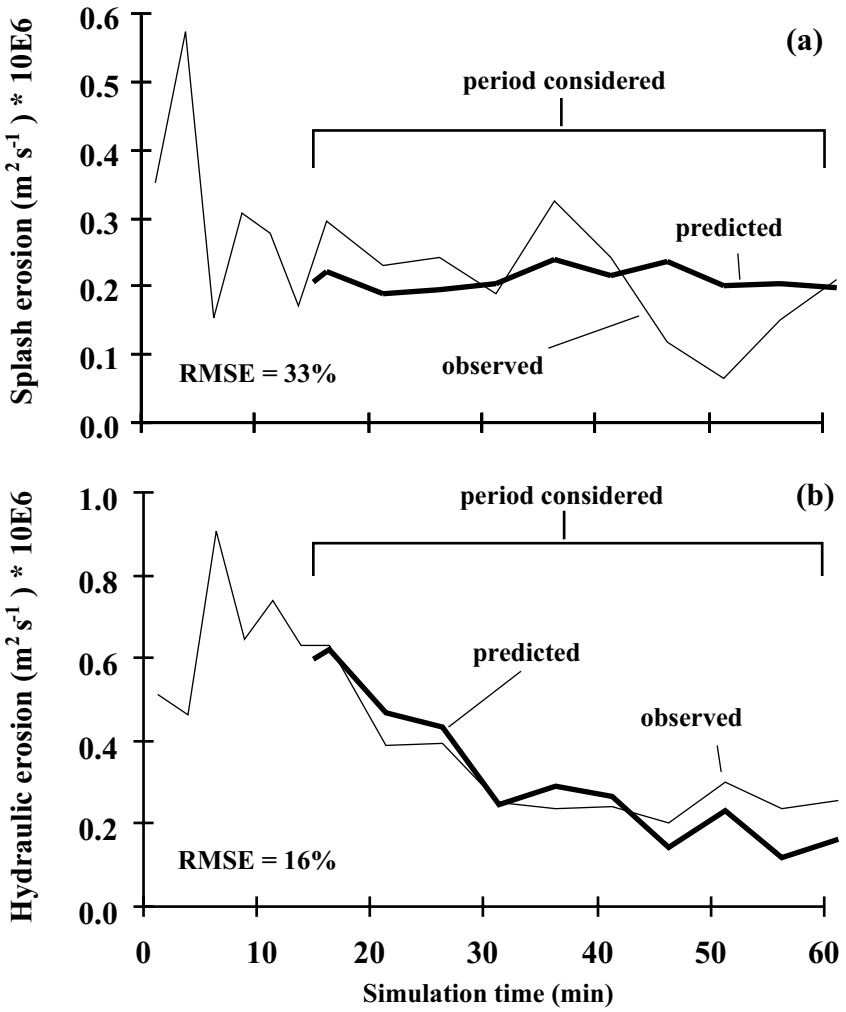

Figure 6.2. Comparison of predicted and observed (a) splash (Eq. 4.1) and (b) hydraulic (Eq. 6.5) erosion for ROAD rainfall simulation events 1,2,4,5, and 7. Coefficients c_f and c_g in Eqs. 4.1 and 6.5 were chosen to reduce the root mean squared error between predicted and observed values over the final 50 min of simulation, following the initial flush of loose material. These optimal values were then used as initial estimates for KINEROS2 c_f and c_g parameters prior to model calibration.

First-guess values of c_f and c_g were assigned by solving Eq. 4.1 and 6.5, respectively, using observed discharge, concentration, and water depth data from Experiment II (Chapter 4). Values of c_f and c_g were selected that produced the lowest RMSE between equation-predicted and

observed splash and hydraulic erosion during the final 45-min of the ROAD rainfall simulation events 1,2,4,5, and 7 (Figure 6.2). The initial 15-min period containing the flush of loose surface material was not included in the calculation, because we wanted the erodibilities to be that of the true road surface. The final values shown in Table 6.2 were determined during model calibration by reducing the initial c_f and c_g values equivalently, to retain the proportionality between splash and hydraulic erosion.

6.4.3 ROAD validation

The results of the ROAD12457 parameter set validation using ROAD events 3, 6, and 8 are shown in Figures 6.3 and 6.4, and Tables 6.4-6.6. Runoff was slightly over-predicted for all events and RMSE error values were higher than those during calibration. During events 3 and 8, total variation in RO was better described than during ROAD12457 (CD = 0.87 and 0.92, respectively); however, model efficiency (R^2) values were lower. Event 6 was poorly modeled, as indicated by comparatively high values for E_{peak} and RMSE, low CD, and a negative value for model efficiency (Table 6.4). Error values for the median ROAD368 event were reasonable. Total RO was under-predicted by only about 4%, E_{peak} was lower than during calibration, and CD was nearly identical. RMSE and R^2 were higher for ROAD368 compared with ROAD12457 because of over-prediction during the first 20 min of simulation.

KINEROS2 over-predicted total sediment transport for ROAD368 by 47%, but under-predicted median peak values by ≈ 42% (Table 6.5; Figure 6.4). For the individual events, E_{total} ranged from -12% to 92%, RMSE values were > 75%, and R^2 was as low as 0.09. As in the calibration simulations, over-prediction of S_t resulted from inability of KINEROS2 to predict the initial flush and subsequent decline in sediment output over time. Unlike the calibration phase, initial under-prediction was not enough to compensate for over-prediction at the end of the events. As a result, errors in predicted concentration values were generally high (Table 6.6).

6.4.4 HILL validation

Simulation of the median HILL time series using the ROAD12457 parameter set is shown in Figure 6.5. The runoff hydrograph was predicted reasonably, with E_{total} = 7.5% and RMSE ≈ 18%

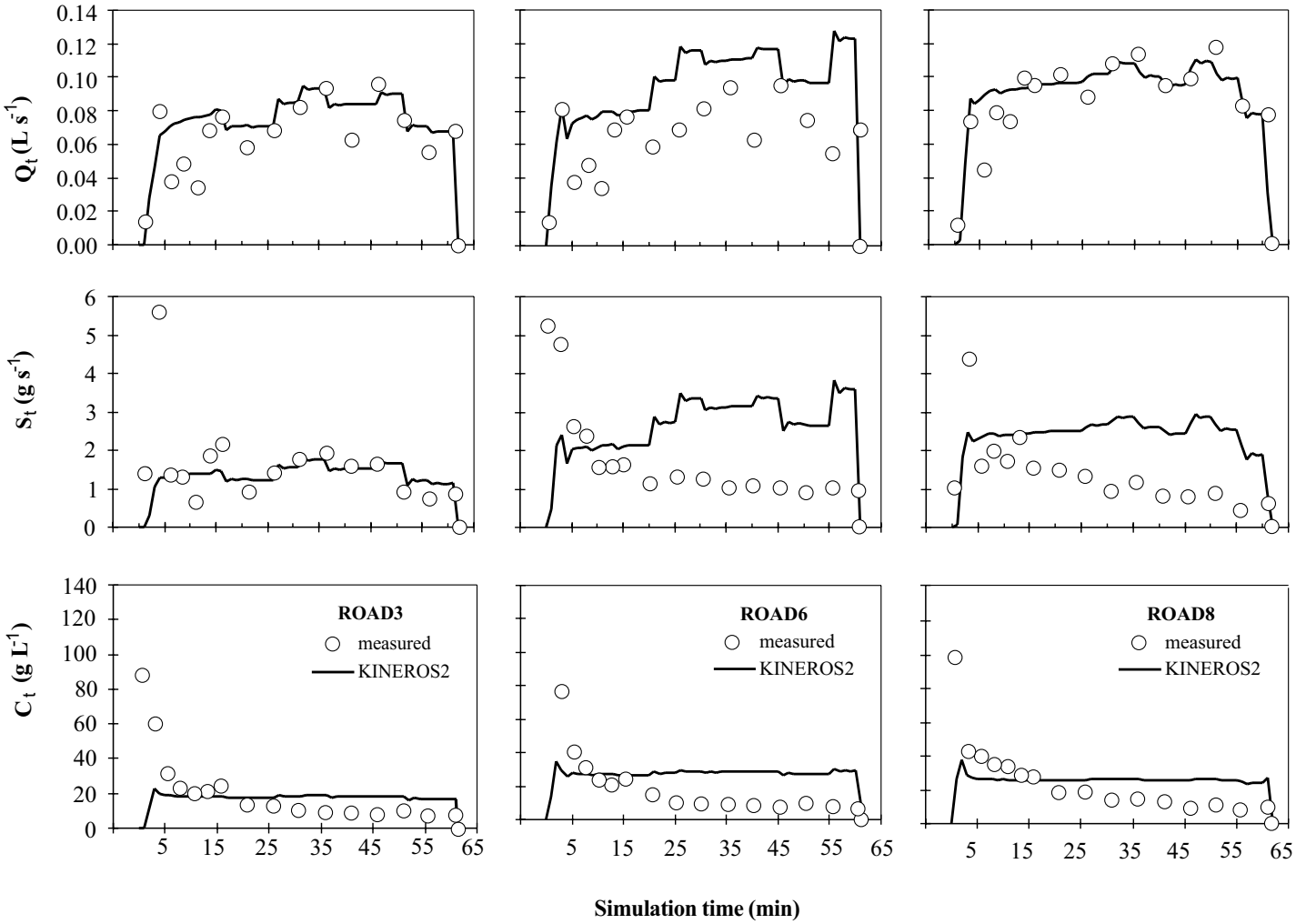

Figure 6.3. Comparison of discharge (Q_t), sediment transport rate (S_t), and concentration (C_t) between measured rainfall simulation data (circles) and KINEROS2-predicted values for ROAD events 3,6, and 8. KINEROS2 results were obtained using the calibration parameter set (Table 6.2).

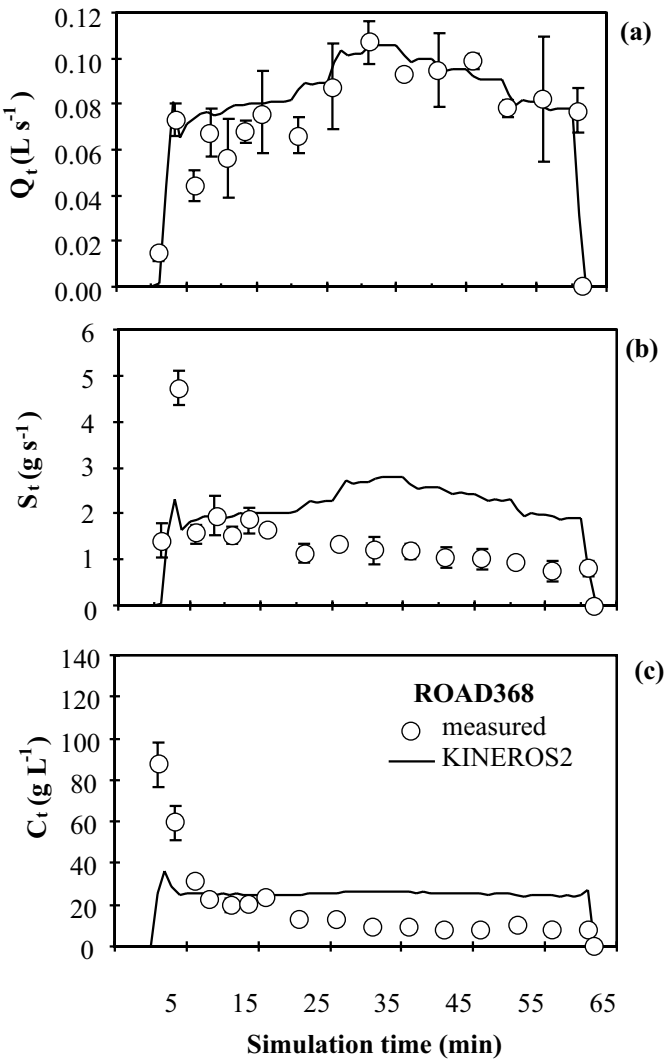

Figure 6.4. Comparison of (a) discharge (Q_t), (b) sediment transport rate (S_t), and (c) concentration (C_t) between measured rainfall simulation data (circles) and KINEROS2-predicted values for ROAD368. Measured values are medians from ROAD events 3,6, and 8; error bars are ± one median absolute deviation about the median. KINEROS2 results were obtained using the calibration parameter set (Table 6.2).

(Table 6.4). CD and ME for the predictions were only slightly lower than those during ROAD12457calibration. In contrast to over-predicting S during ROAD368 validation, KINEROS2 under-predicted sediment transport for HILL. Total error in S and C were ≈ -32% and

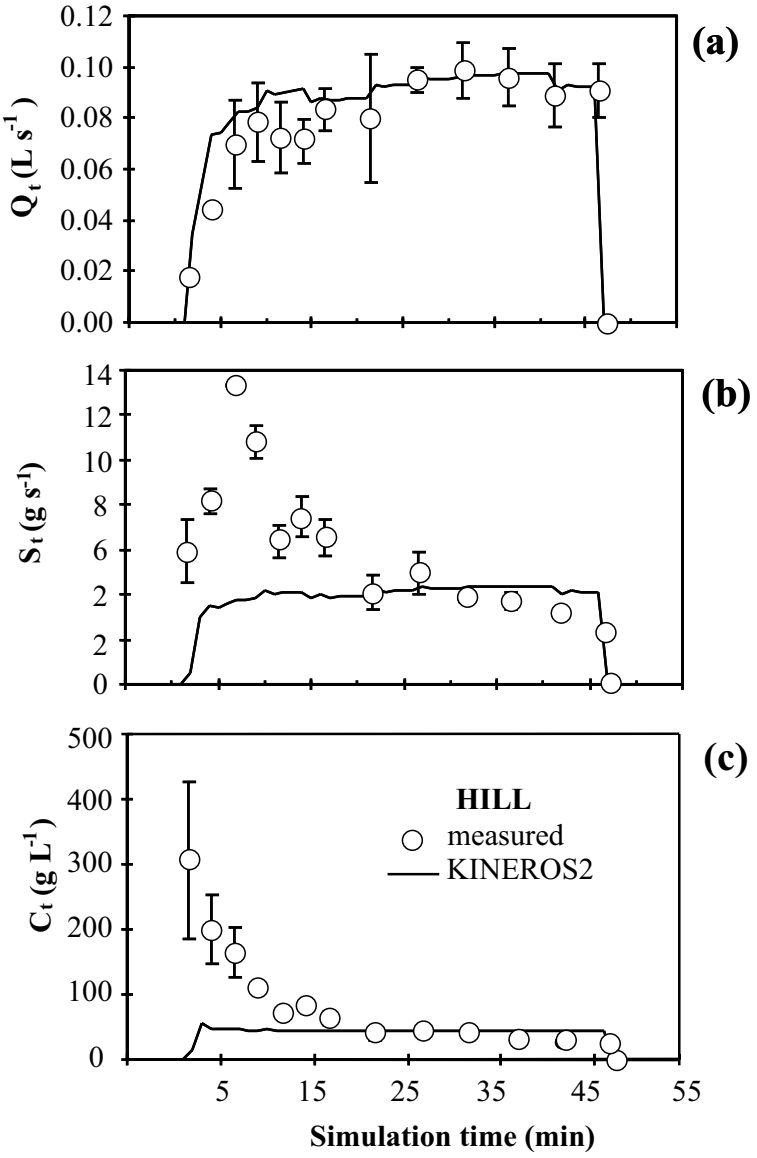

Figure 6.5. Comparison of (a) discharge (Q_t), (b) sediment transport rate (S_t), and (c) concentration (C_t) between measured rainfall simulation data (circles) and KINEROS2-predicted values for the HILL validation. Measured values are medians from four HILL events; error bars are ± one median absolute deviation about the median. KINEROS2 results were obtained using the calibration parameter set (Table 6.2).

-20%, with much larger errors in peak estimates (Tables 6.5, 6.6). RMSE for HILL-predicted S was ≈ 70%, but was smaller than that for ROAD368; RMSE in the C prediction was again greater than 100%.

6.4.5 WET validation

Wet validation results are shown in Figure 6.6 and Tables 6.4-6.6. Predicted discharge was ≈ 19% higher than the observed median value. Much of this error results from over-prediction during the first 5 min of this short event, for which there were few data points for evaluation of model performance. The error in peak output was less than 1%; and model efficiency R^2 was higher than that of the calibration event. Total sediment transport was over-predicted by ≈ 73% on this wet

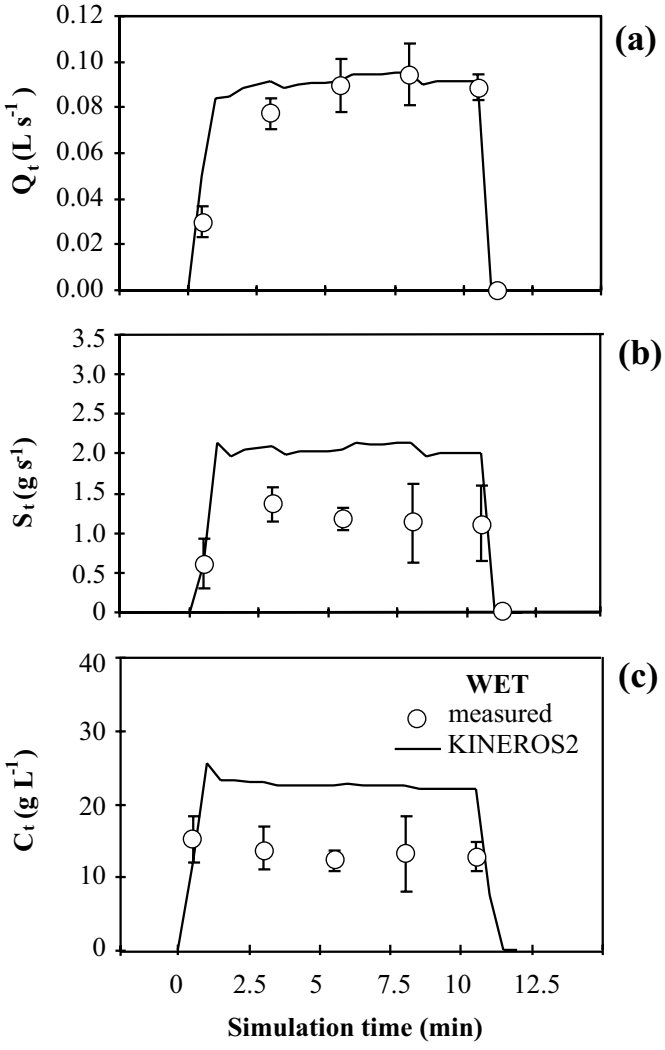

Figure 6.6. Comparison of (a) discharge (Q_t), (b) sediment transport rate (S_t), and (c) concentration (C_t) between measured rainfall simulation data (circles) and KINEROS2-predicted values for the WET validation. Measured values are medians from 8 WET events; error bars are ± one median absolute deviation about the median. KINEROS2 results were obtained using the calibration parameter set (Table 6.2).

surface, where most loose sediment was removed in the previous simulation (Table 6.5, Figure 6.6b). Model efficiency for the S prediction was the lowest of all median-based validation sets.

6.5 DISCUSSION

6.5.1 Soil moisture

Experimental conditions for ROAD368 were similar to those under which the calibration parameter set was produced. HILL sites had greater slope and lower soil moisture content than the ROAD12457 site; and WET had higher initial soil moisture (Table 6.3). Runoff was well predicted in ROAD368 and HILL validation tests (E_{total} was within ± 7.5%). Thus, KINEROS2 handled slope and soil moisture changes on these surfaces. Runoff during the WET validation was over-predicted by ≈ 19%. In comparison, the WEPP model used by Elliot et al. (1995) over-predicted total event runoff values on 46.4 m^2 plots by 3-6% for dry, wet, and very wet soil moisture conditions. Much of the error for our WET simulations is related to the small time series for the observed data during the 10-min rainfall simulations (n = 5 time steps).

6.5.2 Sediment availability

Sediment transport was poorly predicted for ROAD368, HILL, and WET events using the ROAD12457 calibration parameter set (E_{total} = 47, -32, and 73%, respectively). Although, under-prediction of S for HILL could be related to higher erosive energy of hydraulic flow on the steeper slope, we believe the predominant cause for poor prediction at all sites is differences in availability of loose surface material. During the ROAD12457 rainfall simulation experiments, most sediment removed up to some time t was loose, previously detached material. In contrast, sediment output for the WET simulations was comparatively low because most loose material was removed on the previous day of rainfall simulation. KINEROS2 over-predicted S because the erosion parameters were determined for a road having a loose layer of surface material, i.e., the conditions for the ROAD simulations. Similarly, Elliot et al. (1995) reported WEPP did not predict declines in erosion rates with successive storms.

KINEROS2 under-predicted S on HILL plots because these surfaces have more loose material than the ROAD12457 plots. Large quantities of loose surface material on the HILL

plots result from higher vehicle-detachment rates on this comparatively steep surface. The sediment depth survey showed the HILL road section contained 3 times more loose sediment than the ROAD plots (5.4 versus 1.8 kg m^{-2}). HILL total sediment transport is best modeled by KINEROS2 using c_f and c_g values 3.55 times greater than those in the ROAD12457 calibration parameter set (not shown), suggesting that S is largely a function of sediment availability. Disparity in sediment transport between ROAD12457 and ROAD368 is related to high spatial variability in sediment depth on the road surface resulting from variability in interstorm preparation processes, including mass wasting, road maintenance, and traffic.

6.5.3 Dynamic erodibility

In PKEW the road surface at any given time consists of a compacted, resilient surface underlying a layer of loose material of finite depth. Because the supply of road surface sediment is dynamic, road sediment transport response varies both during and between events. Sediment production is often high, such as following a long dry period where traffic has generated a substantial layer of loose material. In general, roads receiving high traffic volumes tend to have high sediment production rates (cf., Reid and Dunne, 1984). Sediment transport is initially controlled by the ability of rain-affected surface flow to remove the loose surface layer, then by the ability to detach previously unavailable material from the compacted road surface. Both the underlying and loose material layers have unique erodibilities, with the loose layer generally being much more erodible. Thus, during a storm event, the road surface passes through two or more 'states' of erodibility. This dynamic erodibility can be represented by the following expression:

$$E_{road} = \begin{cases} E_2 & 0 \le d_{cum} \le c_2 d_s \\ E_1 & c_2 d_s \le d_{cum} \le c_1 d_s \\ E_0 & c_1 d_s < d_{cum} \end{cases} \tag{6.11}$$

where E_{road} is the dynamic erodibility (DE) of the composite road. For implementation in KINEROS2, E_{road} represents a scalar to multiply to baseline c_f and c_g parameters. The variable E_2 is the erodibility of the loose surface material at the start of a storm; E_0 is the baseline erodibility of the compacted road surface; E_1 is an intermediate erodibility value following the initial

flush of loose material; d_s is an index of sediment availability at the beginning of the storm (e.g., mass per area is used herein); c_1 and c_2 are values between 0 and 1; and d_{cum} is a value between 0 and d_s that represents cumulative removal of the surface material. E_{road} at any time t is related to pre-storm sediment availability (via d_s) and the amount of sediment removed during the current storm (d_{cum}). After d_{cum} surpasses thresholds defined by c_2 and c_1, E_{road} drops to that of a lower state. Implementation of the DE method requires empirical experimentation to determine values for c_1, c_2, E_0, E_1, and E_2. Sediment availability values, d_s, are also required for each storm modeled. As a modification to Eq. 6.11, any number of erodibility states could be specified; ultimately, it could be represented as a continuous function.

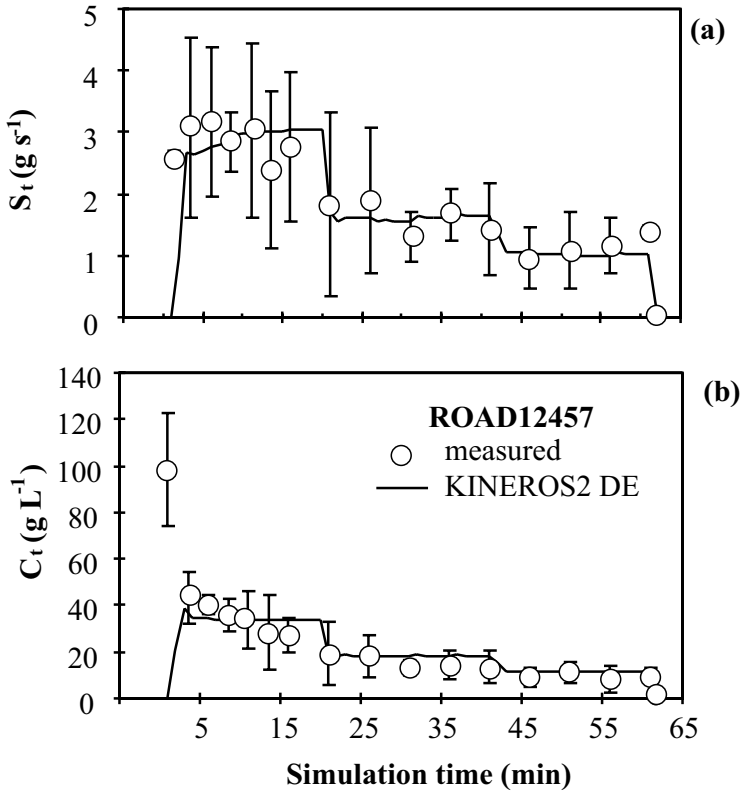

Figure 6.7. Modeling of (a) sediment transport rate (S_t) and (b) concentration (C_t) using the dynamic erodibility methodology (DE, Eq. 6.11). Measured values are medians from ROAD rainfall simulation events 1,2,4,5, and 7 (circles); error bars are ± one median absolute deviation about the median. KINEROS2 results were obtained using the calibration parameter set, but with c_f and c_g of 139.95 and 0.0105, respectively. Table 6.7 lists erodibility values and corresponding transition information used to implement DE modeling on this surface.

Figure 6.7 shows calibration results for KINEROS2 modeling of ROAD12457 using the dynamic erodibility method. Values for E_0, E_1, E_2, d_s, c_1, and c_2 in Eq. 6.11 were assigned as follows: 1. Baseline splash and hydraulic erodibility values for the underlying compacted road surface were established by optimizing KINEROS2 c_f and c_g parameters to minimize RMSE in predicted sediment transport for the 10-min WET simulations. Most loose material was removed from these plots on the previous day; therefore, WET sediment output resulted from detachment of new material from the compacted road surface. Optimization yielded values of 139.95 and 0.0105 for c_f and c_g, respectively.

2. Initial erodibility (E_2 = 3.4) was determined by increasing baseline c_f and c_g values to reduce RMSE for sediment transport during the initial sediment output peak for ROAD12457 (i.e., roughly the first 15 min). Optimization during the period 20-40 min determined E_1 to be ≈1/2 E_2. Finally, E_0 = 1 (i.e, the baseline erodibility values).

3. Sediment availability (d_s) was assigned the value determined during the dry-season cross-section survey (1.8 kg m^{-2}). Sediment transport data for ROAD simulations 1,2,4,5, and 7 suggested that the transitions between states E_2 and E_1, and then E_1 and E_0, occurred after ≈ 53% (c_2) and 84% (c_1) of the material, respectively, had been removed from the plots.

Using the DE method, RMSE for predicted S improved from 52 to 35% (Table 6.5). Although total error increased slightly to 4%, compared with < 0.5% error for the ROAD12457 calibration simulation, CD was reduced from 1.64 to 1.11; and ME R^2 increased to 0.89, indicating the DE-predicted values were better estimates of observed time series than were the KINEROS2-predicted values. The improved estimates of S produced better estimates of concentration; although, errors in the C estimate were still high, owing to poor estimation of the initial concentration spike following runoff generation. Temporal sediment response of ROAD12457 DE more closely describes the observed flush peak and the subsequent decline produced by the depletion of superficial material (Figure 6.7). Although more difficult to implement—for DE requires calibration and validation for all specified erodibilities—the dynamic erodibility method provides an improved approach for physically modeling removal of a loose road surface layer of finite depth. Figure 6.2 highlights the inability of Eq. 4.1 to predict road splash response using observed discharge and water depth data. Predicted splash stabilizes after a few min because water depth,

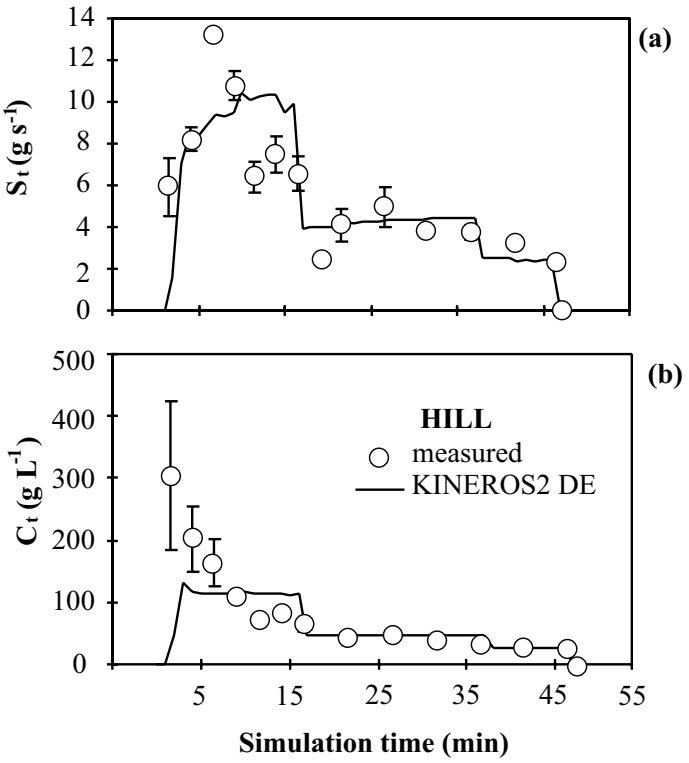

Figure 6.8. Modeling of (a) sediment transport rate (S_t) and (b) concentration (C_t) using the dynamic erodibility methodology (DE, Eq. 6.11). Measured values are medians from all HILL rainfall simulation events (circles); error bars are ± one median absolute deviation about the median. KINEROS2 results were obtained using the calibration parameter set, but with c_f and c_g of 139.95 and 0.0105, respectively. Table 6.7 lists sediment depth, erodibility values, and corresponding transition information used to implement DE modeling on this surface.

which is calculated as a function of runoff, stabilizes on the small-scale plots. Observed splash continues to decline because it is controlled by sediment availability, not increasing water depth, as modeled in Eq. 4.1. The DE methodology addresses the change in sediment availability by modifying model parameters for erodibility.

Results from a second calibration of the DE modeling technique using HILL data are shown in Figure 6.8. Initial erodibility (E_2 = 6.1) was determined by reducing RMSE of KINEROS2-predicted sediment transport during the initial flush of the HILL data. A value of E_1

= 1.9 was determined by optimizing model erosion parameters during the middle 20 min of the HILL simulations. The sediment cross-section survey value of 5.4 kg m^{-2} was used for d_s. Similar to the ROAD12457 DE simulation, c_1 and c_2 were assigned values 53 and 84%, respectively. The KINEROS2-predicted values for HILL DE are shown in Figure 6.8. Simulation using the DE methodology substantially improved the "goodness of fit" of the predicted S_t values: RMSE reduced from 70 to 45%, CD improved from 3.22 to 0.97, and model efficiency R^2 increased from 0.62 to 0.85. The CD value was the best of all simulations; and R^2 was second only to that of the ROAD12457 DE simulation.

6.5.4 General implementation of dynamic erodibility modeling

Using data from the ROAD12457 DE and HILL DE simulations, a predictive relationship between road sediment depth and the E_{road} values was developed (Figure 6.9). This relationship makes possible a general implementation of dynamic erodibility modeling using KINEROS2. Initial erodibility, E_2, is determined from the amount of sediment present on the road surface at the beginning of an event. In Figure 6.9, this value is represented by the thick line fitted through the val-

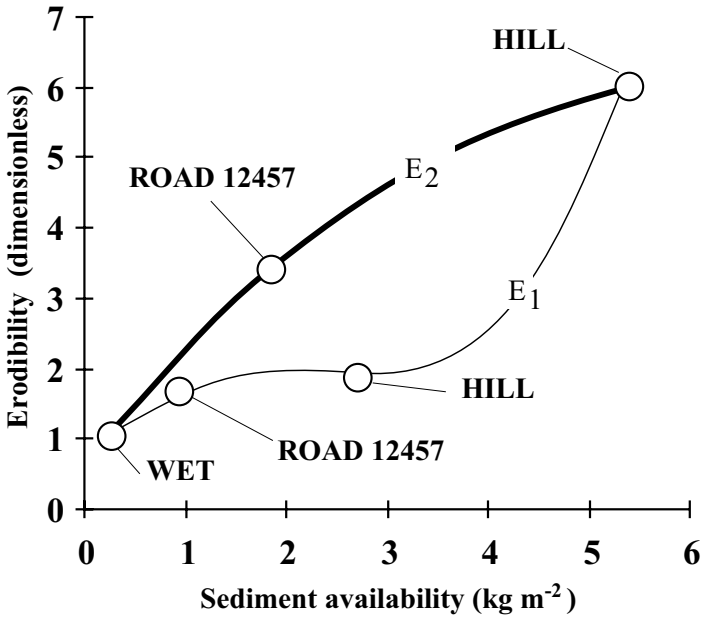

Figure 6.9. Relationship between surface sediment (mass per area) and erodibility values (E_1 and E_2) used to implement the dynamic erosion method (Eq. 6.11).

ues of E_2 used in the WET, ROAD12457 DE, and HILL DE events reported above. E_1 is calculated based on the amount of sediment remaining after some percentage of the initial sediment supply has been removed from the road (represented by c_2 above). The value of E_1 is determined by the thin lined fitted through the values of E_1 used in the WET, ROAD12457 DE, and HILL DE events above. Two unique functions are required for representing E_1 and E_2 because the relationship between erodibility and sediment availability changes following the initial flush of material. Erodibility is initially high, as sediment transport is limited by the transport capacity of the flowing water. After the flush, entrainment becomes more difficult as material must be moved into defined flow channels from upslope sediment sources or detached from the road surface. Armoring occurs as material becomes "lodged" in surface depressions, thereby reducing sediment output. For all DE events, baseline road erodibility, E_0, is 1. Values c_2 = 53% and c_1 = 84% can be used to define transition points between successive erodibility states, or the values could be determined from empirical data. Although based on limited rainfall simulation data, the prediction functions in Figure 6.9 represent a systematic method for estimating Eroad values using pre-storm estimates of road sediment depth.

Figure 6.10 shows the results from modeling ROAD events 3, 6, and 8 employing dynamic erodibility, with E_{road} values predicted from Figure 6.9. Table 6.7 lists sediment depth estimates and corresponding E_2, E_1, and E_0 values for the three modeled events. Predicted values of S and C are shown with prediction errors in Tables 6.5-6.6. Predicted discharge is the same for the DE event as for the standard KINEROS2 predictions presented above (Table 6.4). The DE imple-

Table 6.7. Parameter assignments for DE simulations.

Simulation	d_s† (kg m^{-2})	E_2	E_1	E_0	c_2	c_1
ROAD12457 DE	1.80	3.60	1.70	1	0.53	0.84
HILL DE	5.40	6.10	1.90	1	0.53	0.84
ROAD3 DE	1.62	3.00	1.61	1	0.53	0.84
ROAD6 DE	1.56	3.14	1.69	1	0.53	0.84
ROAD8 DE	1.33	2.59	1.46	1	0.53	0.84

†Variables are defined in Eq. 6.11; E_2, E_1, E_0, c_2, and c_1 are dimensionless.

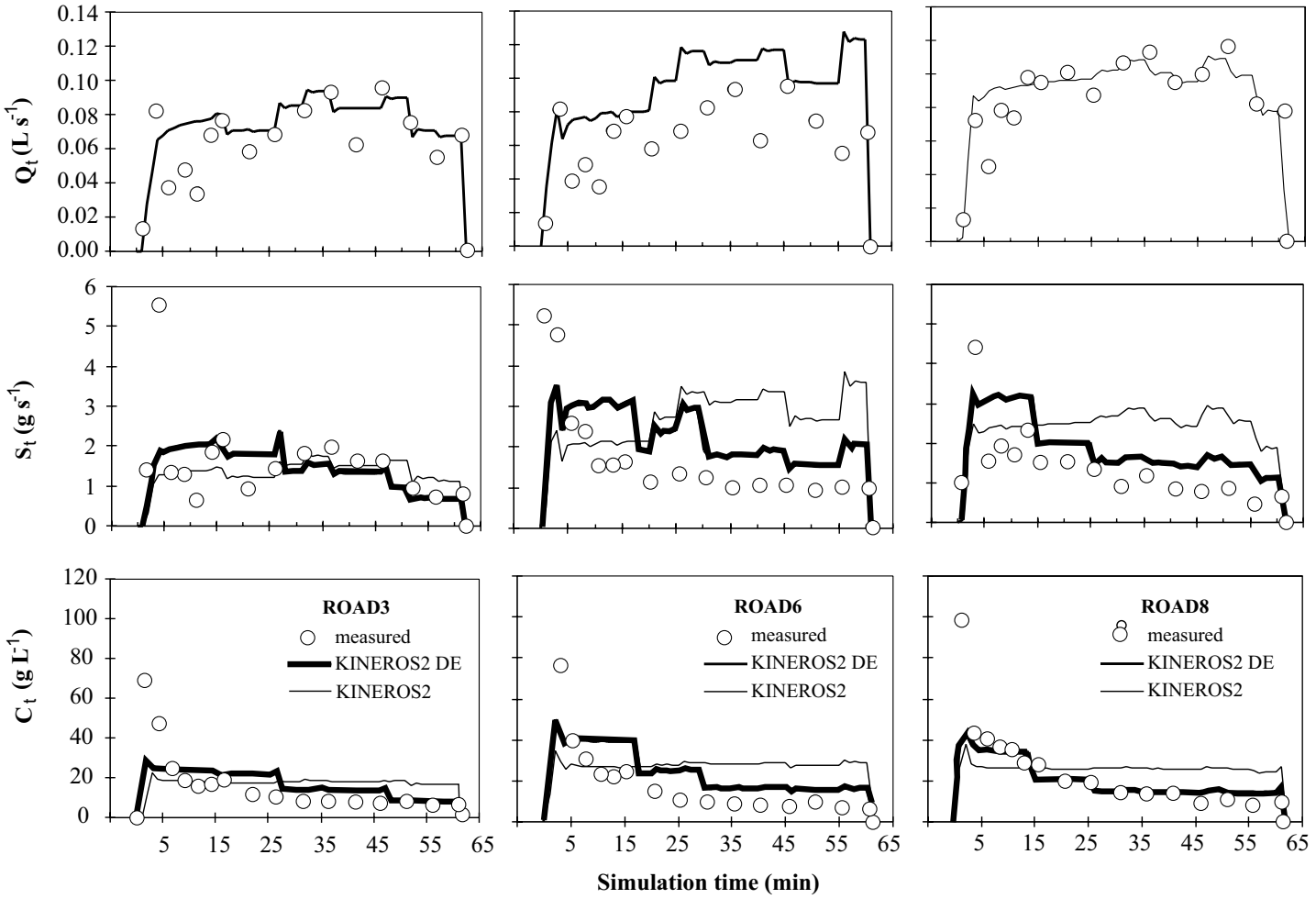

Figure 6.10. Modeling of discharge (Q_t), sediment transport rate (S_t), and concentration (C_t) using the dynamic erodibility methodology (DE, Eq. 6.11). Measured values are for ROAD events 3, 6, and 8 (circles). KINEROS2 DE results (thick line) were obtained using the calibration parameter set, but with c_f and c_g of 139.95 and 0.0105, respectively. Results from standard KINEROS modeling are indicated by thin lines. Table 6.7 lists sediment depth, erodibility values and corresponding transition information used to implement DE modeling on this surface.

mentation greatly improved sediment production estimates for all three events. E_{total} for ROAD events 6 and 8 reduced from 82 and 92% to < 50%. Improvements in RMSE and ME R^2 indicate a better fit of modeled instantaneous values. In general, concentration estimates also improved, although error values remained high, owing to the inability to predict initially high S_t values, associated with the flushing of sediment early in an event. These high S_t and C_t values might be better predicted by adding more erodibility states to the general DE model (Eq. 6.11). Finally, the over-prediction of ending S_t values in ROAD6 and ROAD8 suggest that the baseline erodibility E_0 value may be too high.

Both c_f and c_g were multiplied by E_{road}. One could argue that, based on the poor fit of predicted to observed splash erosion values in Figure 6.2 (as compared with the good fit of the predicted hydraulic erosion values), only the splash parameter c_g need be multiplied by E_{road}. However, as shown in Chapter 4, the splash erosion subcomponent was less than the hydraulic component at all times during the 60-min rainfall simulations on the Thailand road site. Adjusting only the c_g parameter would have violated this relationship. In other physical settings, unique scalar multipliers for c_f and c_g may be required.

6.6 SUMMARY

KINEROS2 can be parameterized to predict discharge hydrographs on small-scale plots under varying slope and soil moisture conditions. Temporal response in sediment transport on unpaved roads in the study area is best modeled when the superficial layer of loose sediment is explicitly considered. The dynamic erodibility approach introduced herein recognizes roads have more than one state of erodibility, which changes both between and during storm events. Initial road erodibility for any storm is related to availability of loose surface material, which is a function of interstorm sediment detachment processes. After removal of this upper layer, road erodibility is that of the compacted road surface itself. Using field rainfall simulation and KINEROS2 simulation data we developed a predictive relationship between sediment availability on the road surface and erosion parameter values needed to model erosion states. By implementing the DE methodology, sediment transport and concentration values, observed during small-scale road rainfall simulation events, were modeled more realistically.

7. Conclusion

7.1 SUMMARY OF RESULTS

Runoff generation and sediment transport are unique on roads, paths, and agricultural land-surfaces in PKEW (Chapter 3). Sediment transport on roads can be high when large amounts of loose material are present on the road surface before a rainfall event. Compacted roads, owing to low saturated hydraulic conductivities, produce runoff after relatively light rainfall. Because HOF is generated on unpaved roads during most rain events, the road system contributes to stream sedimentation throughout the rainy season. Horton overland flow generation within PKEW agricultural fields is rare during dry antecedent soil moisture conditions, except on path surfaces. Footpaths, like roads, accelerate runoff, thereby potentially enhancing in-field surface erosion by acting as source areas for surface runoff.

The partitioning of total erosion on roads into splash and hydraulic components varies over the course of a storm (Chapter 4). In PKEW, hydraulic erosion dominated total erosion at the beginning of an event. Energy associated with overland flow was adequate to transport loose material from the road surface, but once the sediment supply was depleted, rainsplash impact energy was needed to detach previously unavailable material from the compacted road surface. Thus, after 60 min of rainfall simulation, hydraulic and splash components were nearly equivalent. At the Hawaii site where the supply of loose material was limited, splash energy was needed to initiate erosion at the beginning of an overland flow event. The difference between the two sites supports that road erosion in a function of pre-storm availability of loose material, which itself is a function of cumulative surface preparation since the last overland flow event. Importantly, the greater the intensity of preparation (via traffic, maintenance, and mass wasting) and the greater the time interval between flushing events, the more erodible the road will be at the beginning of any given storm.

The road surface at any given time consists of a compacted, resilient surface that underlies a layer of loose material of finite depth. Vehicular activity and road maintenance activities are principal mechanisms generating loose material on the PKEW road surface between storms

(Chapter 5). Vechicle passes during rainstorms detach material that is immediately transported on the road by overland flow. In the absence of incision of tracks by surface flow, during-storm vehicle passes temporarily boost the erodibility of the road until the newly detached material is removed. Because the supply of road surface sediment is dynamic, sediment transport response varies during and between events. Temporal response in sediment transport on PKEW unpaved roads is best modeled when the superficial layer of loose material is explicitly considered (Chapter 6). Because the dynamic erodibility (DE) modeling methodology introduced in this work addresses the changing erodibility of the road surface, it produces a better prediction of road sediment transport and concentration time series than conventional techniques.

7.2 IMPLICATIONS OF THIS WORK

Because the DE modeling technique utilizes sediment depth estimates to determine pre-storm erodibility, it can be implemented in any watershed. It can additionally be used to model vehicle detachment of sediment during storm events provided a relationship between sediment availability and vehicle passes can be established. The versatility of the technique allows managers to quantify road impacts in a variety of environmental settings.

This dissertation extends current scientific knowledge of road versus agricultural impacts in montane mainland SE Asian watersheds. For example, in some basins, the road impacts may be greater than those of seemingly unstable agricultural activities. Some adverse effects of long-term cultivation on steep slopes may be attributed to overland flow generation on compacted path or trails. Because vehicle usage and maintenance activities contribute to road sediment production by generating entrainable surface material, stream sedimentation may in some instances be reduced by regulating traffic volume or improving maintenance practices. This work supports the need to properly design mountain roads to minimize slope angles and lengths, thereby reducing (1) the velocity of overland flow that erodes the road surface, and (2) runoff volumes exiting onto unprotected hillslopes or directly into stream channels. Finally, managers should understand that road development in some watersheds may not be a sustainable practice under any circumstance.

Plate 1

Plate 2

Plate 4

Plate 3

Plate 5

People of Pang Khum. (1) Alima, with other Lisu women at a spirit ritual; (2) Dailom (front) and other Karen friends on a hand-made cart; (3) Ataboo's father (back) and the near-mute Lisu basketmaker; (4) two Karen boys brandishing worldly icons that are now common in Pang Khum: a rose, symbolic of cash-based flower farming; and a football—the world's most popular sport; (5) the young Lisu father, Apon, and his son.

Plate 6

Plate 7

Plate 9

Plate 8

Plate 10

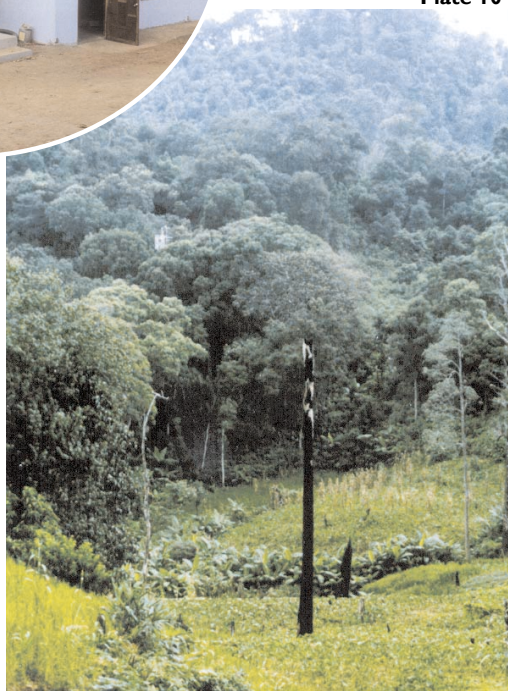

Pang Khum Experimental Watershed. (6) station 406, dedicated to measuring rainfall and road surface soil moisture change, located at the base of the monitored road section; RAS is measuring saturated hydraulic conductivity; (7) station 405, a weir constructed in the Loei stream at the mouth of PKEW; Asu is removing trapped sediment; (8) climate station 402 within Atachichi's upland rice field; (9) the research vehicle parked outside the fieldhouse in the Karen village at Pang Khum; (10) sensors of climate station 401 rest above a 17-m primary forest canopy.

Plate 11

Plate 12

Plate 14

Plate 13

Plate 15

Surface preparation and road-related erosion. (11) surface lowering in excess of 0.5 m was observed on the road from Pang Khum to Pa Pae in 1996; (12) repairing of roads with a tractor and blade usually occurs only on major arteries (the road to Pa Pae, November, 1998); (13) severe gullying on the road from Pa Pae (1996); (14) road sections often terminate at stream channels; thus, road sediment is transported directly to the stream network; (15) hand-filling of ruts is the dominant maintenance method on Pang Khum roads (Paluk and other Karen men, the road to Samoeng, 1999).

Plate 16

Plate 17

Plate 18

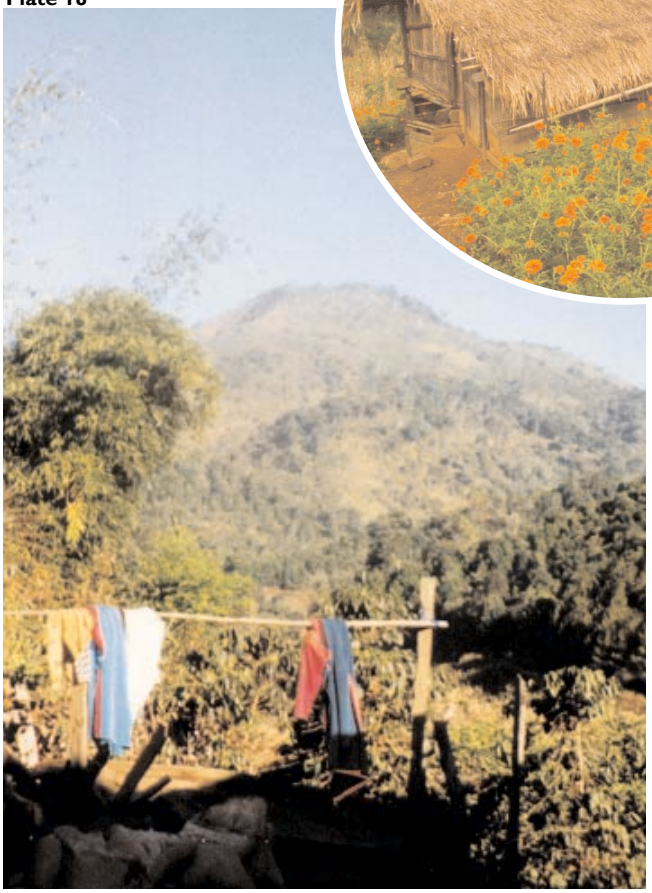

Plate 19

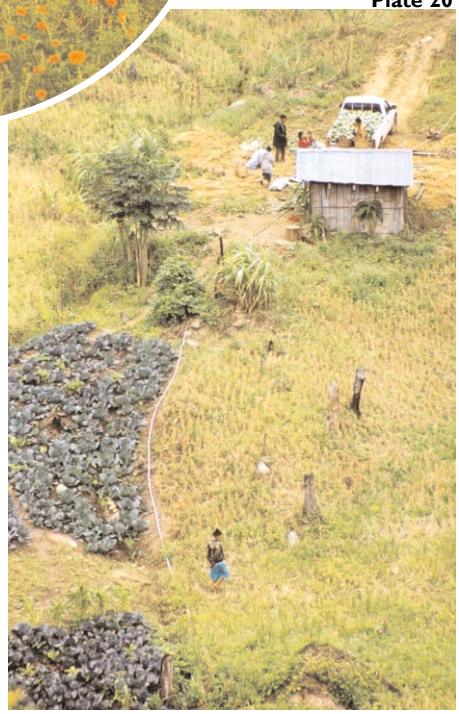

Plate 20

Landscape of Pang Khum. (16) a cleared hillslope awaiting planting; (17) furrows and paths within agricultural fields serve as source areas for overland flow and erosion; (18) Doi Mon Ang Ket, the highest point in PKEW, as seen from the Lisu village in Pang Khum; (19) flower field beside a Lisu field house; (20) mixed swidden field (cabbage, onions, corn, papaya, taro) and Lisu farmers during harvesting season (taken from station 401).

Plate 21

Plate 22

Plate 23

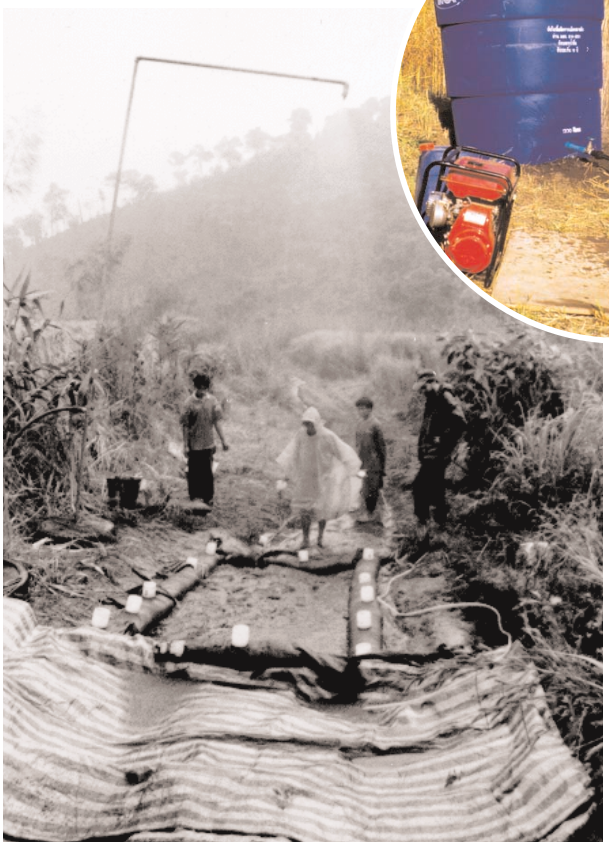

Plate 24

Plate 25

Rainfall simulator. (21) Lisu helpers prepare the FILL plots by filling ruts with material taken from the roadside; (22) Asu draining water from the collection ditch at the plot base, TRUCK simulations, February, 1999; (23) ADZ with pump, generator, and 1500 L supply tank, which was filled with water piped from a stream about 500 m upslope; (24) FILL simulation experiment, February, 1999; (25) practice run on an agricultural field.

Plate 26

Plate 27

Plate 28

Plate 30

Plate 29

Agricultural simulations. (26) Asu, Aluong, and Atachichi creating the NEW PATH treatment, 1998; (27) testing on the HOED FIELD treatment, 1998; (28) ADZ observing NEW PATH (left) and HOED (right) treatments during February, 1998 rainfall simulations; (29) Atachichi burning the rice field to create the UPLAND FIELD treatment, 1998; (30) FALLOW treatments, 1999.

Plate 31

Plate 32

Plate 33

Plate 34

Road-related rainfall simulations. (31) RAS collecting runoff from the SPLASH treatment during the SPLASH/NO SPLASH simulations, 1998; (32) RAS observing a large rut created during the TRUCK simulations, 1999; (33) Ayong driving a motorcycle through the simulation plot during the MOTORCYCLE simulations, 1998; (34) Disrupted road surface following four passes of the Isuzu Rodeo during TRUCK simulations, 1999; Assam looking on in amazement.

Plate 35

Plate 36

Plate 37

Lisu helpers. (35) Atachichi, ADZ, Asu, & Aluong taking measurements during the UPLAND FIELD simulations, 1998; (36) Lisu men and women laying the water pipeline that fed the simulator; (37) Asu and Atachichi showing they too can be hotshot researchers; (38) Asu seeing how one hotshot Western researcher measures up to Lisu standards.

Plate 38

APPENDIX A: Horizon soil properties at the 4 climate stations in PKEW

	H	Depth	ρ_b	ρ_p	K_s	ROOT	Sand	Silt	Clay	pH	OC	TN	CEC	BASE
		cm	Mg m^{-3}	Mg m^{-3}	mm h^{-1}	km m^{-3}	%	%	%	-	%	%	cmol$_c$ kg^{-1}	%
Station 401	A	15-20	1.15	2.44	82	12.0	48.8	16.4	34.8	4.7	3.02	0.19	15.5	22.0
	BA	40-50	1.19	2.46	154	4.0	42.3	19.5	38.2	4.3	1.39	0.24	9.0	14.1
	Bt1	90	1.31	2.58	228	0.3	39.2	18.6	42.2	4.2	0.63	0.06	6.6	11.1
	Bt2	150	1.38	2.48	-	0.8	38.3	22.8	38.9	4.4	0.01	0.07	5.8	10.4
	Bt3	200+	1.36	2.56	-	2.2	43.9	18.5	37.6	4.3	0.34	0.04	4.4	12.1
Station 402	Ap	15-20	1.12	2.46	273	4.3	52.2	26.8	21.0	4.7	2.52	0.18	12.7	26.4
	A2	35-40	1.08	2.50	-	0.0	52.0	21.9	26.1	4.6	1.82	0.15	12.0	33.7
	Bt1	60-70	1.22	2.48	113	0.0	50.9	18.4	30.7	4.9	0.70	0.09	7.6	50.1
	Bt2	100-110	1.44	2.48	89	0.0	47.2	19.2	33.6	4.9	0.30	0.05	6.3	51.4
	Bt3	150	1.50	2.53	-	0.0	46.8	23.7	29.5	4.7	0.45	0.04	6.4	50.1
	Bt4	200	1.56	2.55	-	0.0	48.2	20.3	31.5	5.0	0.23	0.04	5.8	52.8
Station 403	A	5-10	0.96	2.35	201	110.2	51.4	29.5	19.1	5.6	4.38	0.28	22.5	53.2
	AB	20-40	1.03	2.52	87	18.5	49.4	28.5	22.1	4.9	2.69	0.20	14.0	17.7
	Bt1	80	1.26	2.46	-	2.4	52.2	31.2	16.6	4.5	0.48	0.05	8.1	9.5
	Bt2	120	1.36	2.61	76	2.2	54.0	25.5	20.5	4.4	0.28	0.08	5.6	9.7
	Bt3	160	1.47	2.54	-	2.8	59.4	27.1	13.5	4.4	0.20	0.02	4.7	13.5
	Bw	200+	1.60	2.60	-	0.0	67.6	24.9	7.5	4.5	0.13	0.02	3.5	10.7
Station 404	A	5-15	0.87	2.34	113	40.7	49.5	23.7	26.8	4.7	5.12	0.41	26.8	7.9
	AB	30/45	1.03	2.38	79	14.5	45.6	21.6	32.8	4.4	2.20	0.15	11.2	3.8
	Bt1	100-110	1.31	2.51	38	4.2	45.5	19.0	35.5	4.5	0.64	0.06	5.5	5.8
	Bt2	150-160	1.56	2.54	-	1.0	48.6	14.9	36.5	4.6	0.15	0.04	3.7	3.8
	Bt3	200+	1.64	2.68	-	3.7	56.9	26.1	17.0	4.7	0.01	0.02	2.7	5.2

H is horizon; ρ_b is bulk density; ρ_p is particle density; K_s is saturated hydraulic conductivity; ROOT is root density, calculated from 45 cm^3 cores using a modified version of the method of Tennant (1975); OC is organic carbon; TN is total Nitrogen; CEC is cation exchange capacity; and BASE is base saturation. Sample size for most variables is one; n = 4 for K_s, ρ_b, and ROOT. For each site, the three K_s values were determined from disk permeameter measurements at depths of 0, 0.50, and 1.20 m. Clay minerals for all sites include: Kaolinite (small-moderate); Gibbsite (trace-small); Illite, Vermiculite, and interstratisfied 10 & 14A° (trace). Soil orders for the four sites are likely: Ultisol (401), Alfisol (402), Inceptisol (403), and Ultisol (404).

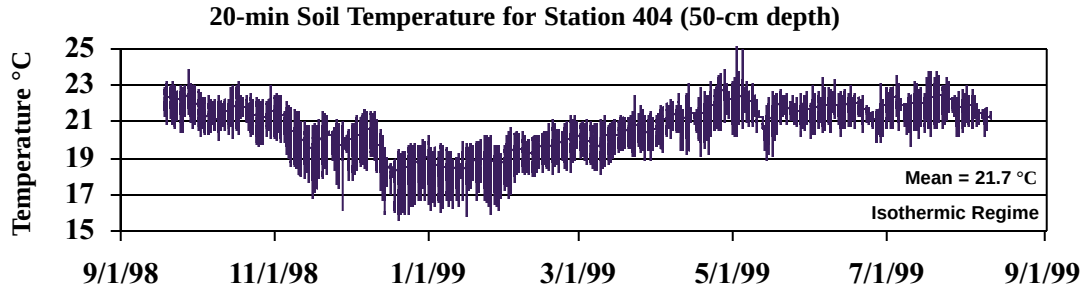

APPENDIX B: Rainfall and Streamflow in PKEW

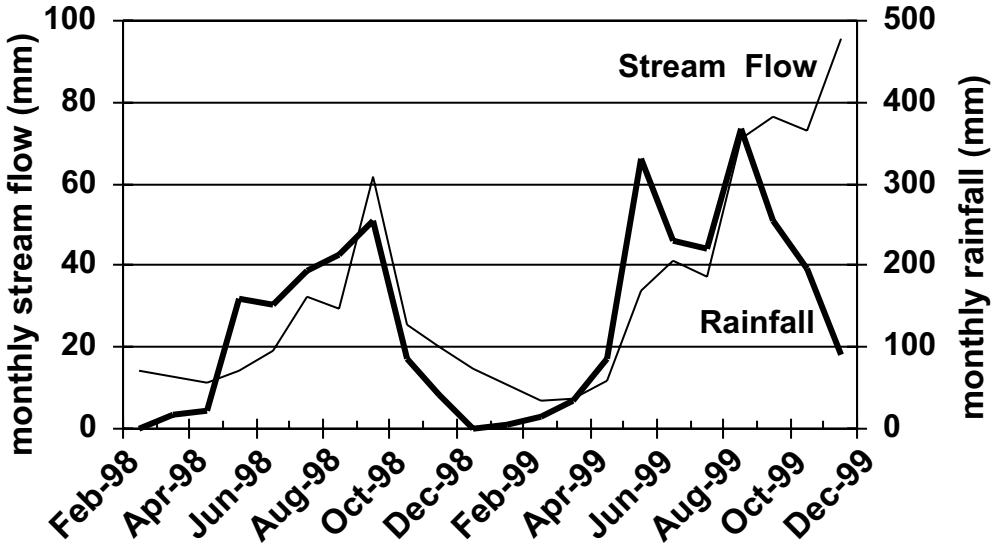

	1997	1998	1999	Median	
Jan	1	0	5	1	
Feb	0	0	16	0	
Mar	6	18	35	18	
Apr	21	22	87	22	
May	125	159	330	159	
Jun	125	151	231	151	
Jul	252	194	220	220	
Aug	298	214	367	298	
Sep	221	255	255	255	
Oct	201	86	197	197	
Nov	40	42	91	42	
Dec	0	0	0	0	
Annual	**1290**	**1141**	**1833**	**1290**	**(annual median)**
				1363	**(sum of monthly medians)**

Rainfall data are based on (a) six rain gauges within PKEW; (b) one rain gauge in Pang Khum village, approximately 3 km SE of PKEW; and (c) one rain gauge at a flower farm, approximately 4 km SW of PKEW. All gauges are tipping bucket, recording at one-min resolution.

Year 1999 was probably an unusually wet year; therefore, typical annual rainfall ranges from 1100-1300 mm.

References cited

Anderson, D.M., and MacDonald, L.H. 1998. Modelling road surface sediment production using a vector geographic information system. *Earth Surface Processes Landforms 23*: 95-107.

Anderson, H.W. 1975. Relative contributions of sediment from source areas and transport processes. In *Present and Prospective Technology for Predicting Sediment Yields and Sources*, 66-73. U.S. Dept. Agriculture, Ag. Research Service, ARS-S-40. Wash., D.C.

Baruah, P.C. 1973. An investigation of drop size distribution of rainfall in Thailand. Ph.D. dissertation. Asian Institute of Technology, Bangkok, Thailand.

Beschta RL. 1978. Long term patterns of sediment production following road construction and logging in the Oregon Coast Range. *Water Resources Research* 14(6):1011-1016.

Best, A.C. 1950. The size distribution of raindrops. *Quarterly Journal of the Royal Meterological Society* 76:16-36.

Bilby R.E., Sullivan K., and Duncan, S.H. 1989. The generation and fate of road-surface sediment in forested watersheds in southwestern Washington. *Forest Science* 35: 453-468.

Black T and Luce C. 1999. Changes in erosion from gravel surface forest roads through time. Proceedings of the International Mountain Logging and 10th Pacific Northwest Skyline Symposium, sponsered by Dept. Forest Engineering, Oregon State University and Internat. Union of Forestry. Research Org., Corvallis, OR March 28-April 1, 1999, pp 204-218.

Bradford, J. M. 1986. Penetrability. In Klute, A.(Editor), *Methods of Soil Analysis, Part 1*. Physical and Mineralogical Methods-Agronomy Monograph no. 9 (Second edition). American Society of Agronomy-Soil Science Society of America, Madison, WI, pp. 463-478.

Bruijnzeel, L.A. and Bremmer, C.N. 1989. Highland-lowland interactions in the Ganges Brahmaputra River Basin, A review of published literature. ICIMOD Occasional Paper 11, International Centre for Integrated Mountain Development, Kathamandu, Nepal.

Bryan, R. B. 1996. Erosional response to variations in interstorm weathering conditions. In: Anderson, M.G. and Brooks, S.M. (Editors), *Advances in Hillslope Processes*, Vol. 1. John Wiley & Sons Ltd., Chichester, England, pp. 589-612.

Bryan, R.B. and Poesen, J. 1989. Laboratory experiments on the influence of slope length on runoff, percolation and rill development. *Earth Surface Processes and Landforms* 14: 211-231.

Burroughs Jr., E.R., Watts, F.J., and Haber, D.F. 1984. Surfacing to reduce erosion of forest roads built in granitic soils. In O'Loughlin, C.L. and Pierce, A.J., (Editors), *Proceedings of a Symposium on Effects of Forest Land Use on Erosion and Slope Stability*, pp. 255-264, May 7-11, 1984. Honolulu, HI: University of Hawai'i, East-West Center.

Coker R.J., Fahey, B.D., and Payne, J.J. 1993. Fine sediment production from truck traffic, Queen Charlotte Forest, Marlborough Sounds, New Zealand. *Journal of Hydrology* (NZ) 31: 56-64.

Cook, F.J., Lilley, G.P., and Nunns, R.A. 1993. Unsaturated hydraulic conductivity and sorptivity: Laboratory measurement. In Carter, M.R.(Editor), *Soil Sampling and Methods of Analysis*. Baco Raton, FL: CRC Press, Inc.

Elliot, W.J., Foltz, R.B., and Luce, C.H. 1995. Validation of Water Erosion Prediction Project (WEPP) model for low-volume forest roads, in *Proceedings of Sixth International Conference on Low-Volume Roads*, vol 1, 178-186, Minneapolis, MN, June, 1995. National Acadamy Press, Washington, D.C.

Elliot, W.J., Laflen, J.M., and Foster, G.R. 1993. Soil erodibility nomographs for the WEPP model, Paper no 932046, American Society of Agricultural Engineers & Canadian Society of Agricultural Engineering meeting, Spokane WA, June. 22 p.

Flanagan, D.C., and Nearing, M.A.(Editors). 1995. USDA-Water Erosion Prediction Project: technical documentation. NSERL Rep. no. 10. Natl. Soil Erosion Res. Lab., West Lafayette, IN.

Flanagan, D.C., Foster, G.R. and Moldenhauer, W.C. 1988. Storm pattern effect on infiltration, runoff and erosion. *Transactions of the American Society of Agricultural Engineers* 31:337-350.

Flerchinger, G.N., and Watts, F.J. 1987. Predicting infiltration parameters for a road sediment model. *Transactions of the American Society of Agricultural Engineers* 30(6): 1700-1705.

Foltz R.B. 1996. Traffic and no-traffic on an aggregate surfaced road: sediment production differences, paper for FAO seminar on *Environmentally Sound Forest Road and Wood Transport*, Sinaia, Romania. Intermountain Research Station, USDA, Forest Service, Moscow, ID.

Fox, J., Krummel, J., Yarnasarn, S., Ekasingh, M. and Podger, N. 1995. Landuse and landscale dynamics in northern Thailand: Assessing change in three upland watersheds since 1954. *Ambio* 24(6): 328-334.

Gagnon J, Roth J.M., Finzer W.F., Haycock K.A., Feldman Jr, D.S., and Simpson J. 1989. *Super ANOVA™ - Accessible General Linear Modeling*. Abacus Concepts, Inc., Berkeley, CA.

Geological Map of Thailand, Scale 1:250 000. A. Hess and K.E. Koch compilers, Federal Inst. for Geosciences and Natural Resources, Stuttgart, Germany, 1979.

Gilbert, G. K. 1917. Hydraulic-mining debris in the Sierra Nevada, *U.S. Geological Survey Professional Paper* 105, 154 pp.

Gimenez, D., Dirksen, C., Miedema, R., Eppink, L.AA..J. and Schoonderbeek, D. 1992. Surface sealing and hydraulic conductances under varying-intensity rains. *Soil Science Society of America Journal 56*: 234-242.

Grayson R.B., Haydon S.R., Jayasuriya M.D.A., and Finlayson, B.L. 1993. Water quality in the mountainous ash forest—separating the impacts of roads from those of logging operations, *Journal of Hydrology* 150: 459-480.

Green, I.R.A., and Stephenson, D. 1986. Criteria for comparison of single event models. *Hydrological Sciences Journal* 31: 395-411.

Hafley, W.L. 1975. Rural road systems as a source of sediment pollution—A case study, in *Watershed Management*, pp. 393-405, Irrigation and Drainage Division, American Society of Civil Engineers, New York.

Hillel, D. 1982. *Introduction to Soil Physics*. Academic Press, San Diego, CA, 364 p.

Hudson, N.W. 1957. Progress report on experiments at Henderson Research Station 1953-1956. *The Rhodesia Agricultural Journal. 54(3)*: 297-323.

Jones, J.A. and Grant, G.E. 1996. Peak flow responses to clear-cutting and roads in small and large basins, western Cascades, Oregon. *Water Resources Research* 32: 959-974.

Ketcheson, G.L., Megahan, W.F, and King, J.G. 1999. "R1-R4" and "BOISED" sediment prediction model tests using forest roads in granitics. *Journal of the American Water Resources Association* 35 (1): 83-98.

Kinnell, P.I.A. 1991. The effect of flow depth on sediment transport induced by raindrops impacting shallow flows. *Transactions of the American Society of Agricultural Engineers* 34:161-168.

Klute, A. 1986. Water retention: Laboratory methods. In Klute, A. (Editor), *Methods of Soil Analysis, Part 1. Physical and Mineralogical Methods-Agronomy Monograph no. 9* (2nd edition). American Society of Agronomy-Soil Science Society of American, Madison, WI, pp. 636-662.

Kubiniok J. 1992. Soils and weathering as indicators of landform development in the mountains and basins of Northern Thailand. *Zeitschrift für Geomorphologie* 91: 67-78.

La Marche, J., and Lettenmaier, D. P. 1998. Forest road effects on flood flows in the Deschutes River Basin, Washington. Water Resource Series Tech. Report. No 158, University of Washington, Department of Civil Engineering, 178 p.

Loague, K.M., and Freeze, R.A. 1985. A comparison of rainfall-runoff modeling techniques on small upland catchments, *Water Resources Research* 21: 229-248.

Loague, K., and Green, R.E. 1991. Statistical and graphical methods for evaluating solute transport models: Overview and application. *Journal of Contaminant Hydrology* 7: 51-73.

Luce, C.H., and Black, T.A. 1999. Sediment production from forest roads in western Oregon. *Water Resources Research* 35 (8): 2561-2570.

Luce, C.H., and Cundy, T.W. 1994. Parameter identification for a runoff model for forest roads.*Water Resources Research* 30: 1057-1069.

Mbagwu, J.S.C. 1997. Quasi-steady infiltration rates of highly permeable tropical moist savannah soils in relation to landuse and pore size distribution. *Soil Technology* 11:185-195.

Megahan, WF. 1974. Erosion over time: a model. USDA-Forest Service Research Paper Report INT-156. Intermountain Research Station, Ogden UT, 14 p.

Megahan, W.F. 1975. Sedimentation in relation to logging activities in mountains of central Idaho. In *Present and Prospective Technology for Predicting Sediment Yields and Sources*, 74-92. USDA, Ag. Research. Serv., ARS-S-40, Washington, D.C., 285p.

Megahan, W.F, and Ketcheson, G.L. 1996. Predicting downslope travel of granitic sediments from forest roads in Idaho, *Water Resources Bulletin* 32(2): 371-382.

Megahan, W.F, and Kidd, W.J. 1972. Effects of logging and logging roads on erosion and sediment depostition from steep terrain. *Journal of Forestry* 7:136-141.

Merz W. and Bryan, R.B. 1993. Critical conditions for rill initiation on sandy loam Brunisols: Laboratory and field experiments in southern Ontario, Canada. *Geoderma* 57: 357-385.

Meyer, L. D. 1994. Rainfall simulators for soil erosion research. In Lal, R. (Editor), *Soil Erosion Research Methods* (Second edition). St. Lucie Press, Delray Beach, FL, pp. 83-103.

Montgomery, D.R. 1994. Road surface drainage, channel initiation, and slope stability. *Water Resources Research* 30: 1925-1932.

Morgan, R.P.C. 1995. Soil Erosion and Conservation. Longman Group Limited, Esses, UK. 198 p.

Moss, A. J. and Green, P. 1983. Movement of solids in air and water by raindrop impact: effects of drop-size and water-depth variations. *Australian Journal of Soil Research* 21: 257-269.

Mualem, Y. and Assouline, S. 1986. Mathematical model for rain drop distribution and rainfall kinetic energy. *Transactions of the American Society of Agricultural Engineers* 29(2):494-500.

Nash, J.E. and Sutcliffe, J.V. 1970. River flow forecasting through conceptual models. Part I - A discussion of priniciples. *Journal of Hydrology* 10: 282-290.

Perroux, K.M. and White. I. 1988. Designs for disc permeameters. *Soil Science Society of America Journal 52*: 1205-1215.

Philip, J.R. 1957. The theory of infiltration: 1. The infiltration equation and its solution. *Soil Science* 83: 345-357.

Pransutjarit, C. 1983. Impacts of land use evolution on streamflow and suspended sediment in Mae Taeng watershed, Chiengmai. M.S. Thesis. Environmental Science, Department of Forestry, Kasetsart University, Bangkok, Thailand.

Rawls, W.J., Brakensiek, D.L., and Saxton, K.E. 1982. Estimation of soil water properties, *Transactions of the American Society of Agricultural Engineers* 25(5):1316-1320, 1328.

Reid, L.M. 1993. Research and cumulative watershed effects. US Dept. Ag., Forest Service, General Tech. Report, PSW-GTR-141. 118 p.

Reid, L.M. and Dunne, T. 1984. Sediment production from forest road surfaces. *Water Resources Research* 20: 1753-1761.

Reid L.M., Dunne T., and Cederhom, C.J. 1981. Application of sediment budget studies to the evaluation of logging road impact, *Journal of Hydrology (NZ)* ***29***: 49-62.

Rijsdijk, A., and Bruijnzeel, L.A. 1990. Erosion, sediment yield and land-use patterns in the upper Konto watershed, East Java, Indonesia, Part II: Results of the 1987 - 1989 measuring campaign. Project Communication 18, Konto River Project, Kingdom of the Netherlands, Ministry of Foreign Affairs, Director General of International Cooperation.

Rijsdijk, A., and Bruijnzeel, L.A. 1991. Erosion, sediment yield and land-use patterns in the upper Konto watershed, East Java, Indonesia, Part III: Results of the 1989 - 1990 measuring campaign. Project Communication 18, Konto River Project, Kingdom of the Netherlands, Ministry of Foreign Affairs, Director General of International Cooperation.

Riley, SJ. 1988. Soil loss from road batters in the Karuah State Forest, Eastern Australia. *Soil Technology* 1: 313-332.

Römkens, M.J.M., Prasad, S.N., and Parlange, J.Y. 1990. Surface seal development in relation to rainstorm intensity. *Catena Supplement* 17:1-11.

Schmidt-Vogt, D. 1998. Defining degradation: The impacts of swidden on forests in northern Thailand. *Mountain Research and Development* 18 (2): 135-149.

Schmidt-Vogt, D. 1999. *Swidden farming and fallow vegetation in northern Thailand.* Geoecological Research, vol 8. Franz Steiner Verlag, Stuttgart, Germany, 373 p.

Simons, D.B., Li, R.M., and Ward., T.J. 1978. Simple road sediment yield model, Colorado State University Report CER77-78DBS-RML-TJW-LYS41, Ft. Collins, CO, USA, 70 p.

Simons, D.B., Li, R.M., and Anderson, B.A. 1982. Soil erosion and sedimentation analysis of forest roads in northern California. Colorado State University Report CER81-82DBS-RML-BAA74, Ft. Collins, CO, USA, 113 p.

Simons, D.B., Li, R.M., and Shiao, L.Y. 1977. Formulation of a road sediment model. Colorado State University Report CER76-77DBS-RML-LYS50, Ft. Collins, CO, USA, 107 p.

Smetten, K.R.J., Ross, P.J., Haverkamp, R., and Parlange, J.Y. 1995. Three-dimensional analysis of infiltration from the disk infiltrometer. 3. Parameter estimation using a double-disk tension infiltrometer, *Water Resources Research* 31: 2491-2495.

Smith, R.E. 1976. Field test of a distributed watershed erosion/sedimentation model. *Soil Erosion, Prediction, and Control*. Soil Conservation Society of America Special Publication 21. Ankeny, IA, pp. 201-209.

Smith, R.E., Goodrich, D.C., and Quinton, J.N. 1995. Dynamic, distributed simulation of watershed erosion: the KINEROS2 and EUROSEM models. *Journal of Soil and Water Conservation* 50(5): 517-520.

Soil Conservation Service 1981. *Erosion and Sediment Control, Guide for Hawaii*. United States Dept. Ag., Soil Conservation Service, Honolulu, HI, 178 p.

Stearns, H. 1966. *Geology of the State of Hawaii*. Pacific Books, Palo Alto, CA. 266 pp,

Storck, P., Bowling, L., Wetherbee, P., and Lettenmaier, D. 1998. Application of a GIS-based distributed hydrology model for prediction of forest harvest effects on peak stream flow in the Pacific Northwest. *Hydrological Processes* 12: 889-904.

Sutherland, R.A., Wan, Y., Ziegler, A.D., Lee, C-T. and El Swaify, S.A. 1996. Splash and wash dynamics: An experimental investigation using an Oxisol. *Geoderma* 69: 85-103.

Tennant, D. 1975 A test of a modified line intersect method of estimating root length. *Journal of Ecology* 63: 995-1001.

Thomas, R.B., and Megahan, W.F. 1998. Peak flow responses to clear-cutting and roads in small and large basins, western Cascades, Oregon: A second opinion. *Water Resources Research* 34(12): 3393-3403.

Ulman, P.L., and Lopes, V.L. 1995. Determining interrill soil erodibility parameters for forest roads. *Carry the Torch for Erosion Control: An Olympic Task*. Proceedings of Conference XXVI, Feb. 25 - March 3, 1995, Atlanta, GA. International Erosion Control Association, pp. 345-357.

Van der Plas, M.C., and Bruijnzeel, L.A. 1993. Impact of mechanized selective logging of rainforest on topsoil infiltrability in the Upper Segama Area, Sabah, Malaysia. *Hydrology of Warm Humid Regions* (Proceedings of the Yokohama Symposium, July 1993, IAHS Publ. 216)

Wald, A.R. 1975. Impact of truck traffic and road maintenance on suspended sediment yield for 14' standard forest roads. M.S. Thesis, University of Washington, Seattle, WA, USA, 38 p.

Ward T.J. 1985. Sediment yield modeling of roadways, in El-Swaify S.A., Moldenhauer W.C., Lo, A. (Editors), *Soil Erosion and Conservation*. Soil Cons. Society of America, Ankeny, IA., pp. 188-199.

Ward, T.J. and Seiger, A.D. 1983. *Adaptation and Application of a Surface Erosion Model for New Mexico Forest Roadways*. Tech. Completion Rep. Proj. Nos. 1423669 & 1345667. New Mexico Water Resour. Research. Inst., New Mexico State University, Las Cruces, NM.

Wemple, B.D. 1998. Investigations of Runoff Production and Sedimentation on Forest Roads. Ph.D. dissertation. Forest Science, Oregon State University, Corvallis OR, 30 Nov. 1998, 168 p.

Wigmosta, M.S., Vail, L.W. and Lettenmaier, D.P. 1994. A distributed hydrology-vegetation model for complex terrain. *Water Resources Research 30 (6)*: 1665-1679.

Wischmeier, W.H. and Smith, D.D. 1978. Predicting rainfall erosion losses, *USDA Agricultural Research Service Handbook 537*, Washington DC.

Wold, W., Dube, K., and McCalmon, M. 1998. Technical Documentation for SEDMOD, Boise Cascade Road Erosion/Delivery Model, draft .

Woolhiser, D.A., Smith, R.E., and Goodrich, D.A. 1990. *KINEROS, A Kinematic Runoff and Erosion Model: Documentation and User Manual*. USDA-Agricultural Research Service, ARS-77, 130 p.

Zevenbergen, L.W., and M.R. Peterson. 1988. Evaluation and testing of storm-event hydrologic models. Proceedings of ASCE National Conference on Hydraulic Engineering. Colorado Springs, CO, Aug. 6-12, pp. 467-472.

Zhang, X.C., Nearing, M.A., Miller, W.P., Norton, L.D., and West, L.T. 1998. Modeling interrill sediment delivery. *Soil Science Society of America Journal* 62:438-444.

Ziegler, A.D. and Giambelluca, T.W. 1997a. Importance of rural roads as source areas for runoff in mountainous areas of northern Thailand. *Journal of Hydrology* 196 (1/4): 204-229.

Ziegler, A.D. and Giambelluca, T.W. 1997b. Simulation of runoff and erosion on mountainous roads in northern Thailand: a first look. In: *Human Impact on Erosion and Sedimentation* (Proceedings of Rabat Symposium S6, April 1997) IAHS Publ. no 245: 21-29